LABORATORIO DE MICROSCOPÍAS AVANZADAS

ANNUAL REPORT 2014-2015

LMA
LABORATORIO
DE MICROSCOPÍAS
AVANZADAS

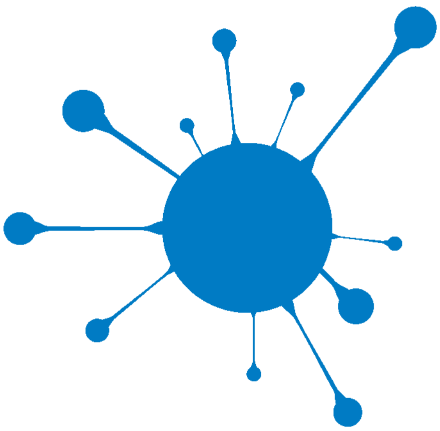

Laboratorio de Microscopías Avanzadas

Annual Report 2014-2015

LABORATORIO DE MICROSCOPÍAS AVANZADAS

EDITA
Laboratorio
de Microscopías Avanzadas
C/ Mariano Esquillor, s/n.
50018 Zaragoz (Spain)
Tel. +34 976 762 980
Fax +34 976 762 777
Email: lma@unizar.es
http://ina.unizar.es/lma

DISEÑO GRÁFICO
José Luis Lizano

Index

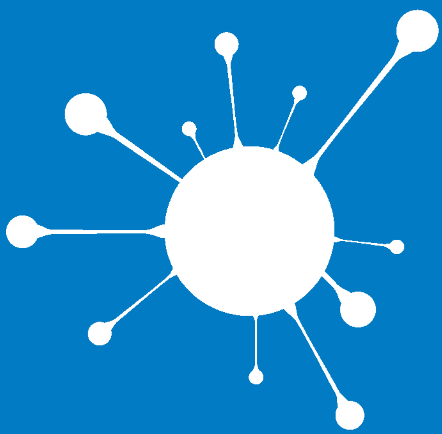

Introduction

Manuel Ricardo Ibarra García
Director

The Laboratory of Advanced Microscopies has consolidated a set of top level infrastructures in different fields of microscopies, establishing the necessary instrumentation and expertise to attend the demand of scientists and companies to face new challenges based in nanoscience and nanotechnology. Our mission is to attract world class science, creating a high research level atmosphere and based in the selective criteria of access and internalization of the laboratory. Several international partnerships have promoted synergies which allowed raising cutting edge scientific and technological outputs. The international collaboration with Midi Pyrenees Region through the Associate Laboratory CNRS-UNIZAR (TALEM II) and the participation in the European ESTEEM2 consortium allowed a fluent scientific exchange with top level researchers.

Our facilities have been completely settled during this period and world-class groups are frequently using our laboratories. The combination of expertise in nanofabrication and nanocharacterization at the same facility constitutes one of the most valuable characteristic that envision a promising future for the LMA.

Our scientific and technical staff cover a wide range of experimental facilities in advanced microscopies. Our challenge for the next period is to become an international reference Laboratory to promote and to establish new bridges among scientists and companies.

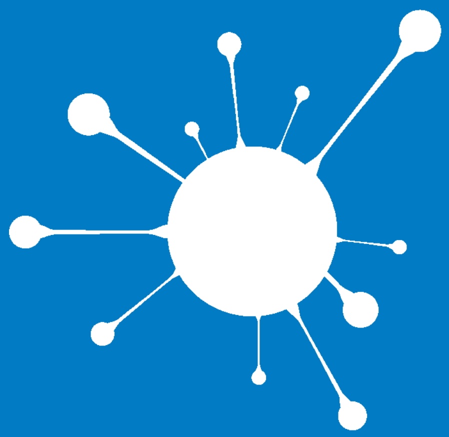

Foreword

Pilar Cea Mingueza
Scientific Coordinator

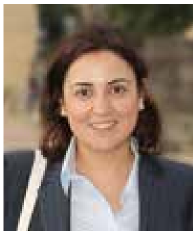

Since its creation in 2007, the Laboratory for Advances Microscopies (LMA) has worked very hard to locate Aragon and, in particular the city of Zaragoza, in the map of prestigious facilities for the nanofabrication and characterization of nanostructured materials. Less than one decade after the birth of the LMA, such an objective has been achieved and nowadays the LMA is recognized by the Ministry of Economy and Competitivity of Spain (MINECO) as a National Facility or a Singular Scientific and Technical Infrastructure (ICTS) and together with the Center for National Microscopy of Spain (CNME) from the University Complutense of Madrid conforms the so called ELECMI (Electron Microscopy for Materials Characterization) ICTS. ICTS' are defined by MINECO as are large installations, resources, facilities and services, unique in its kind, that are dedicated to cutting edge and high quality research and technological development, as well as to promote exchange, transmission and preservation of knowledge, technology transfer and innovation. In this context, as the reader can verify throughout this biennial report, the LMA scientists, technicians and users have achieved an unprecedented research level. Among the achieved goals, more than 128 publications, 26 with an impact factor higher than 10 deserve a special mention. Also, the increase of the industry demand to use the LMA facilities in 2014-15 which has doubled with respect to 2012-13 is another exponent of this laboratory expansion and growth. More than 66 proposals have been accepted in 2014-15 and the corresponding experiments performed in the LMA facilities. An important milestone is also the grant given by the MINECO in 2015 to the LMA and the CNME with the aim of stablishing a collaborative network to boost the ELECMI ICTS. Several research and training activities have been launched in this period including the regular scientific seminars of LMA open to the whole scientific and technical community as well as practical courses oriented to either advanced users or to potential industrial users.

Reaching such an excellent scientific and transfer to industry level has been a difficult task that required from the collaboration of scientists, technicians and LMA managers but also from University authorities as well as local and national politicians that provided LMA with the required infrastructure and financial support. However, as most of things in life, reaching a goal is not the most difficult challenge, the real challenge is to keep this goal alive and go a step further. In this context, the LMA needs more than ever the required support to invest in the maintenance of the already existing facilities, achieve the stability of our highly prepared and competitive staff as well as investing in the next generation of instruments that will build the LMA future.

About LMA

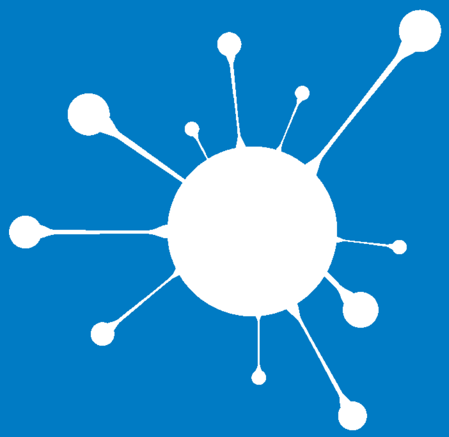

About LMA

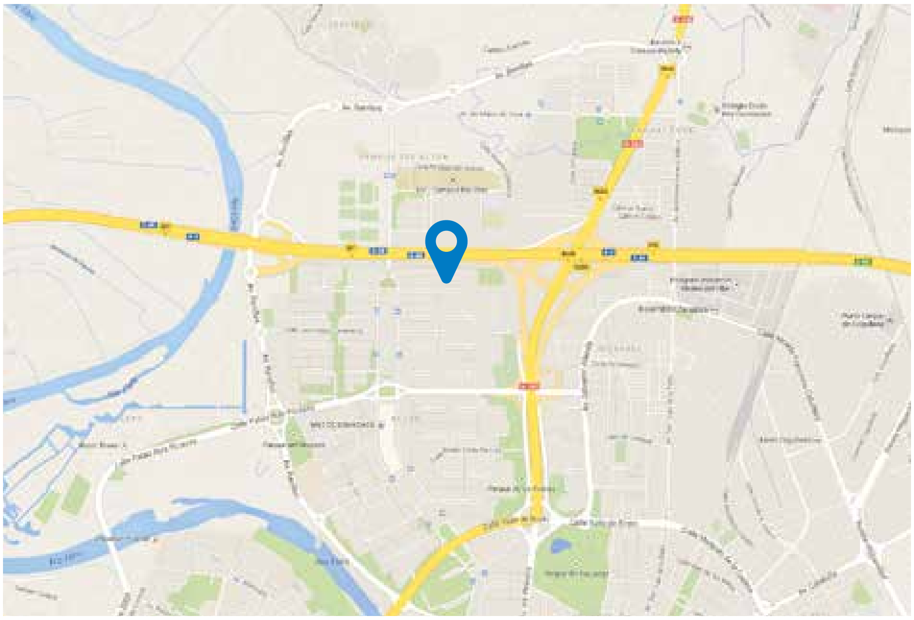

Laboratorio de Microscopías Avanzadas (LMA)
***Advanced Microscopies Laboratory* (LMA)**
Edificio I+D
Campus Río Ebro
Universidad de Zaragoza
C/ Mariano Esquillor, s/n.
50012 Zaragoza (Spain)
Tel: +34 976 762 980
Fax: +34 976 762 776
Email: lma@unizar.es
http://ina.unizar.es/lma

University Research Institutes Building – Campus Río Ebro.

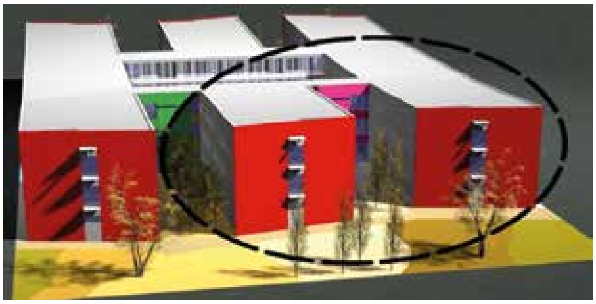

LMA Laboratories.

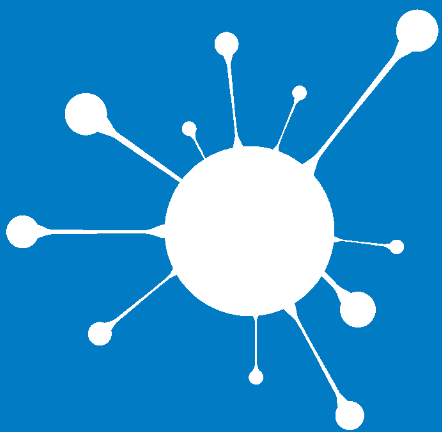

Organization Chart

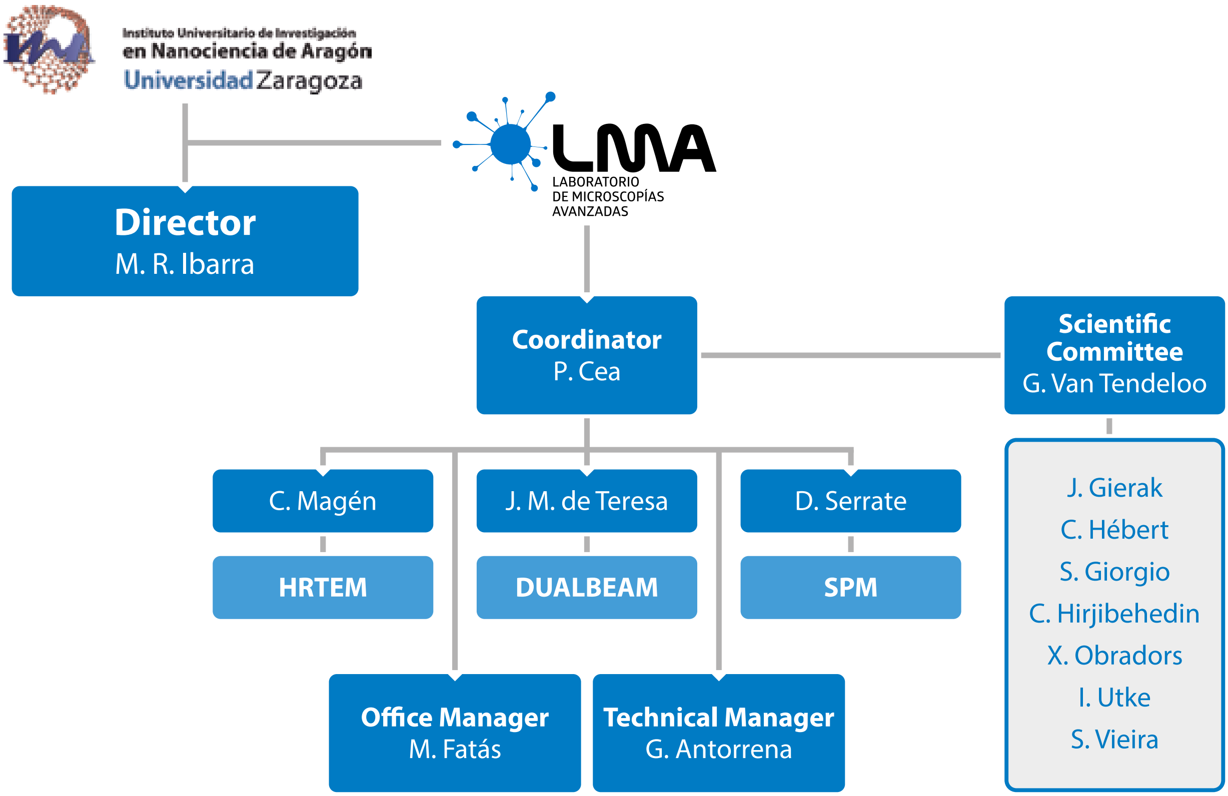

Human Resources 2014-2015

LMA staff

Personnel	
Scientific & Technical staff	17
Administration	2

LMA Associated members

Personnel	
Scientific	19

Management

M. Ricardo Ibarra	**Director**
Pilar Cea	**Scientific Coordinator**
Guillermo Antorrena	*Technical Manager*
Mercedes Fatás	*Office Manager*
Mª Jesús Calvera	*Administrative Support*

TEM

Aguirre, Myriam	*Researcher, Ramón y Cajal Program*
Arenal, Raúl	*Researcher, ARAID Foundation*
Custardoy, Laura	*Sample Prep Technician*
Fdez. Pacheco, Rodrigo	*TEM Technician*
Guzmán, Roger	*Postdoctoral Researcher*
Ibarra, Alfonso	*TEM Technician*
Luc Lajeunie	*Postdoctoral Researcher*
Mayoral, Álvaro	*Area Instrument Supervisor*
Peláez, Mario	*PhD Student*
Rodríguez, Luis Alfredo	*PhD Student*
Magén, César	**Head of TEM Area**

SPM

Arnaudas, José Ignacio	*Professor*
Cea, Pilar	*Associate Professor*
Coffey, David	*PhD Student*
Díez José, Luis	*SPM Technician*
Gracia, Ana Isabel	*Researcher, ARAID Foundation*
González, Alejandro	*Postdocotral Researcher*
Herrer, Lucía	*PhD Student*
Marcuello, Carlos	*PhD Student*
Martín, Carlos	*SPM Technician*
Moro, María	*PhD Student*
Piantek, Marten	*Area Instrument Supervisor*
Serrate, David	**Head of SPM Area**

DUAL BEAM

Casado, Laura	*Dual Beam Technician*
Cuestas, Carlos	*SEM Technician*
De Teresa, José Mª	**Head of DUAL BEAM Area**
Goya, Gerardo	*Associate Research Professor*
Irusta, Silvia	*Associate Research Professor*
Pablo, Javier	*PhD Student*
Pardo, José Ángel	*Associate Professor*
Rivas, Isabel	*Clean Room Technician*
Serrano, Luis	*PhD Student*
Sesé, Javier	*Associate Research Professor*
Simón, Gala	*Clean Room Technician*
Tejero, Luis	*Technician*
Torres, Teobaldo	*Dual Beam Technician*
Valero, Rubén	*Clean Room Technician*

The Scientific Committee

The Scientific Committee is in charge of providing scientific and advisory support to the Management Board. It is composed of internationally prominent scientists in the field of advanced microscopies, with outstanding professional and scientific track record in line with LMA objectives.

Members

Prof. G. Van Tendeloo (Chair)	*University of Antwerp (Belgium)*
Dr. Jacques Gierak	*LPN – CNRS (France)*
Prof. Suzanne Giorgio	*CINM – CNRS (France)*
Prof. Cecile Herbert	*EPFL (Switzerland)*
Dr. Cyrus Hirjibehedin	*London Center for Nanotechnology (UK)*
Prof. Xavier Obradors	*ICMAB – CSIC (Spain)*
Dr. Ivo Utke	*EMPA (Switzerland)*
Prof. Sebastián Vieira	*Universidad Autónoma de Madrid (Spain)*

Functions

> Provide advice in relation with the scientific policy guidelines

> Evaluate and inform on the Annual Report of activities and on the proposals for the Annual Action Plans

> Provide feedback on the usefulness of programs, resources and capabilities of the different laboratories.

> Assess on the technology transfer strategy

> Assess on the recruitment policy for scientific personnel

> Inform on the creation of research programs.

Description of the access offered to the R&D community

To achieve the goals of expanding the microscopy techniques both to industry and the scientific community we offer the use of our facilities to experienced users as well as novel users and groups not directly connected with microscopy methods. Users find at LMA a flexible and competent center to carry out their characterization and research studies with the support of specialized technical staff and scientists.

In accordance with the range of experimental tools and methods, we offer access to our facilities either as a service (studies and nanofabrication carried out by our technical staff) or as project-oriented collaborations (demanding studies requiring the active participation of our scientific personnel). Our experience is that, depending on the user and the type of measurement, the support by the LMA staff varies.

LMA offers the following type of activities:

> Structural and chemical TEM studies of materials and devices

> Studies of local magnetic configuration by electron holography and magnetic force microscopy

> Plasmon mapping

> Cryo-TEM studies of soft materials

> Nanostructuration by Focused Ion Beam

> Surface analysis by scanning probe microscopy, including atomic manipulation, follow-up of catalytic reactions and thin-film growth modes.

> Studies of single molecule configuration and spectroscopy by UHV Tunneling microscopy

> Magnetic microscopy under high magnetic fields in combination with electric transport measurements.

There are three types of access depending on the experience of the applicant, on the instrument, and on the challenge of the proposed measurements:

> **Service:** measurements are carried out by our technical staff. In general the attendance of the applicant is desired. This modality is applied to industrial partners, as well as to scientific users not directly working with similar instruments, who in general seek for a measurement complementary to their own techniques.

> **Scientific Use:** Some of our equipments are used by external experience users, who do not have at hand at their institutes of the specific tools like the ones available at LMA. In this case, users are advised by our technical staff about the use of the system and allowed to work independently.

> **Collaborative Use:** when challenging measurements are required, we offer the possibility to realize collaborative works together with scientific personnel of the LMA. In this case, our scientists get deeply involved in the measurements and analysis of the results.

Administrative and scientific and technical support to users

The LMA offers to potential users all types of local supports in terms of additional equipment for sample preparation and characterization, and technical, scientific and administrative staff.

> **Before the arrival:** For each accepted project, a "local contact" is designated, who will organize with the external user(s) his/her visit (together with the administration staff) and experiment (together with the technical staff) at the infrastructure. The local contact is chosen among the respective local experts of the corresponding infrastructure, depending on their own expertise and on the equipment that has been requested. This local contact is also in charge of checking that the equipment and samples are ready for the experiment, the viability of the measurements, and of reserving enough time in advance for preparing the experiment.

> **During the measurement:** All equipment offered are continuously maintained by highly specialized technical operators, who support and train the user in their initial use, as well as in the preparation of samples for measurement. They consider each specific requirement to ensure the success of the measurement. For some specific measurements in which special sophisticated methods are needed, the local contact will be also available to assist the user(s) in performing measurements, as well as in the data analysis.

> **After the measurement:** When leaving the infrastructure, the user(s) will take away all the raw images and spectra obtained with the LMA equipment and when carried out, the data that have been analyzed with the LMA researchers. In some special cases, LMA researches could offer subsequent support in terms of interpretation, and discussion of obtained results, especially in those cases when the local contacts were particularly involved in the scientific project.

Access protocol.

To gain access to the LMA facilities, eligible users need to submit a research proposal describing their requirements. A standardized proposal form is available in the LMA website and can be filled on-line (http://ina.unizar.es/lma)

The research proposal to gain access contains the administrative location of the requesting person or group leader and describes:

> The scientific aim of the project, including

- The state of the art
- The expected output
- The potential industrial applications
- Possible special requests (for example: use of particular stages, precautions, low temperature, gas atmosphere, low voltages…)

> The requested instrument(s) including measuring conditions and sample preparation facilities, if needed.

> The requested access time to the instrument and sample preparation time (if any)

> The preferred dates for the measurements.

> The requested time for computing / data treatment and analysis time (if any).

Currently there is a permanently open call for submission of proposals, which are evaluated by at least one member of the Access Committee. Successful proposals enjoy experimental time as soon as possible. The feedback time to the user is very fast, in the range of 1-2 weeks, warranting the timeliness of the experiment.

For every successful proposal, the area leader of the LMA selects a scientific in-house correspondent (local contact). The applicant is then notified of the acceptance of the proposal and invited to communicate details and dates of the experiment with the local contact at the LMA.

Access Committee

The evaluation of the proposals is performed by specialized committees in each of the three scientific divisions of the LMA. The committees are chaired by the corresponding responsible scientist of the TEM, SPM and Dual Beam areas and are formed by the following experienced external scientists.

TEM Experts

> Dr. B. Warot (CEMES- CNRS, Toulouse) – Expertise: EELS, in-situ TEM

> Dr. J. Verbeek (EMAT, Antwerpen) – Expertise: EELS, STEM-HAADF, Tomography

> Pr. J. Arbiol (ICMAB, Barcelona) – Expertise: HREM, HRSTEM, EELS

> Dr. Luca Ortolani (University of Bologna) – Expertise : Holography, HREM

> Dr. E. Snoeck (Coordinator TEM division of LMA) – Expertise: Lorentz, Holography, HREM

SPM Experts

> Dra. Agustina Asenjo (ICMM, Madrid). Expertise: Magnetic Force Microscopy.

> Dr. Carlos Untiedt (Univ. Alicante). Expertise: low temperature transport through nanostructures.

> Prof. José Ignacio Pascual. Expertise: Surface Science and low temperature UHV-SPM

Dual Beam Experts

> F. Pérez-Murano (UAB, Barcelona). Expertise: Electron Beam Lithography

> J. Gierak (LPN-CNRS – Marcoussis, France). Expertise: Ion Beam Lithography

> José Luis García Fierro (ICP-CSIC, Madrid). Expertise: XPS.

> Bruno Humbel (Univ. Lausanne, Switzerland). Expertise: Cryo Dual Beam.

> Prof. José María de Teresa (Coordinator Dual Beam division of LMA). Expertise: Nanolithography

Description of the evaluation procedure

Depending on the requested instrument, each research proposal is sent via the WEB site to the heads of the area i.e. Prof. E. Snoeck for TEM, Prof. J.I. Pascual for SPM and Prof. J.M. de Teresa for Dual Beam, who transfers it to a member of the Access Committee.

Each proposal is assessed by the Access Committee against the following selection criteria:

> **Technological or Scientific Merit of the proposal** (rank: weak: 0 – outstanding: 10)

> **Capabilities of the user team** (rank: weak: 0 – outstanding: 10)

> **Feasibility of the experiment:** the experiment must be feasible, this is discussed with the technicians and the scientists of the LMA.

Proposals are accepted provided that the threshold mark of 5 is reached in the first two criteria and the experiment is found to be feasible. Proposals with a total ranking less than 10 are rejected and the users are normally invited to resubmit their proposal following the advice of the reviewer report to improve their application. Accepted proposals designate a local person who is the contact for the user(s) to organize and perform the experiment.

LMA as one of the nodes of the Singular Scientific and Technical Facility ICTS ELECMI

LMA was recognized (7th October 2014) by the Government of Spain as a joint National Facility together with the CNME (from Universidad Complutense of Madrid). They both constitute ELECMI, a Singular scientific and technological infrastructure (ICTS, for its Spanish acronym) distributed in two nodes: the National Center for Electron Microscopy (CNME) at Complutense University of Madrid, and the Advanced Microscopies Laboratory (LMA) at University of Zaragoza. ELECMI appears in Spain's scientific panorama as a consequence of the fruitful activity in the field of materials and of the need to respond to the demand of techniques to characterize matter.

This ICTS allows users from research centers, national and international laboratories and industry to carry out experiments and pursue groundbreaking research by providing them with with an extraordinary range of cutting-edge microscopy and spectroscopy tools that support in depth research and drive scientific breakthroughs.

ELECMI is currently working to establish and implement the best way to provide competitive access to ELECMI, which will be unique, simple and open both to public and private research centers, and to industry. Those beneficiaries will have the possibility to perform experiments with last-generation equipment, triggering I+D+I in our country and giving rise to transational cooperation which will place our country's electron microscopy in the World's map.

ELECMI is currently setting up a joint access website which will be available shortly.

The Laboratories

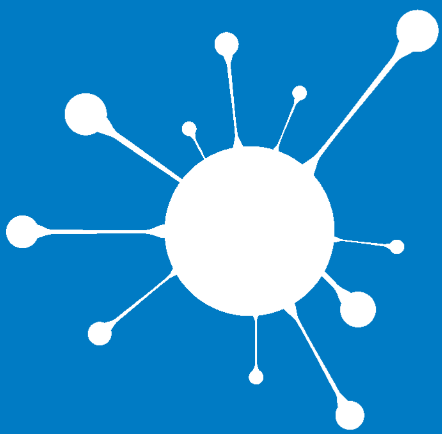

The Laboratories

Transmission Electron Microscopy Laboratories

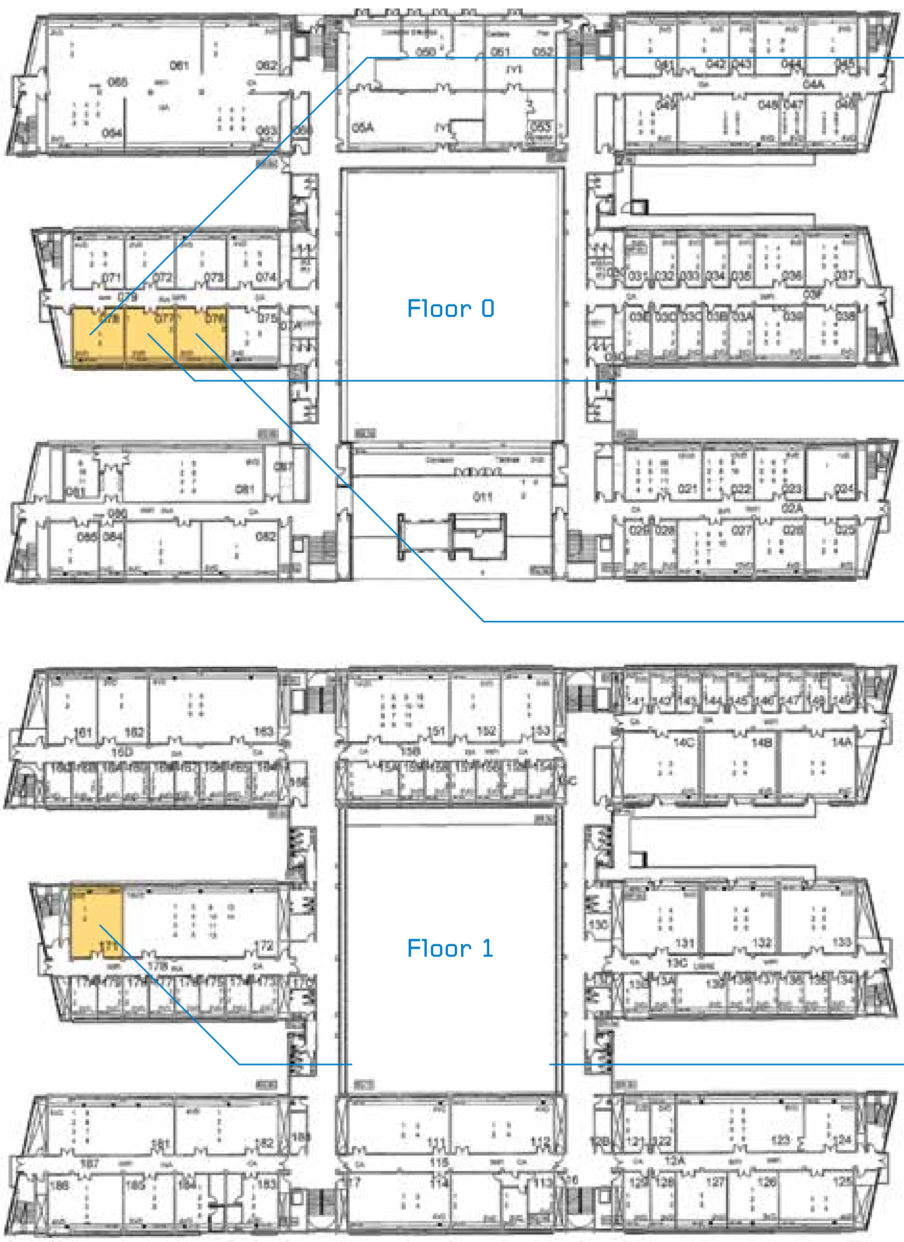


TITAN^3


TITAN STEM

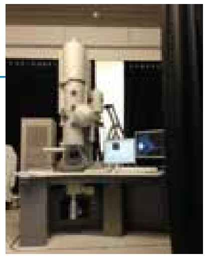
F30


Sample Preparation

a) Transmission Electron Microscopy Laboratories (UHRTEM snd HRTEM) & Sample Preparation

There are three HRTEM instruments working up to 300 kV available: a F30 TEM and two TITAN Cs corrected microscopes of the very last generation.

a.1) High resolution transmission electron microscope (F30) .

This 300 kV Field Emission Gun (FEG) TEM is fitted with a SuperTwin® lens allowing a point resolution of 1.9 Å. This TEM can work in TEM and STEM mode. For Z-contrast imaging in STEM mode, it is fitted with a High-Angle Annular Dark Field (HAADF) detector. This TEM is equipped for spectroscopy experiments performed either in EDS (X-Ray Microanalysis) or in Electron Energy Loss spectroscopy (EELS). For the latter, it is fitted with the "Tridiem" Gatan Energy Filter (GIF). This EELS set-up allows Energy Filtered TEM (EFTEM) images to be recorded as well as line spectra or spectrum imaging experiments to be performed. A 2K x 2K Ultrascan CCD camera (Gatan) is located before the GIF for TEM imaging. In addition to these capabilities the F30 TEM is also fitted with a Lorentz lens which permit the study of magnetic materials in an environment free of magnetic field (for magnetic domain imaging). Furthermore, the F30 allows tomography experiments to be performed both in TEM and STEM mode using a dedicated single tilt holder (+/- 70°) from Fischione.

a.2) Cs probe corrected STEM microscope (TITAN Low base) dedicated to EELS and STEM HAADF studies.

This Scanning Transmission Electron Microscope works either in TEM or in STEM mode at voltages between 60 kV and 300 kV. It can be used at low voltage to analyse electron irradiation sensitive materials. It is fitted with the last generation of a high brightness Schotky emitter developed by FEI (the so called "X-FEG" gun) a monochromator and a Gatan 2k x 2k CCD camera.

STEM: As this microscope is devoted for STEM and EELS experiments, it is equipped with a CETCOR Cs-probe corrector from CEOS Company allowing for the formation of an electron probe of 0.08 nm mean size. The TEM is equipped with all the STEM facilities (BF, DF, ADF and HAADF detectors) and 0.08 nm spatial resolution has indeed been achieved in STEM-HAADF mode.

EELS and EDS: For EELS experiments, the microscope is fitted with a Gatan Energy Filter Tridiem 866 ERS and a monochromator. An energy resolution of 0.14 eV has been recently achieved with this setup. In addition, an EDS (EDAX) detector allows performing EDX experiments in scanning mode with a spatial resolution of about ~0.2 nm.

Lorentz and holography: Beside these analytical capabilities, the Titan STEM corrected microscope is fitted with a Lorentz lens and an electrostatic biprism allowing Lorentz and medium resolution electron holography experiments to be carried out in a field-free environment (as needed for magnetic materials studies). Tomography: In addition, a tomography set-up with a +/- 70° single tilt stage permits to perform 3D analyses either in TEM or STEM modes.

a.3) Cs objective lens corrected microscope (TITAN3) dedicated to Ultra High Resolution TEM imaging

This TEM also works at voltages between 60 and 300 kV. It is located in a "box" (cube) to avoid mechanical and thermal perturbation (see figure). It contains a normal FEG (Shottky emitter) and a Gatan 2k x 2k CCD camera for (HR)TEM images acquisition.

HREM: As this microscope is devoted for High Resolution Transmission Electron Microscopy (HRTEM) studies, it is equipped with a SuperTwin® objective lens and a CETCOR Cs-objective corrector from CEOS Company allowing a point to point resolution of 0.08 nm.

STEM: In addition this Titan3 is equipped with the basic STEM facilities (BF, DF detectors) for STEM imaging at medium resolution

EELS: a Gatan Energy Filter Tridiem 863 allows Titan3 to perform EELS experiments in a standard and routine way (energy resolution of ~0.7 eV).

Lorentz and holography: As for the dedicated Titan STEM, beside these spectroscopy capabilities, the Titan3 corrected microscope is fitted with a Lorentz lens and an electrostatic biprism allowing Lorentz and medium resolution electron holography experiments to be carried on.

a.4) Sample Preparation Laboratory

TEM is based in the use of transmitted electrons to form images of the materials. However, the electron is a strongly interacting charged particle and TEM samples are required to be extremely thin (tens of nm) to be electron transparent. Some materials are inherently electron transparent (nanoparticles, nanotubes…), but most of them (bulk materials, thin films, devices…) have much larger dimensions and it is frequently required to carry out a TEM sample preparation procedure to make them thin. The LMA has set the most advanced Sample Preparation Laboratory equipped with the necessary instruments to perform this task. Among the many procedures to produce electron transparent specimens, the most important and frequently used is based on mechanical thinning of the materials in a highly controlled way. This produces a flat specimen of a few microns thickness with defect-less surfaces that afterwards follows a low-angle, low-energy ion milling of the surfaces to achieve extremely thin areas ready for TEM observation. Nowadays, this task can be also performed in many cases by means of Focused Ion Beam (FIB) techniques in the DualBeam equipment available at the LMA providing large flat electron transparent areas selected with high accuracy, which is ideal, for instance, in the TEM sample preparation of nanodevices.

Sample Preparation Laboratory

Ion mill equipment to obtain electron transparent areas in the samples for the TEM observation.

DUAL BEAM Laboratories

Dual Beam in Clean Room

µ-structural chacterization & Spectroscopy

Life Sciences

b) Dual Beam Laboratories & Microcharacterization

b.1) Dual Beams Laboratory in Clean Room

In the Clean Room facilities of the institute, several lithography facilities permit to pattern structures at the micro- and nanometer scale and to create devices. In particular, the two dual beam equipment assigned to nanolithography and lamellae preparation are placed on two concrete platforms inside the 125 m2 10000-class Clean Room.

Helios 600 dual beam equipment installed inside the Clean Room of the INA building.

Dual Beam #1

The first dual beam equipment is the Helios 600 model and has been working since December 2009 at the same place. It consists of a 30 kV field-emission scanning electron column and a 30 kV Ga focused ion beam placed at 52º one from each other. The ion column is able to work properly at low voltage (5 kV and lower), allowing the preparation of lamellae with low ion damage. Thus, in this equipment 54 lamellae have been prepared in 2011 by the technical staff, with high enough quality for atomic-resolution TEM imaging. In this equipment, there are five gas injectors as well, allowing the growth of nanodeposits with high resolution. In this equipment it has been possible to grow W-based superconducting nanodeposits with lateral size of 40 nm and Co-based ferromagnetic nanodeposits with lateral size 30 nm, these ultranarrow dimensions being at the forefront of the research in these topics.

Dual Beam #2

The second dual beam inside the Clean Room was installed in December 2010 and the model is Helios 650. Such a model is an improved version of the Helios 600 one. Thus, the SEM column has resolution of 0.9 nm and it bears a monochromator and beam deceleration. The FIB column is differentially vacuum-pumped at the lowest part, allowing a well-defined beam profile impacting on the sample surface. Preliminary results with such a column indicate that ultranarrow nanodeposits can be grown. This FIB column is nicely suited for lamellae preparation too, in combination with the Omniprobe nanomanipulator. The equipment has got 5 gas injectors and electrical microprobes. This equipment is expected to work properly for the requested main tasks: lamellae preparation and nanolithography based on ion patterning, electron beam lithography and nanodeposition.

Helios 650 equipment installed inside the Clean Room of the INA building.

Nova 200 dual beam equipment and the cryo-transfer setup, installed at INA building .

b.2) Cryogenic Dual Beam

The third dual beam equipment is used for electron sensitive materials and life sciences and has been installed in the same room as the environmental SEM and the field-emission SEM. This instrument is based on the Nova 200 model (existing in our laboratory since November 2006) but upgraded with a cryo-transfer chamber. This equipment has worked properly since 2007 and in combination with the cryo-transfer set-up is being used to produce series of ion-cuts of cells embedded in resin or frozen with the help of liquid nitrogen. These images will be used to produce 3-dimensional reconstructions. Appropriate software for 3-dimensional compositional reconstructions based on energy-dispersive x-ray micro-analysis is also included in this equipment. If needed, the equipment also holds an Omniprobe nanomanipulator for lamellae preparation as well as 5 gas injectors.

b.3) Other facilities for micro and surface characterization

Environmental SEM-FEG

An environmental SEM, model Quanta 250, is installed in the same room as the Nova 200 dual beam. The SEM column allows beam deceleration, which permits to keep resolution of 1.4 nm even at 1 kV electron landing voltage. The Quanta equipment can work under three different pressure ranges, the maximum pressure being 4000 Pa, thus close to ambient pressure. This allows observation of life-sciences samples without previous metallic coating. The equipment allows the use of a Wet-STEM, which permits to inspect samples with controlled humidity, this being crucial in life-science samples in order to maintain the same conditions as hold when functional. The equipment can also use a heater to perform observation on samples heated up to 1000 Celsius degrees.

Environmental SEM, Quanta FEG 250 equipment, installed at the INA building.

Field-emission SEM, INSPECT equipment, installed at the INA building.

SEM-FEG

The last SEM equipment, the Inspect model, is a general-purpose field-emission SEM for high-resolution imaging and composition analysis by energy-dispersive x-ray microanalysis.

Laboratory of Microstructural Characterization and Spectroscopy

> The XRD and the XPS-AES equipments are installed in the room devoted to microstructural and spectroscopy sample analysis. Those equipments have been working since 2006 and providing a great variety of useful results for most of the research groups at INA and other centres and companies mentioned later. In the following, the main characteristics of these equipments are mentioned:

> XRD (Bruker D8 Advance, four-circle diffractometer).

- Copper anode.
- Eulerian cradle.
- Parallel-beam optics.
- Incident- and diffracted-beam monochromators.
- Scintillation counter and 2D detector (GADDS).
- Analysis software and database.

> XPS-AES (Kratos):

- Analysis chamber with base pressure < 10-9 Torr
- Multi-detector energy analyser and 2D image in parallel
- Monochromator
- Ar ion milling
- Electron gun for AES
- Charge neutralizer
- Sample holder for 4-axis high-precision displacements

XRD (left image) and the XPS-AES (right image) equipment, installed at LMA

Laboratories for Local Probe Microscopy

High Magnetic Field

UHV-LT (II)

Environmental

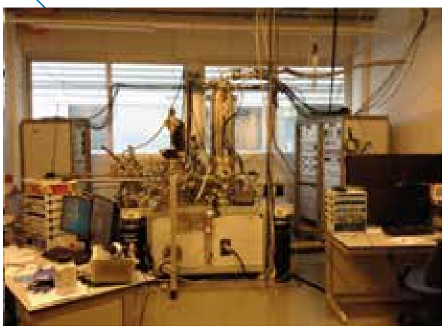

UHV-LT (I)

c) Laboratories for Local Probe Microscopy

The available facilities in the SPM section of the LMA are composed by six SPM instruments combined in three different laboratories:

Low-temperature, ultra high vacuum (UHV-LT) scanning probe microscopy Laboratory

The laboratory of UHV-LT is specifically designed for surface science microscopy and spectroscopy methods. The aim is to cover a wide variety of problems in surface science, from molecular chemistry to atomic magnetism. Three systems are equipped with different preparation techniques under UHV conditions, as well as with large variety of epitaxial growth facilities. Force- and Tunnel-based methodologies can be combined, allowing the investigation of samples with different electronic properties. The accessible temperature range for experiments is from 0.5 K to 1300 K. The laboratory is composed by three UHV microscopes hosting four different SPM heads, each with complementary characteristics:

c.1) 1 Kelvin STM with axial magnetic field and variable temperature SPM.

This equipment is specifically oriented to investigate atomic scale magnetism and to high resolution spectroscopy of molecules and atoms, as well as to study the surface dynamics with atomic resolution as a function of temperature and gas partial pressure. It includes two UHV STMs, one of them running at a base temperature of 1.1 K (0.5 K using He3) and a variable temperature STM (from 100 K to 1300 K), with a fast and flexible measurement approach.. In the last year, this facility has provided the scientific community with spin-polarized STM on a regular basis, being the only laboratory offering worldwide this technique via a competitive proposal scheme.. The details of the equipment are the following:

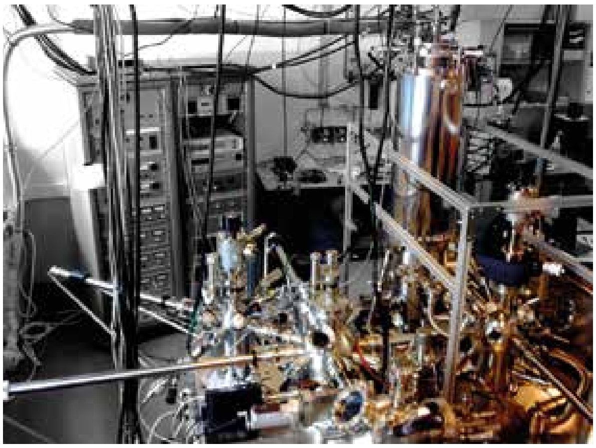

SPECS JT-STM:

Joule Thomson cryostat (1K-10K) UHV-STM; 3 T axial B field; energy resolution 0.15 meV; Metal and organic epitaxy in situ

AAHRUS VT-STM/AFM:

Aarhus variable temperature (100K-1300K) STM, Non-contact-AFM, in-situ evaporation

Attached UHV facilities

Surface conditioning, LEED/Auger characterization; 9 Molecular Beam Epitaxy pockets (5 of them with fast reload option), 3 crucible evaporators

c.2) Low Temperature STM in UHV.

This equipment is oriented to investigate metal-on-metal epitaxy of rare earths. It is specially oriented to the growth of magnetic thin films and nanostructures. The equipment runs at a base pressure of 4.3 K and has been optimized to deposit rare-earth metals on tungsten substrates

OMICRON LT-STM:

Low temperature (5K) UHV STM

Preparation:

Surface conditioning, Metal epitaxy

c.3) Low temperature STM/AFM in UHV.

OMICRON LT-qPlus:

Low temperature (4.3 K-40 K) UHV STM equipped with a qPlus sensor allows users to correlate resonance frequency shifts of a quartz tuning fork with the gradient of forces between tip and sample.

Preparation:

Surface conditioning, LEED/Auger, metal epitaxy, and sublimation of organic materials by one K-cell and two crucible evaporators

This set up includes the last development in UHV non-contact AFM. Working at a base temperatureof 5K, the use of a qPlus sensor allows to simultaneously acquire local tunneling spectroscopy and forces spectroscopy. Measurement of both forces and conductance is especially interesting in the field of molecular physics on surfaces.

Force microscopy is also especially suitable to work on insulating surfaces. This experimental set up has been equipped with various methods to deposit organic materials on inorganic surfaces. The research lines are oriented to molecular interactions, self-assembly and magnetic, electronic and structural properties of hybrid metal-organic films.

Laboratory of SPM under high magnetic field

c.4) High field SPM

The laboratory of high magnetic fields offers the possibility of combining probe measurements (AFM, MFM, STM) with ultra-low temperatures and a high vector magnetic field. It is especially suitable for combination of local probe and magneto-transport measurements as, for example, scanning gate microscopy. Therefore, it runs research lines oriented towards low temperature magnetism, transport through nanodevices, spintronics and superconductivity.

-ATTOCUBE AFM/STM: STM/AFM/MFM head inserted into a large bore superconducting magnet reaching 8T/2T vector magnetic field. The equipment has a quick load facility, allowing an easy sample replacement and measurements. A variable temperature module allows one to continuously change the temperature from 2 Kup to 300 K. The laboratory. Further characteristics: in-situ optical access, compatible chip carrier with dual-beam facilities

Laboratory AFM/STM in ambient conditions

c.5) Near ambient SPM heads

The biology, chemistry and physics community, all of them potential users of the SPM facilities, demands a set of microscopy tools with large versatility and able of working under different environments close to ambient conditions. The laboratory contains both force and tunnel microscopies that allows users a quick investigation of samples in liquid, electrolytes, or in atmosphere with controlled humidity and/or temperature.

Atomic Force Microscopy

AFM is a key technique in Nanosciences, supporting multidisciplinary activities. Hence it is a central facility in the LMA. The microscopes are mounted on vibration isolation stages. In addition, a highly specialized technical scientist is in charge of the support to external users, training of frequent and experienced users and maintenance of the equipment, which features a remarkable completeness.. They can perform high sensitive Force spectroscopy and workunder magnetic field in the Magnetic Force Microscopy mode.

Multimode 8 from Veeco-Bruker

Equipment:

1. Nanotec: Cervantes Fullmode SPM from Nanotec Electrónica S.L. AFM/MFM/STM equipped with variable magnetic field and liquid cell.
2. Veeco: Multimode 8 from Bruker. SPM equipped with KPM, conductive AFM, liquid and electrochemistry cells, PicoForce module for force spectroscopy measures, and variable temperature (-40 ºC to 100 ºC).

Cervantes Fullmode SPM from Nanotec Electrónica

Scientific Activity

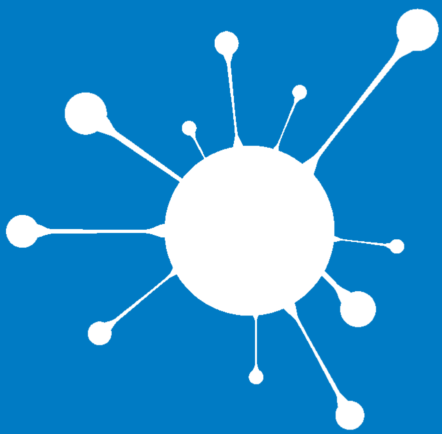

Highlights

Artificial chemical and magnetic structure at the domain walls of an epitaxial oxide

Strained oxide thin films oxides often present radically different physical properties than bulk materials. For instance, they often contain high density of ferroelastic domains to accommodate the epitaxial strain. This symmetry breaking can induce properties absent from the domains themselves, such as magnetic or ferroelectric order and other functionalities, as well as the formation of new structural and chemical phases. In this sense, domain walls can function as nanoscale chemical reactors.

In this work, a new 2D ferromagnetic phase is synthesized at the domain walls of the orthorhombic perovskite terbium manganite ($TbMnO_3$) thin films grown under epitaxial strain on strontium titanate ($SrTiO_3$). Aberration corrected STEM has enabled a comprehensive characterization of the structure and chemical composition of this novel ferromagnetic phase by means of atomically resolved High Angle Annular Dark Field (HAADF) imaging and Electron Energy Loss Spectroscopy (EELS). This new phase, yet to be created by standard chemical routes, is characterized by the selective substitution of alternate Tb atoms in the perovskite structure by Mn atoms in the B positions of the perovskite structure (ABO_3). The density of these 2D sheets can be tuned by changing the film thickness, and they can grow as densely as to represent up to 25 per cent of the film volume. The general concept of using domain walls of epitaxial oxides to promote the formation of unusual phases may be applicable to other materials systems, thus giving access to new classes of nanoscale materials for applications in nanoelectronics and spintronics.

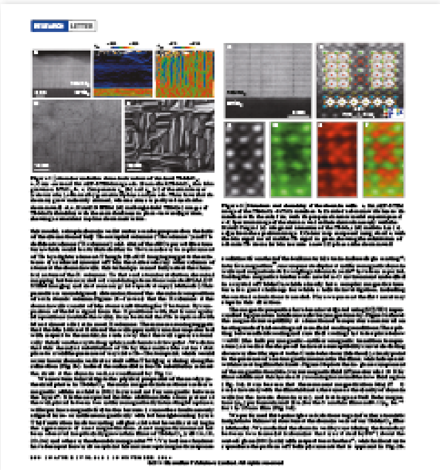

Figure caption. (a) HAADF-STEM image of the TbMnO3–SrTiO3 interface. b) Domain wall of TbMnO3 close to the interface with the SrTiO3 substrate, with the proposed atomic model superimposed. (c–f) STEM-EELS spectrum image of the domain wall; (c) HAADF signal, (d) Tb signal, (e) Mn signal, (f) color map of Tb (green) and Mn (red).

Reference:

S. Farokhipoor, C. Magén, S. Venkatesan, J. Íñiguez, C.J.M. Daumont, D. Rubi, E. Snoeck, M. Mostovoy, C. de Graaf, A. Müller, M. Döblinger, C. Scheu and B. Noheda. Nature 2014, 515, 379–383.

Highlights

Observation of magnetic dead layers in the surface of strained La2/3Ca1/3MnO3 films

Most technological applications of spintronics (such as low power electronics or high density data storage) require the use of the chosen functional material in the form of thin film. These may present physical properties remarkably different from bulk due to scale reduction or the influence of a substrate. These factors need to be taken into account so that thin film specimens present the same or even optimized functional properties with respect to their bulk counterparts. An ideal benchmark to study these effects is single crystalline $La_{2/3}Ca_{1/3}MnO_3$ (LCMO), a colossal magnetoresistive spin-polarized ferromagnetic material which often presents a dramatic reduction or weakening of their magnetic and transport properties in thin films with due to the strain by epitaxy on a single crystalline substrate.

In this work, we show the first experimental images of the magnetization state of strained LCMO thin films obtained by electron holography demonstrating that epitaxial strain induces the segregation of a non-FM (magnetically dead) layer with antiferromagnetic (AFM) character at the top surface of a FM layer, the whole film being chemical and structurally homogeneous at room temperature. For different substrates and growth conditions the tetragonality of LCMO at room temperature, a critical tetragonal distortion is found above which this phase coexistence takes place. Theoretical calculations prove that the increased tetragonality changes the energy balance of the FM and AFM ground states in strained LCMO, enabling the formation of magnetically inhomogeneous states. This work gives the key evidence that opens a new route to synthesize strain-induced exchanged-biased FM–AFM bilayers in single thin films, which could serve as building blocks of future spintronic devices.


NANO

Figure caption. Magnetic flux lines of weakly strained LCMO films grown on LSAT (left) and tensile-strained LCMO film on STO (right). The strained LCMO on STO shows a non-ferromagnetic layer near the film surface segregated from the ferromagnetic layer near the substrate. The cartoons illustrate the type of lattice distortion induced and the predicted magnetic coupling in each case.

Reference:

L. Marín, L. A. Rodríguez, C. Magén, E. Snoeck, R. Arras, I. Lucas, L. Morellón, P. A. Algarabel, J. M. de Teresa, M. R. Ibarra. Nano Letters 2015, 15, 492–497.

Highlights

Title: "In-situ Growing of Carbon Nanotubes Encapsulated within Boron Nitride Nanotubes via Electron Irradiation"

Text: In the last 15 years several studies have demonstrated the capability of electron-irradiation for modifying the behavior of carbon-based and related nanomaterials under extreme conditions and radiation. Here we report the synthesis and growth of crystalline carbon nanotubes (NTs) inside a larger diameter boron nitride (BN) NT via in-situ electron irradiation in a TEM. The resulting CNT remains stable and encapsulated within the outer BN tube which provides a protective shell against environment perturbations, suggesting an alternative method for the fabrication of BNC-based electronic devices.

Electron beam irradiation and HRTEM studies were performed using an imaging-side aberration-corrected FEI Titan-Cube microscope working at 80 kV. Complementary spatially-resolved EELS-STEM measurements were also carried out using a FEI Titan Low-Base microscope, which is equipped with a Cs probe corrector. Single-walled (SW) BNNT were produced by laser vaporization technique and some of them can be partially filled by amorphous carbon. Furthermore, density functional theory (DFT) simulations were conducted for determining the structural stability and electronic properties of the hybrid system.

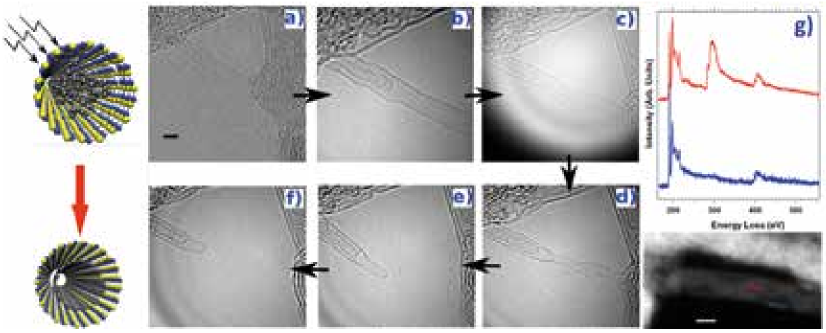

Figure caption: On the left sketch showing the in situ transformation/growing of an hybrid DW-BN@C NT. (a)-(f) Six-frame HRTEM image sequence displaying the formation process of a crystalline CNT from amorphous C encapsulated in a BNNT under electron beam irradiation (high doses for short periods of time, see Fig. 1 (c)) in a TEM. (g) EEL spectra recorded in 2 different areas (marked in the HAADF-STEM image showed below), displaying B-K, C-K and N-K edges. Scale bars in Fig. 1 (a) and (g) are 2 nm.

Reference:

R. Arenal and A. Lopez-Bezanilla, ACS Nano 8, 8419-8425 (2014).

Highlights

3D magnetic induction maps of ferromagnetic nanowires revealed by electron holographic tomography

The investigation of three-dimensional (3D) ferromagnetic nanoscale materials carries great potential to impact areas such as magnetic data storage, sensing, and biomagnetism. The properties of Such nanoscale ferromagnets present complex 3D magnetic configurations which are closely connected with their morphology. Thus the correlation between these factors require the reconstruction of both the shape and magnetic induction fields produced by the nanostructure in 3D. Only recently substantial efforts have been made to obtain quantitative 3D maps providing both the internal magnetic and electric configuration of the same specimen with high spatial resolution. In this work, we demonstrate the quantitative 3D reconstruction of the dominant axial component of the magnetic induction and electrostatic potential within a cobalt focused electron beam induced deposition (FEBID) nanowire of 100 nm in diameter with spatial resolution below 10 nm by applying electron holographic tomography. The tomogram was obtained using a dedicated TEM sample holder for acquisition, in combination with advanced alignment and tomographic reconstruction routines. The powerful approach presented here is widely applicable to a broad range of 3D magnetic nanostructures and may trigger the progress of novel spintronic nonplanar nanodevices.

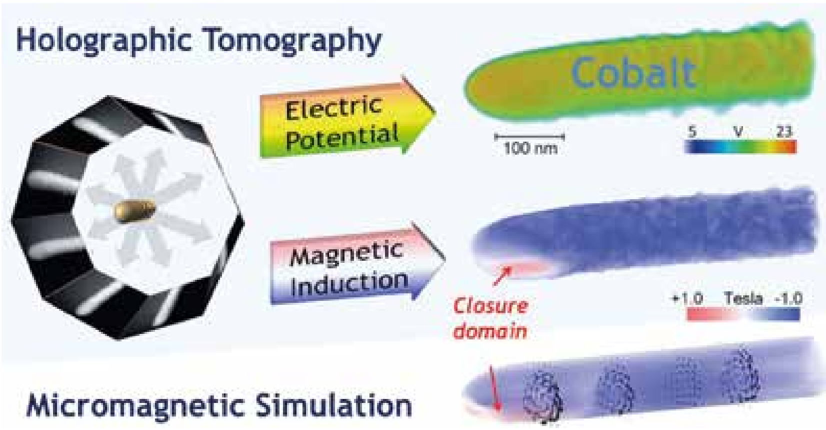

Figure caption. Sketch of the holographic tomographic reconstruction of the Co-FEBID three-dimensional nanowire. 1) 360º tilt phase series are obtained and prealigned. 2) Pairs of 180º rotated phase images are added and subtracted to obtain the electrostatic and magnetic phase images. 3) Electrostatic phase images are accurate aligned and 3D reconstructed. 4) Alignment parameters of the electrostatic phase alignment are applied to the magnetic phase images to obtain 3D reconstruction of the magnetic induction. Phase gradients of the latter provides the magnetic induction vector along the tilt axis, showing a closure domain at the tip.

Reference:

D. Wolf, L. A. Rodriguez, A. Bećhé, E. Javon, L. Serrano, C. Magen, C. Gatel, A. Lubk, H. Lichte, S. Bals, G. Van Tendeloo, A. Fernańdez-Pacheco, J. M. De Teresa and E. Snoeck.

Chemistry of Materials 2015, 27, 6771–6778.

Highlights

A novel Co@Au structure formed in bimetallic core@shell nanoparticles

Core@shell nanparticles composed of a nucleus of Co and a shell of Au of around 8 nm have been successfully synthesized by inert gas condensation technique, reveling that most of the nanoparticles adopted icosahedral shapes in agreement with the theoretical prediction. A new structure is reported for the very first time where the core is a Co icosahedron which is coated by a fcc Au structure linked by several twin planes and intergrowths formed in order to release the strain that these nanoparticles present. Due to the bimetallic nature, they can carry out two functions at a time. Thus this type of material is of great interest in multiple applications in catalytic reactions or Nanomedicine. For the current case, the nanoparticles exhibit magnetic and optical properties.

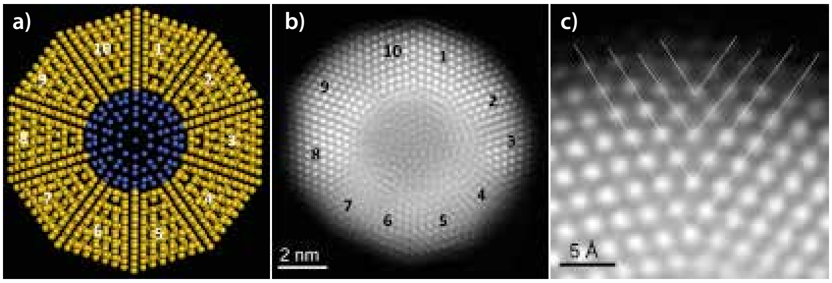

Figure caption. (a) Schematic model of a sliced icosahedral core fully occupied by Co atoms (blue) and a shell formed by 10 fcc projected domains formed by Au atoms (yellow). (b) Aberration-corrected STEM-HAADF image of the corresponding Co@Au nanoparticle. In both figures the 10 Au fcc domains are numbered. (c) Triangular junction unit that links two fcc domains.

Reference:

A. Mayoral, D. Llamosa and Y. Huttel. Chem. Commun. 2015, 51, 8442.

Highlights

Plasmonic response studies following the morphological transformation of hollow gold nanoparticles to nanorings"

Text: In recent years, noble metal nanostructures have been extensively studied owing to their fascinating properties, in particular the optical ones. In this sense, it is well known that the morphology, the size, and the local dielectric environment of these metallic nanostructures have strong impact on their optical properties. These properties are being elucidated, at the local scale (nanometer level), using monochromated electron energy loss spectroscopy (EELS) conducted in the low-loss (0-30 ev) region of the EEL Spectrum. Here, the use of a monochromator in a TEM has opened new avenues to study the optical, dielectric and electronic properties of materials all at unprecedented spatial information. In addition, in order to interpret the plasmonic EELS experimental results, we have carried out discrete dipole approximation (DDA) simulations.

In the present work, we have locally investigated by EELS the plasmonic response of hollow gold nanostructures, which have suffered a controlled top-down morphological modification (from spheres to nanorings (NR) with various aspect ratio).Thus, we have demonstrated that a fine tuning of the optical response is possible. In particular, we have followed the shift of the dipolar mode of the gold nanorings as a function of their aspect ratio.

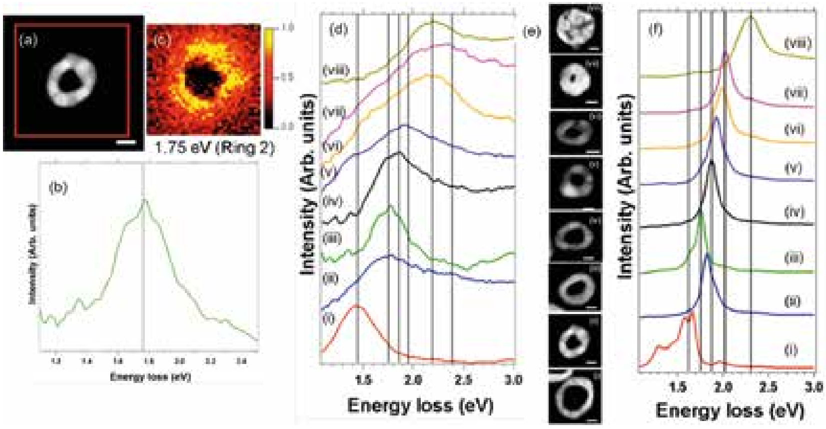

Figure caption: (a) HAADF-STEM image of an Au nanoring, where an EELS SPIMs has been recorded in the red marked area. (b) EEL spectrum, after background subtraction, corresponding to the sum of 12 spectra collected from the green marked area of (c). (c) Intensity maps showing the spatial distribution of the SPR mode (1.75 eV.) for this Au NR. (d) EEL spectra recorded on different NR of different aspect ratios (σ), noted as (i) to (vii). (e) HAADF images of these nanostructures. (f) EELS DDA simulations for the corresponding (same sizes) nanoparticles. Scale bar is 10 nm for all these micrographs.

Reference:

M. Prieto, R. Arenal, L. Henrard, L. Gomez, V. Sebastian, M. Arruebo, J. Phys. Chem. C 118, 28804–28811 (2014).

Highlights

Atomic Observations of Microporous Materials Highly Unstable under the Electron Beam: The Cases of Ti-Doped $AlPO_4$-5 and Zn-MOF-74

In this work the analysis of nanoporous networks was taken into a further level in terms of resolution and beam sensitivity. Both materials studied here, an aluminophosphate TAPO-5 and a metal organic framework Zn-MOF-74, are highly attractive materials for catalytical applications due to their composition and particular structural features. The high resolution data acquired for TAPO-5 allows a clear observation of the aluminophosphate framework, making able of locate all "T" atoms forming the structure. In the case of the metal organic framework Zn-MOF-74 proves that under certain conditions electron microscopy can provide invaluable information of an increasing variety of molecular sieves.

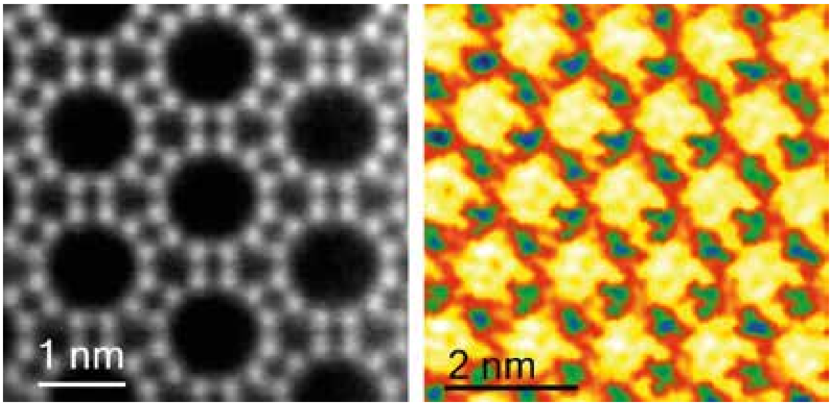

Figure caption: Aberration corrected STEM images of microporous materials: (a) HAADF image of the aluminophosphate TAPO-5 doped with Ti, and (b) artificially colored ultrahigh resolution image of Zn-MOF-74 material (Zn in green blue).

Reference:

Manuscript published in the special issue "Microscopy and Spectroscopy for Catalysis". A. Mayoral, M. Sanchez-Sanchez, A. Alfayate, J. Perez-Pariente, I. Diaz. Chem. Cat. Chem. 2015, 7, 3719-3724.

Highlights

Enhancement of long range correlations in a 2D vortex lattice by incommensurate 1D disorder potential

We create a 2D vortex lattice at 0.1 K in a superconducting thin film with a well-defined 1D thickness modulation—the symmetry-breaking disorder—and track the field-induced modification using scanning tunnelling microscopy. We find that the 1D modulation becomes incommensurate with the vortex lattice and drives an order–disorder transition, behaving as a scale-invariant disorder potential. We show that the transition occurs in two steps and is mediated by the proliferation of topological defects. The resulting critical exponents determining the loss of positional and orientational order are far above theoretical expectations for scale-invariant disorder and follow instead the critical behaviour describing dislocation unbinding melting. Our data show that randomness disorders a 2D crystal, with enhanced long-range correlations due to the presence of a 1D modulation.

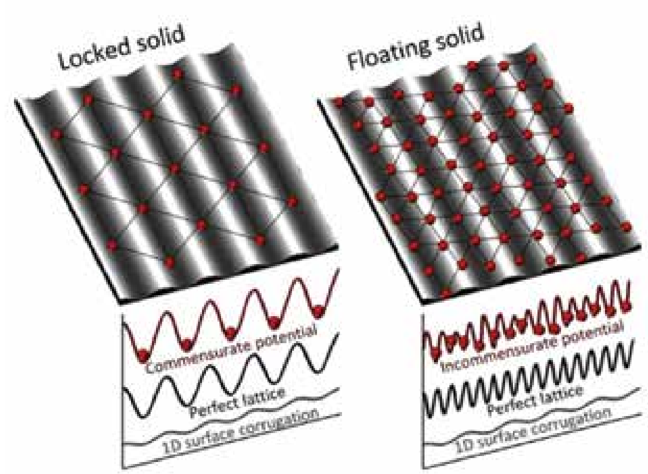

Figure caption: Vortices in a hexagonal lattice are shown as red points. A linear modulation acts on the vortex positions. When the vortex density is low, vortices are confined to the minima of the linear modulation, and the interaction among them is essentially confined to the lines along the potential minima, as schematically in the left panel. However, when the vortex density increases, one can accommodate many vortices within one modulation's wavelength. In the right panel we schematically show this situation (for clarity, we only draw a small amount of vortices). In that case, the lattice and 1D potential modulation have incommensurate spatial periods and the orientation of the lattice no longer follows the linear modulation. The resulting vortex landscape is quasi-random. The vortex positions are slightly displaced with respect to the ordered lattice. In this work, we show that the displacement grows logarithmically with distance, a feature which demonstrates that the disorder created by this situation is scale-invariant.

Reference:

I.Guillamón, R. Córdoba, J. Sesé,J. M. De Teresa, M. R. Ibarra, S. Vieira, H. Suderow, Nature Physics 10, 851-856 (2014)

Highlights

Enhanced Magnetotransport in Nanopatterned Manganite Nanowires

We have combined optical and focused ion beam (FIB) lithographies to produce large aspect-ratio (length-to-width >300) single-crystal nanowires of $La_{2/3}Ca_{1/3}MnO_3$ that preserve their functional properties. It is the first time that FIB is able to pattern such narrow single-crystal oxide nanowires without producing significant damage to the sample. Remarkably, an enhanced magnetoresistance value of 34% in an applied magnetic field of 0.1 T in the narrowest 150 nm nanowire is obtained. The strain release at the edges together with a destabilization of the insulating regions is proposed to account for this behavior. This opens new strategies to implement these structures in functional spintronic devices.

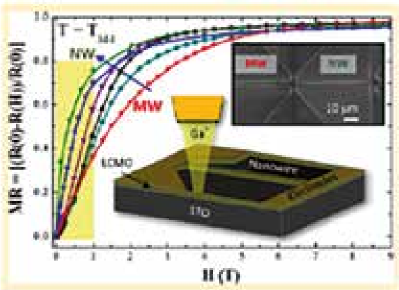

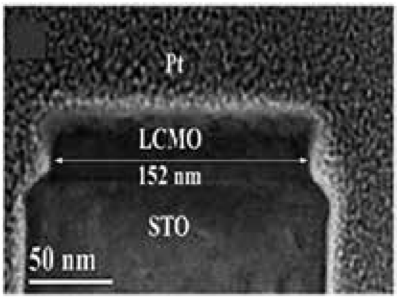

Figure caption: The left image shows a sketch of the lithography process used to pattern the manganite nanowires, implying optical lithography and focused ion beam, as well as the magnetoresistance measurements, highlighting the enhancement of the low-field magnetoresistance as the nanowire lateral size decreases. The right image shows the TEM- experiments carried out on the narrowest nanowire using the image-corrected Titan microscope.

Reference:

Marín, L.A. Morellón, P. Algarabel, L.A. Rodríguez, C. Magén, J. M. De Teresa, M.R. Ibarra, Nano Letters 14, 423 (2014)

Highlights

Focused Electron and Ion Beam Induced Deposition on Flexible and Transparent Polycarbonate Substrates

The successful application of focused electron (and ion) beam induced deposition techniques for the growth of nanowires on flexible and transparent polycarbonate films is reported. After minimization of charging effects in the substrate, sub-100 nm-wide Pt, W, and Co nanowires have been grown and their electrical conduction is similar compared to the use of standard Si-based substrates. Experiments where the substrate is bent in a controlled way indicate that the electrical conduction is stable up to high bending angles, 50 degrees, for low-resistivity Pt nanowires grown by the ion beam. On the other hand, the resistance of Pt nanowires grown by the electron beam changes significantly and reversibly with the bending angle. Aided by the substrate transparency, a diffraction grating in transmission mode has been built based on the growth of an array of Pt nanowires that shows sharp diffraction spots. The set of results supports the large potential of focused beam deposition as a high-resolution nanolithography technique on transparent and flexible substrates. The most promising applications are expected in flexible nano-optics and nanoplasmonics, flexible electronics, and nanosensing.

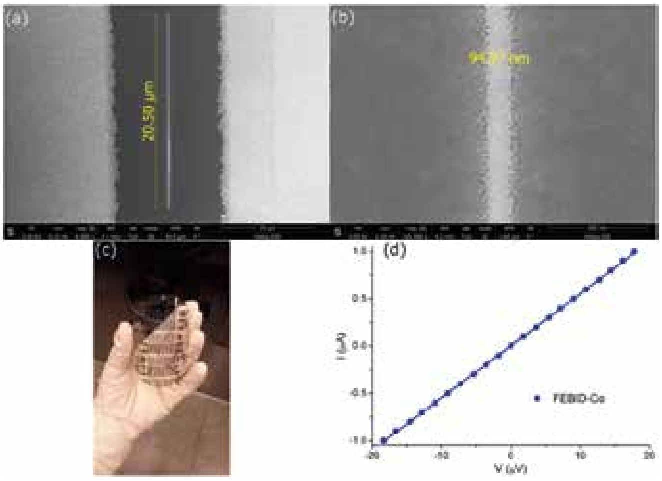

Figure caption: (a) Cobalt nanowire grown by FEBID with length of 20 mm grown on a Polycarbonate flexible substrate and transparent; (b) zoom-in of the nanowire, where the width is 100 nm; (c) overall image of the substrate where the flexibility and transparency are revealed; (d) electrical measurements on the nanowires where the good electrical conductivity is verified.

Reference:

P. Peinado, S. Sangiao, J. M. De Teresa, ACS Nano 9, 6139-6146 (2015)

Highlights

Arrays of Densely Packed Isolated Nanowires by Focused Beam induced Deposition Plus Ar^+ Milling

One of the main features of any lithography technique is its resolution, generally maximized for a single isolated object. However, in most cases, functional devices call for highly dense arrays of nanostructures, the fabrication of which is generally challenging. Here, we show the growth of arrays of densely packed isolated nanowires based on the use of focused beam induced deposition plus Ar^+ milling. The growth strategy presented herein allows the creation of films showing thickness modulation with periodicity determined by the beam scan pitch. The subsequent Ar^+ milling translates such modulation into an array of isolated nanowires. This approach has been applied to grow arrays of W-based nanowires by focused ion beam induced deposition and Co nanowires by focused electron beam induced deposition, achieving linear densities up to 2.5×10^7 nanowires/cm (one nanowire every 40 nm). These results open the route for specific applications in nanomagnetism, nanosuperconductivity, and nanophotonics, where arrays of densely packed isolated nanowires grown by focused beam deposition are required.

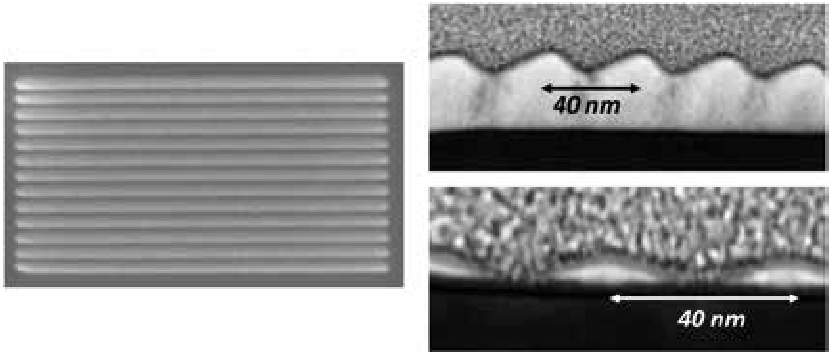

Figure caption: The image on the left shows the top-view vision of the growth of densely-packed cobalt nanowires with periodicity of 40 nm. The images on the right show the cross-section of the same array before and after the Ar^+ milling process.

Reference:

J. M. De Teresa and R. Córdoba, ACS Nano 9, 6139 (2014)

Highlights

Supramolecular Architectures from Bent-Core Dendritic Molecules

Control of the self-assembly of small molecules to generate architectures with diverse shapes and dimensions is a challenging research field. We report unprecedented results on the ability of ionic, bent dendritic molecules to aggregate in water. A range of analytical techniques (TEM, SEM, SAED, and XRD) provide evidence of the formation of rods, spheres, fibers, helical ribbons, or tubules from achiral molecules. The compact packing of the bent-core structures, which promotes the bent-core mesophases, also occurs in the presence of a poor solvent to provide products ranging from single objects to supramolecular gels. The subtle balance of molecule/solvent interactions and appropriate molecular designs also allows the transfer of molecular conformational chirality to morphological chirality in the overall superstructure. Functional motifs and controlled morphologies can be combined, thereby opening up new prospects for the generation of nanostructured materials through a bottom-up strategy.

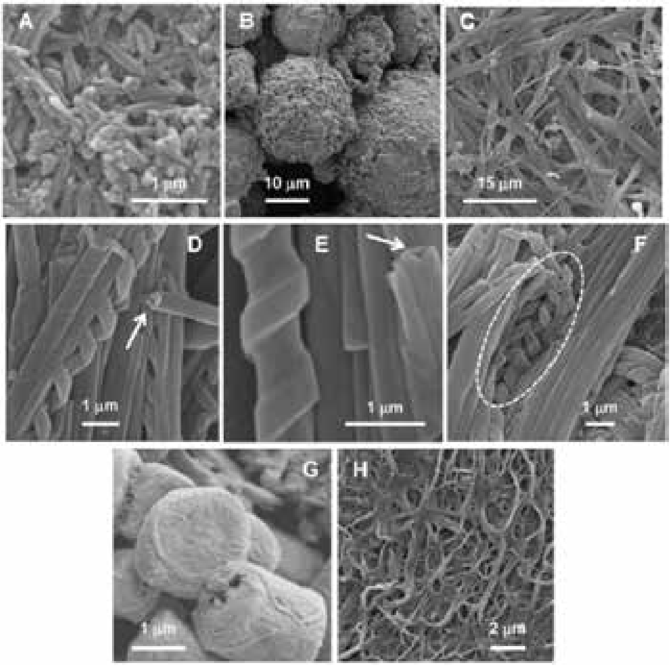

Figure caption: Scanning electron microscopy (SEM) images of dialyzed aqueous solutions of PPI1-B1-10-14 (A), PPI1-B1-10-8 (B), PPI1-B1-4-8 (C–F), PPI1-B1-4-8 (G), and PPI1-C1-4-8 (H).*

Reference:

Miguel Cano, Antoni Sánchez-Ferrer, José Luis Serrano, Nélida Gimeno and M. Blanca Ros. Angew. Chem. Int. Ed. 2014, 53, 13449 –13453

Highlights

The effect of surface charge of functionalized Fe_3O_4 nanoparticles on protein adsorption and cell uptake

Nanoparticles engineered for biomedical applications are meant to be in contact with protein-rich physiological fluids. These proteins are usually adsorbed onto the nanoparticle's surface, forming a swaddling layer that has been described as a 'protein corona', the nature of which is expected to influence not only the physicochemical properties of the particles but also the internalization into a given cell type. We have investigated the process of protein adsorption onto different magnetic nanoparticles (MNPs) when immersed in cell culture medium, and how these changes affect the cellular uptake. The role of the MNPs surface charge has been assessed by synthesizing two colloids with the same hydrodynamic size and opposite surface charge: magnetite (Fe_3O_4) cores of 25-30 nm were in situ functionalized with (a) positive polyethyleneimine (PEI-MNPs) and (b) negative poly(acrylic acid) (PAA-MNPs). After few minutes of incubation in cell culture medium the wrapping of the MNPs by protein adsorption resulted in a 5-fold increase of the hydrodynamic size. After 24 h of incubation large MNP-protein aggregates with hydrodynamic sizes of ≈ 1500 nm (PAA-MNPs) and ≈ 3000 nm (PEI-MNPs) were observed, each one containing an estimated number of magnetic cores between 450 and 1000. These results are consistent with the formation of large protein-MNPs aggregate units having a 'plum pudding' structure of MNPs embedded into a protein network that results in a negative surface charge, irrespective of the MNP-core charge. Quantitative analysis showed that SHSY5Y cells can incorporate 100% of the added PEI-MNPs up to ≈ 100 pg/cell, whereas for PAA-MNPs the uptake was less than 50%. The final cellular distribution showed also notable differences regarding partial attachment to the cell membrane. These results highlight the need to characterize the final properties of MNPs after protein adsorption in biological media, and demonstrate the impact of these properties on the internalization mechanisms in neural cells.

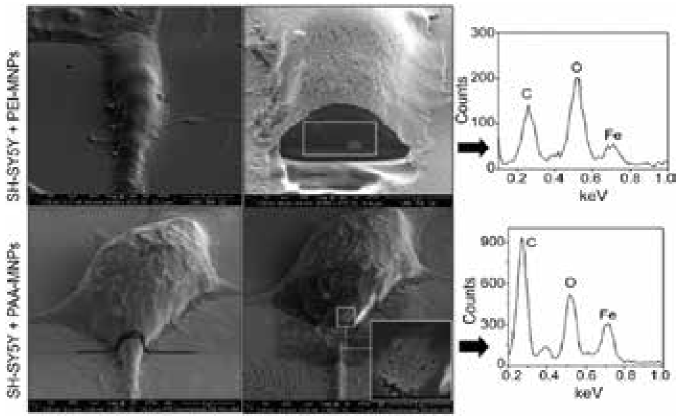

Figure caption: FIB-SEM dual beam analysis of SH-SY5Y cells incubated with 10 µg/ml PEI-MNPs and PAA-MNPs for 24 h

Reference:

M.P: Calatayud et al. Biomaterials, 35 (24): 6389-99, 2014

Highlights

Development of Noncytotoxic Chitosan–Gold Nanocomposites as Efficient Antibacterial Materials

Text: This work describes the synthesis and characterization of non-cytotoxic nanocomposites either colloidal or as films exhibiting high antibacterial activity. The biocompatible and biodegradable polymer chitosan (CS) was used as reducing and stabilizing agent for the synthesis of gold nanoparticles (AuNPs) embedded in it. Herein, for the first time three different chitosan grades varying in the average molecular weight and deacetylation degree (DD) were used with an optimized gold precursor concentration. Several factors were analyzed in order to obtain antimicrobial but not cytotoxic nanocomposite materials. Films based on chitosan with medium molecular weight (Mw) and the highest DD exhibited the highest antibacterial activity against biofilm forming strains of *Staphylococcus aureus* and *Pseudomonas aeruginosa*. The resulting nanocomposites did not show any cytotoxicity against mammalian somatic and tumoral cells. They produced a disruptive effect on the bacteria wall while their internalization was hindered on the eukaryotic cells. This selectivity and safety make them potentially applicable as antimicrobial coatings in the biomedical field.

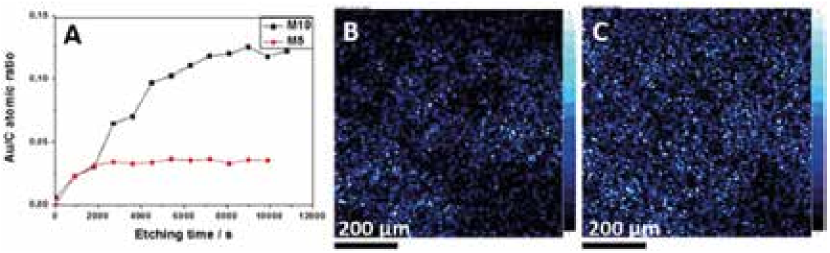

Figure caption: XPS depth profiling results of chitosan-gold films (A). XPS maps of Au nanoparticles distribution. The lighter the blue color, the higher the Au concentration present (B and C).

Reference:

Anna Regiel-Futyra, Małgorzata,Kus-Liśkiewicz, Victor Sebastian, Silvia Irusta, Manuel Arruebo, GrażynaStochel, and Agnieszka Kyzioł, ACS APPLIED MATERIALS & INTERFACES 7 (2015) 1087-1099.

Highlights

Magnetic antidot-to-dot crossover in Co and Py nano-patterned thin films

The crossover from antidot to dot magnetic behavior on arrays patterned in a ferromagnetic thin film has been achieved by modifying only the geometry. A series of antidot arrays has been fabricated on cobalt with fixed diameter d and by reducing the period of the array p from p>>d to p < d. A dramatic change in the coercivity dependence with p, correlated with a significant modification in the magnetic domain structure observed by x-ray photoemission electron microscopy, evidences the crossover. An intermediate regime has been found between the superdomain structure present in antidot arrays and the array of astroid-state noncorrelated dots. The study has been reproduced for a different ferromagnetic material, permalloy, and supported by micromagnetic simulations.

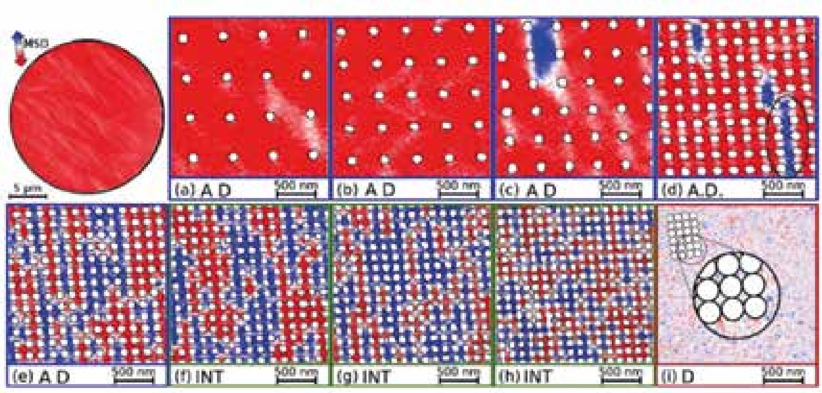

Figure caption: XPEEM images of the unpatterned film, and the arrays of p = (a) 500, (b) 400, (c) 300, (d) 200, (e) 150,(f) 140, (g) 130, (h) 120, and (i) 105 nm. In a zoom the astroid-like shape of the dots formed by the intersection of the antidots can be apreciated. Blue and red colors in the images mean magnetization projection along the MSD pointing up and down, respectively. White color corresponds to magnetization either zero or perpendicular to the MSD. A superdomain is encircled in (d). A blue, green, or red frame surrounding each image indicates whether it belongs to the antidot (AD), intermediate (INT), or dot (D) regime.

Reference:

C. Castán-Guerrero, J. Herrero-Albillos,J. Bartolomé, F. Bartolomé, L. A. Rodríguez, C. Magén, F. Kronast, P. Gawronski, O. Chubykalo-Fesenko, K. J. Merazzo, P. Vavassori,P. Strichovanec, J. Sesé, and L. M. García,PhysicalReview B 89, 144405 (2014)

Highlights

Serrate 2014-2015
Antiferromagnetic Spin Coupling between Rare Earth Adatoms and Iron Islands Probed by Spin-Polarized Tunneling

Understanding the spin polarization mechanisms of single magnetic atoms is a key aspect to realize ultra-high density magnetic storage and advanced spintronic devices. Here, spin-polarized scanning tunneling microscopy and first-principles calculations show that the 5d electrons spin induced moments of thulium and lutetium adatoms deposited on monolayer iron islands couple antiferromagnetically with the 3d electrons magnetic moment of iron. These results reveal the non-contribution of 4f electrons to the spin-polarized tunneling processes in rare earths.

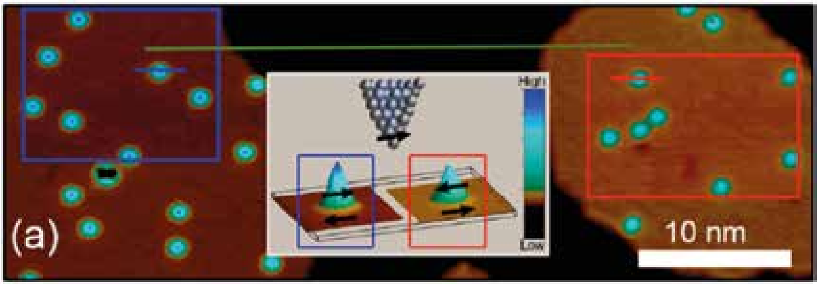

Figure caption: (JT-STM)(a) Constant height map of spin dependent magnetoconductance of Tm atoms on Fe monolayer islands on W(110). The image is obtained by dI/dV mapping of the sample with a Fe-coated W tip in tunnelling regime, at a base temperature of 1.15 K. The colour scale represents the conductance over each part of the surface, which in Spin-Polarized STM is contributed by the bare density of states and the magnetic term dependent on the relative magnetization orientations of tip and sample. The two structurally identical Fe islands exhibit opposite magnetization direction. According to the spin dependent conductance, the magnetic moment of the Tm atoms (as well as Nb and Lu, not shown) is antiparallel to that of the island, indicating the AFM coupling between 4f atomic states and ferromagnetic substrates. The inset highlights the correspondence between conductance to tip-Tm-Fe magnetic moments.

Reference:

Coffey, D.; Diez-Ferrer, J.L.; Serrate, D; Ciria, M.; de la Fuente, C.; Arnaudas, J.I., Scientific Reports 2015, 5, 13709; doi: 10.1038/srep13709 (2015)

Highlights

Enhanced Hydrogen Dissociation by Individual Co Atoms Supportedon Ag(111)

By means of scanning tunneling microscopy, individual Co atoms adsorbed on Ag(111) are found to behave as a model catalyst for the hydrogen oxidation reaction. The dosing of H2 in a cryogenic environment produces the otherwise unstable CoH3 molecule, which results in the complete suppression of the Kondo resonance of the host Co atom. Short voltage pulses over Co hydrides permit reversible dehydrogenation and so, the identification of the intermediate compounds. The electric polarizability of CoH3 allows controlling molecular diffusion via an external electric field, from the range of tens of nm down to the assembly of larger hydride complexes at the molecular scale.

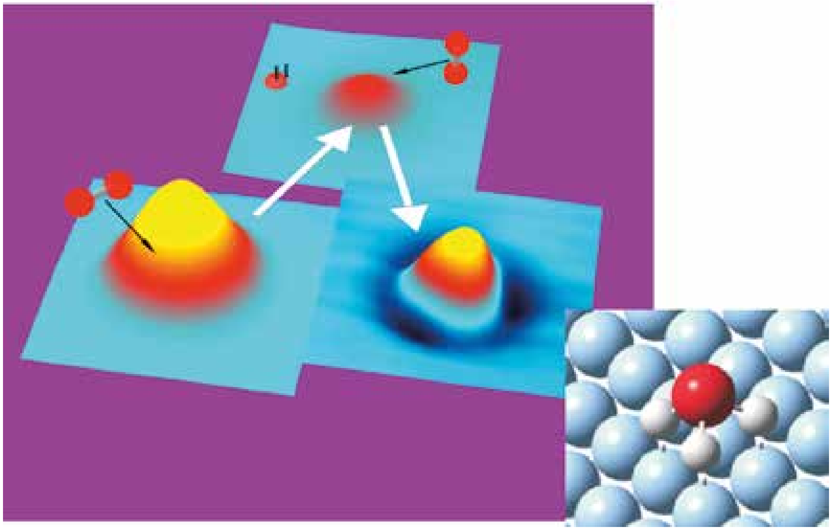

Figure caption: (JT-STM) STM topography (3D rendering) of two intermediate steps of the reaction Co+H_2àCoH_3 supported by Ag(111) surface. The Co adatom (left) dissociates the H_2 molecule dosed in an environment of Ultra-High-Vacuum. The yield of Co atoms toward H2 dissociation is at least 1 order of magnitude better than previously reported Co surfaces, and could be a feasible alternative to the costly Pt-based catalyzers. The intermediate product CoH (middle) is able to dissociate another H_2 molecule to form the final product CoH_3 (right).

Reference:

Serrate, D.; Moro-Lagares, M.; Piantek, P.; Pascual, J.I.; Ibarra, M.R., J. Phys. Chem. C 2014, 118, 5827, doi: 10.1021/jp411860b

Highlights

Dynamic Interplay between Catalytic and Lectin Domains of Galnac-Transferases Modulates Protein O- Glycosylation

Protein O-glycosylation is controlled by polypeptide GalNAc-transferases (GalNAc-Ts) that uniquely feature both a catalytic and lectin domain. The underlying molecular basis of how the lectin domains of GalNAc-Ts contribute to glycopeptide specificity and catalysis remains unclear. Here we present the first crystal structures of complexes of GalNAc-T2 with glycopeptides that together with enhanced sampling molecular dynamics simulations demonstrate a cooperative mechanism by which the lectin domain enables free acceptor sites binding of glycopeptides into the catalytic domain. Atomic force microscopy and small-angle X-ray scattering experiments further reveal a dynamic conformational landscape of GalNAc-T2 and a prominent role of compact structures that are both required for efficient catalysis. Our model indicates that the activity profile of GalNAc-T2 is dictated by conformational heterogeneity and relies on a flexible linker located between the catalytic and the lectin domains.

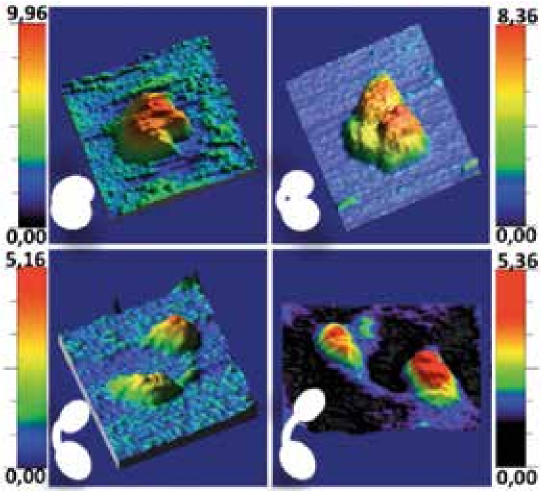

Figure caption: (Veeco Multimode 8) Three-dimensional topography AFM images of single molecules of GalNAc-T2 in different conformations. (a) (Top-left panel) A very compact structure image of the apo form showing an overlap of a domain on the other. The average height of these features is around 9 nm. Compact image of the enzyme bound to UDP-GalNAc/Mn+2 and extended structures images of the enzyme bound to UDP/Mn+2 and the EA2 peptide are shown in the top-right and bottom panel, respectively. Small white figures representing different conformations of GalNAc-T2 are shown for clarification purposes.

Reference:

E. Lira-Navarrete, M. de las Rivas, I. Compañón, M.C. Pallarés, Y. Kong, J. Iglesias-Fernández, J.M. Peregrina, C. Rovira, P. Bernadó, P. Bruscolini, H. Clausen, A. Lostao, F. Corzana, and R. Hurtado-Guerrero. Nature Communications 2015, 6, 6937, doi: 10.1038/ncomms7937

Highlights

Tunnel Conduction in Epitaxial Bilayers of Ferromagnetic LaCoO3/La2/3Sr1/3MnO3 Deposited by a Chemical Solution Method

We report magnetic and electronic transport measurements across epitaxial bilayers of ferromagnetic insulator LaCoO3 and half-metallic ferromagnet La2/3Sr1/3MnO3 (LCO/LSMO: 3.5 nm/20 nm) fabricated by a chemical solution method. The I–V curves at room temperature and 4K measured with conducting atomic force microscopy (CAFM) on well-defined patterned areas exhibit the typical features of a tunnelling process. Our results demonstrate that this chemical method is able to produce epitaxial heterostructures with the quality required for this type of fundamental studies and applications.

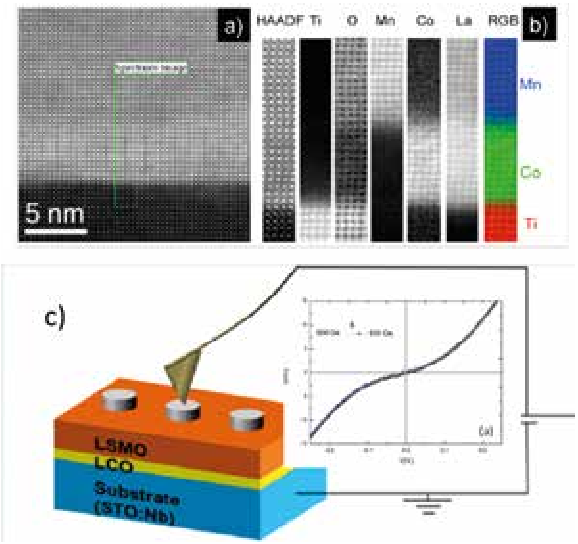

Figure caption: (Attocube, Titan^3, Dual Beam). This work is an archetypal example of transversal application of the three LMA areas. Spectrum imaging of the LCO/LSMO bilayer grown on STO. (a) HAADF reference image. (b) Integrated intensity maps of the simultaneously acquired HAADF, Ti $L_{2,3}$, OK, Mn $L_{2,3}$, Co $L_{2,3}$ and La $M_{4,5}$ signals. c) Sketch of the conducting AFM set up to measure the device I-V characteristic at 4 K (inset) of a nanopatterned sample fabricated by FIB shadow mask technology.

Reference:

Lucas I.; Vila-Fungueiriño, J.M.; Jiménez-Cavero, P.; Rivas-Murias, B.; Magén, C.; Morellón, L.; Rivadulla, F., ACS Applied Materials & Interfaces 2014, 6, 21279, DOI: 10.1021/am506259p

Highlights

Mechanostability of the Single-Electron-Transfer Complexes of Anabaena Ferredoxin–NADP+ Reductase

The complexes formed between the flavoenzyme ferredoxin–NADP+ reductase (FNR; NADP+ =nicotinamide adenine dinucleotide phosphate) and its redox protein partners, ferredoxin (Fd) and flavodoxin (Fld), have been analysed by using dynamic force spectroscopy through AFM. A strategy is developed to immobilise proteins on a substrate and AFM tip to optimise the recognition ability. The differences in the recognition efficiency regarding a random attachment procedure, together with nanomechanical results, show two binding models for these systems. The interaction of the reductase with the natural electron donor, Fd, is threefold stronger and its lifetime is longer and more specific than that with the substitute under iron-deficient conditions, Fld. The higher bond probability and two possible dissociation pathways in Fld binding to FNR are probably due to the nature of this complex, which is closer to a dynamic ensemble model. This is in contrast with the onestep dissociation kinetics that has been observed and a specific interaction described for the FNR:Fd complex.

Figure caption: (Nanotec Cervantes). Journal front cover: FNR is a paradigmatic enzyme, exchanging electrons with two different proteins that bind to the same site. Through AFM using oriented molecules, distinct binding models for the original protein and its replacement are proposed

Reference:

Marcuello, C ; de Miguel, R ; Martinez-Julvez, M; Gomez-Moreno, C ; Lostao, A, CHEMPHYSCHEM 2015, 16, 3161, DOI: 10.1002/cphc.201500534

Other relevant results

Imaging PbI2 Single-Layered Inorganic Nanotubes Encapsulated Within Carbon Nanotubes

When a single layer of material is seamlessly wrapped into a cylinder, the resulting nanotube combines the characteristics of both two-dimensional (2D) and one-dimensional (1D) materials. Yet, despite their interest, reports on single-layered nanotubes are limited because multiwalled species are in general favoured during growth. Here we report the formation of high-quality, single-crystalline single-layered inorganic PbI_2 nanotubes synthesized by a solvent-free high temperature route using the inner cavities of carbon nanotubes as a hosting template.

Aberration corrected HRTEM assisted by image simulations and STEM-EDX chemical analysis has revealed that PbI_2 single-layered nanotubes, ranging from 3.5 to 8 nm in diameter, were prepared by this methodology. This analyses show that above the 4 nm threshold the PbI2 nanotube diameter is only determined by the template diameter, enabling the possibility of tailoring nanotube's dimensions. In situ HRTEM imaging has also demonstrated that electron irradiation is able to transform remnant pieces of PbI_2 nanorods grown on the templates into single-layered PbI_2 nanotubes.

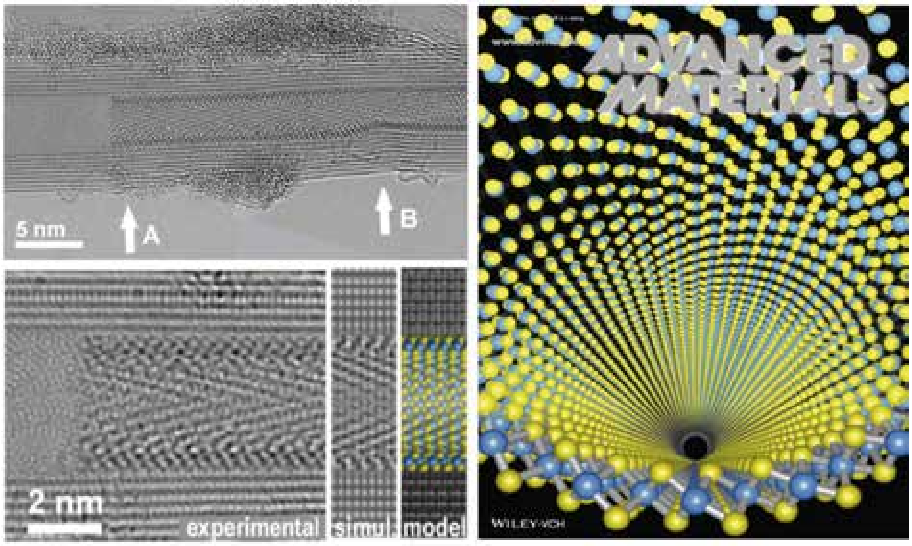

Figure caption. Top left, aberration corrected HRTE image of a PbI_2 nanotube encapsulated in a multiwalled carbon nanotube template. Bottom left, HRTEM close up of the structure, together with an HRTEM image simulation and the atomic model proposed. Right, back cover of Advanced Materials Journal, Issue of 2 April 2014 (Vol. 26, No. 13).

Reference:

L. Cabana, B. Ballesteros, E. Batista, C. Magén, R. Arenal, J. Oró-Solé, R. Rurali, G. Tobias, Advanced Materials 2014, 26, 2016-2021.
Featured Article of the Back Cover of the Advanced Materials Journal, Issue of 2 April 2014 (Vol. 26, No. 13).

Atomic Scale Strain Relaxation in Axial Semiconductor III–V Nanowire Heterostructures

Combination of mismatched materials in semiconductor nanowire heterostructures offers a freedom of band structure engineering that is impossible in standard planar epitaxy. Nevertheless, the presence of strain and structural defects directly influence the optoelectronic properties of these nanomaterials and their potential applications in photonic technologies.

In this work, aberration corrected HAADF-STEM imaging is exploited to investigate with atomic accuracy how mismatched heterostructures release or accommodate strain, therefore, is highly desirable. Geometrical phase analysis (GPA) of the atomically resolved images of InAs/InSb and GaAs/GaSb nanowire heterostructures combined with computer simulations have enabled to establish the relaxation mechanisms (including both elastic and plastic deformations) triggered to release the mismatch strain in these systems. Formation of misfit dislocations, diffusion of atomic species, polarity transfer, and induced structural transformations are studied with atomic resolution at the intermediate ternary interfaces.

Figure caption. (a) Low magnification HAADF image of one analyzed GaAs/GaSb NW. (b–d) Atomic resolution images of the three different crystallographic phases contained in the NW. (e,f) Dilatation/rotation maps calculated by means of GPA on the (−11−1) plane. (g) 3D model of the GaAs/GaSb NW system, with core–shell like interface.

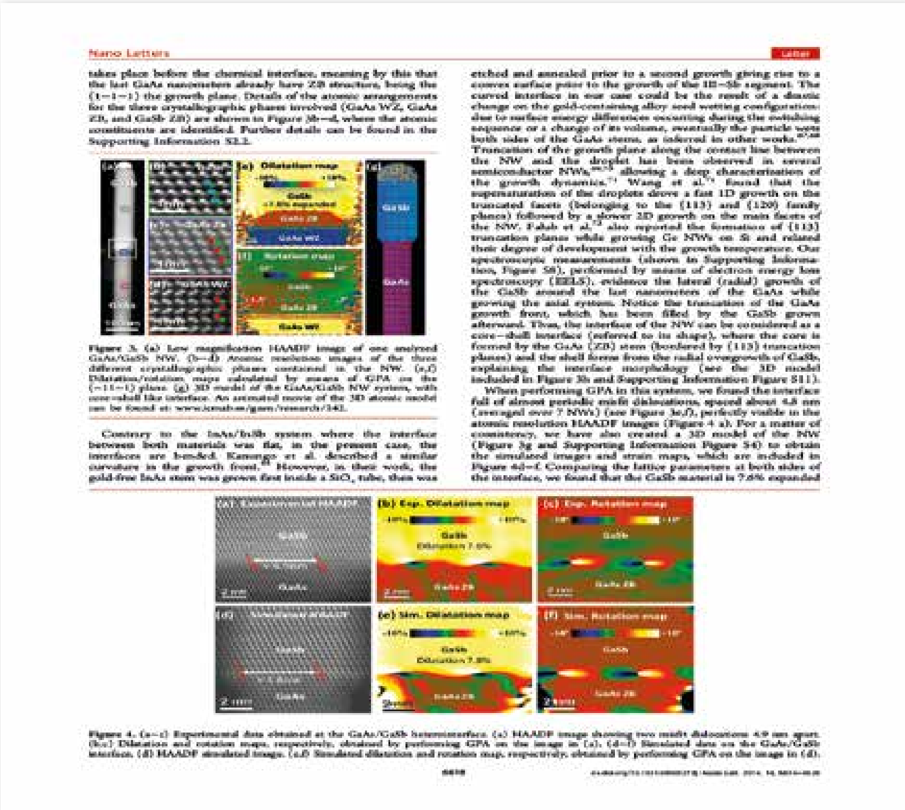

Reference:

M. de la Mata, C. Magén, P. Caroff, J. Arbiol, Nano Letters 2014, 14, 6614–6620.

Dynamic HAADF STEM observation of single atom chain as transient state of Au ultrathin nanowire breakdown

We report a dynamic study of the degradation of ultrathin gold nanowires under electron beam irradiation. High-angle annular dark field (HAADF)-scanning transmission electron microscopy (STEM) imaging performed with an aberration corrected microscope enabled to evidence the formation of atomic chains prior to breaking and free clusters aside.

Ultrathin Au nanowires have recently attracted intense researches due to their high potentiality for multiple applications, such as SERS probes or building block for nanoelectronic. However, these objects are highly fragile and tend to break under external stimuli. The exact process of this atomic reconstruction is of key importance for the future application. Thanks to our HAADF study, expulsion of Au atoms and the formation of reactive clusters is for the first time evidenced. Such clusters are known to have enhanced catalytic properties for CO oxidation.

Moreover, the sub atomic resolution enabled us to follow the formation of atomic chains with either 3-4 atoms or a single atom thickness. Such result was unexpected since ultrathin Au nanowires are single crystalline objects. This duplicity will lead to two different quantized conductance behaviors. Such results open great perspective for massive production of breaking junction at low cost.

Figure caption: Snapshots extracted from a video of e-beam induced wire breaking which proceeds through the decrease of the channel diameter from a) 3 atoms to b) single atom. c) Resulting 7 nm rods surrounded by Au atoms and dimers. As insets, schematic 3D views of a) multi-atom chain and, b) single-atomic chain, and c) dimer and isolated atoms. Scale bar: 1 nm. White arrows indicate twin planes.

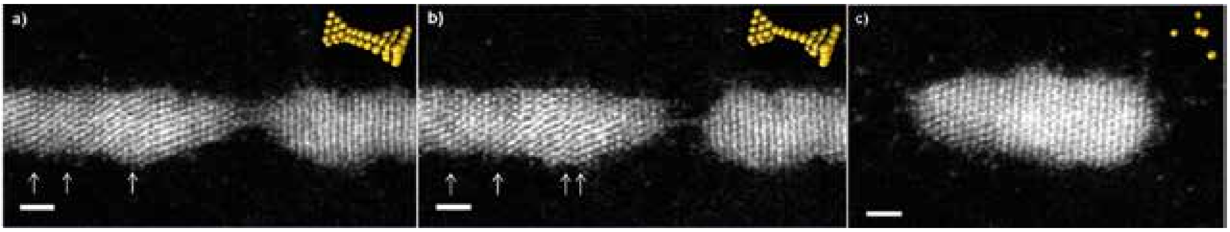

Reference:

L.M. Lacroix, R. Arenal, G. Viau, "Dynamic HAADF STEM observation of single atom chain as transient state of Au ultrathin nanowire breakdown", J. Am. Chem. Soc. 136, 13075–13077 (2014).

Identification of transition metal dichalcogenides phases by HAADF-HRSTEM studies

Inorganic 2D transition metal dichalcogenides (TMDs), with analogous structure to that of graphene, represented by the general formula MX_2 (M = Mo, W, Ti, etc; X = S, Se, Te), are realized in two crystal structures, depending on the metal coordination by six chalcogens, specified as 2H-MX_2 (trigonal prismatic structure) and 1T-MX_2 (octahedral structure). Markedly, the electronic properties for each phase are dissimilar, namely, the 2H-phase is semiconducting and emissive, while the 1T-phase is metallic without photoluminescent properties. Aberration-corrected STEM was employed to investigate the atomic structure of the exfoliated MoS_2 and WS_2 materials. The atomic resolution HAADF-STEM imaging (Fig. b) confirms the 2H-MoS_2 crystalline structure of the particular sheet, which is more evident in the zoomed image (Fig. c).

Figure caption: (a) Low magnification HAADF-STEM image of a MoS_2 flake. (b) HAADF-STEM micrograph showing one of the areas at the edge of the MoS_2 flake examined in Fig. a. Scale bar is 1nm. (c) Zoom of the red-marked area shown in Fig. b. (d) Intensity profile extracted from the white line plotted in Fig. c. (e, f) Low and high magnification HAADF-STEM images of a WS2 flake. (g) HAADF-STEM micrograph showing one of the areas at the edge of the WS_2 flake examined in Fig. f. Scale bar is 1nm. (h, j) Zoom of the red and green marked areas shown in Fig. g. Scale bars are 0.5 nm. (i, k) Intensity profiles extracted from the dotted red lines plotted in Fig. i and k.

In the latter micrograph, the difference in intensity between the spots forming the hexagonal network indicates their different chemical nature, Mo (Z=42) and S (Z=16), respectively. An intensity profile, obtained from the white line marked in this figure, is plotted in Fig. (d). Notably, from the latter intensity profile and micrograph, as well as based in recent works, it is deduced that this area is composed by three layers of MoS_2 possessing semiconducting properties. Atomically-resolved HAADF-STEM analyses were also confirmed the 2H crystalline structure of exfoliated WS_2.

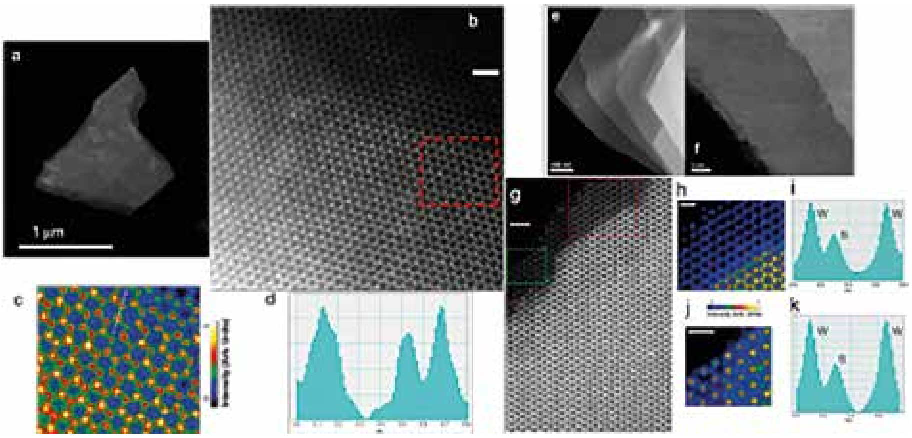

Reference:

G. Pagona, C. Bittencourt, R. Arenal, N. Tagmatarchis, "Exfoliated semiconducting pure 2H-MoS_2 and 2H-WS_2 assisted by chlorosulfonic acid", Chem. Comm. 51, 12950-12953 (2015).

Atomic structural and chemical investigations of misfit layered nanotubes

Misfit layered compounds can be considered as inter-grown materials with a general formula $[(MX)_1+x]m[TX_2]_n$, where M is rare earths, Pb, Sb, etc; T is Ti, V, Cr, Nb, etc. and X is S, Se. They constitute an heterostructure formed by the stacking of TX_2 dichalcogenides layers with MX layers. In order to improve the synthesis conditions, detailed structural and chemical analyses at the nanoscale are highly needed.

In this work, few layers thick nanotubes based on the TbS-CrS_2 system are reported. Their detailed structure and chemical composition are elucidated by different TEM techniques including high-resolution scanning TEM (HR-STEM) and spatially-resolved EELS (SR-EELS). Surprisingly, structural modulation and composition variation along the thin nanotubes axis were observed. In light of this new structural and chemical information, a growth mechanism for these nanotubes is proposed. In addition, we will also show how the coupling between HR-STEM, SR-EELS and DFT calculation can shed light not only on the atomic structure of misfit nanotubes but also on their opto-electronic properties.

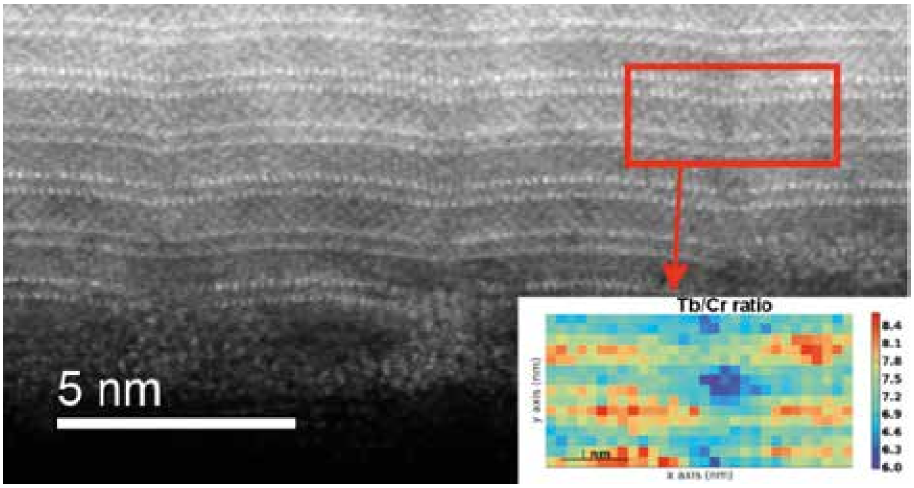

Figure caption: HR-STEM ADF micrograph of a wavy TbS-CrS2 NT. The inset shows the Tb/Cr ratio obtained from SR-EELS elemental quantification performed on the area delimited by the red square.

Reference:

L.S. Panchakarla, L. Lajaunie, R. Tenne, R. Arenal. J. Phys. Chem. C (2015), J. Phys. Chem. C, 2016, 120 (29), pp 15600–15607. DOI: 10.1021/acs.jpcc.5b05811

Magnetization reversal processes in cobalt antidote arrays: magnetic superdomains

Magnetic antidot arrays are periodic assemblies of holes produced in ferromagnetic thin films. As the hole period is reduced, strong demagnetizing fields around the antidots aligns magnetization along the antidot rows. This stabilizes Magnetic Superdomains (SDs), where the average magnetization (not the magnetization itself) is constant.

High resolution Lorentz microscopy has been used to obtain quantitative mapping of the SD configurations of a series of cobalt antidot arrays fabricated by in-house Focused Ion Beam

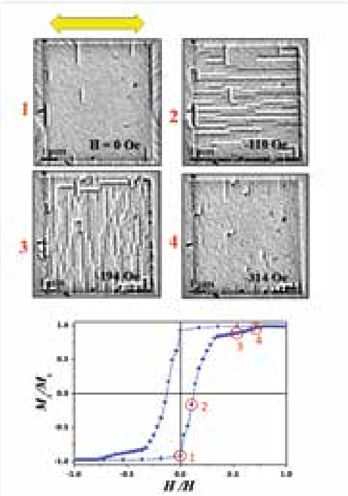

Figure caption. Magnetic Chain structure as a function of the magnetic field in a 160-nm-period antidot array in four steps of the magnetization reversal processes (top left). These corresponds with the positions of the antidote array hysteresis loop (bottom left). Map of Magnetic Superdomains featured in the Cover of the Nanotechnology journal, Vol. 25, No. 38, 2014 (right).

etching. To study periodicities as low as 95 nm, a new low-frequency Fourier filtering method was implemented to remove the contrast produced by the physical holes and enhance the magnetic signal. SDs are observed in periodicities below 160 nm, many of them confined between two antidot rows forming Magnetic Chains. LMA's in situ Lorentz microscopy capabilities has enabled the study of magnetization reversal processes along the easy and hard magnetization axes as a function of the magnetic field, which is driven by the nucleation and propagation of Magnetic Chains parallel to the applied magnetic field. This fact has been successfully supported by micromagnetic simulations. The current study sheds new light on the magnetization reversal processes of high periodicity antidot arrays, and proposes new experimental approaches to investigate periodic arrays of nanomagnets.

Reference:

L. A. Rodríguez, C. Magén, E. Snoeck, C. Gatel, C. Castán-Guerrero, J. Sesé, L. M. García, J. Herrero-Albillos, J. Bartolomé, F. Bartolomé and M. R. Ibarra. Nanotechnology 2014, 25, 385703. Featured Article of the Cover of the Nanotechnology Journal, Issue of 28 September 2014 (Vol. 25, No. 38).

Low Temperature Stabilization of Nanoscale Epitaxial Spinel Ferrite Thin Films by Atomic Layer Deposition

In this work heteroepitaxial stabilization with nanoscale control of the magnetic Co2FeO4 phase at 250 ºC is reported. Ultrasmooth and pure Co2FeO4 thin films (5–25 nm) with no phase segregation are obtained on perovskite SrTiO3 single crystal (100) and (110) oriented substrates by atomic layer deposition (ALD). High resolution structural and chemical analyses confirm the formation of the Co-rich spinel metastable phase. The magneto-crystalline anisotropy of the Co2FeO4 phase is not modified by stress anisotropy because the films are fully relaxed. Additionally, high coervice fields, 15 kOe, and high saturation of magnetization, 3.3 μB per formula unit (at 10 K), are preserved down to 10 nm. Therefore, the properties of the ALD-Co2FeO4 films offer many possibilities for future applications in sensors,

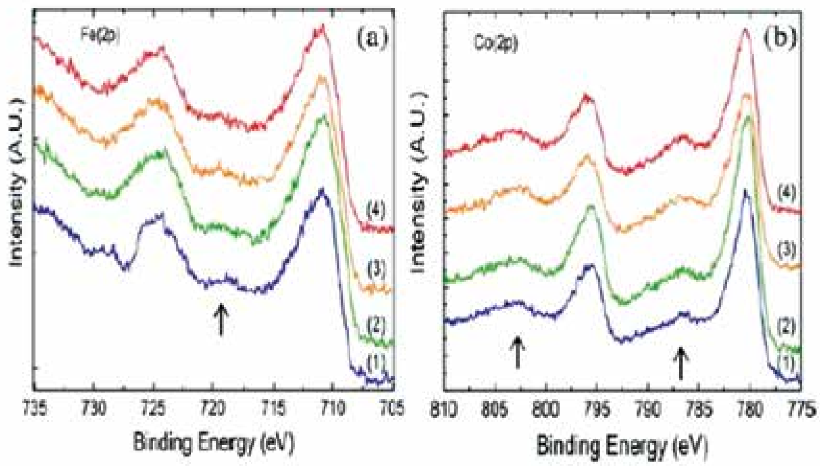

Figure caption: High resolutuionXPS spectra of a) Fe(2p) and b) Co(2p) regions for (1) 5nm CFO on STO (110), (2) 5 nm CFO on STO (100), (3) 15 nm CFO on STO (110), and (4) 15 nm CFO on STO (100). Arrows indicate the position of the satellite peaks.

actuators, microelectronics, and spintronics. In addition, these results are promising for the use of ALD compared to the existing thin-film deposition techniques to stabilize epitaxial multicomponent materials with nanoscale control on a wide variety of substrates for which the processing temperature is a major drawback.

Reference:

MarionaColl,* Josep M. Montero Moreno, JaumeGazquez, KorneliusNielsch, Xavier Obradors, and Teresa Puig, Adv. Funct. Mater.2014, 00, 1–6

Amphiphilic dendritic derivatives as nanocarriers for the targeted delivery of antimalarial drugs

It can be foreseen that in a future scenario of malaria eradication, a varied armamentarium will be required, including strategies for the targeted administration of antimalarial compounds. The development of nanovectors capable of encapsulating drugs and of delivering them to Plasmodium-infected cells with high specificity and efficacy and at an affordable cost is of particular interest. With this objective, dendritic derivatives based on 2,2-bis(hydroxymethyl) propionic acid (bis-MPA) and Pluronic® polymers have been herein explored. Four different dendritic derivatives have been tested for their capacity to encapsulate the antimalarial drugs chloroquine (CQ) and primaquine (PQ), their specific targeting to Plasmodium-infected red blood cells (pRBCs), and their antimalarial activity in vitro against the human pathogen Plasmodium falciparum and in vivo against the rodent malaria species Plasmodium yoelii. The results obtained have allowed the identification of two dendritic derivatives exhibiting specific targeting to pRBCs vs. non-infected RBCs, which reduce the in vitro IC50 of CQ and PQ by ca. 3- and 4-fold down to 4.0 nM and 1.1 mM, respectively. This work on the application of dendritic derivatives to antimalarial targeted drug delivery opens the way for the use of this new type of chemicals in future malaria eradication programs.

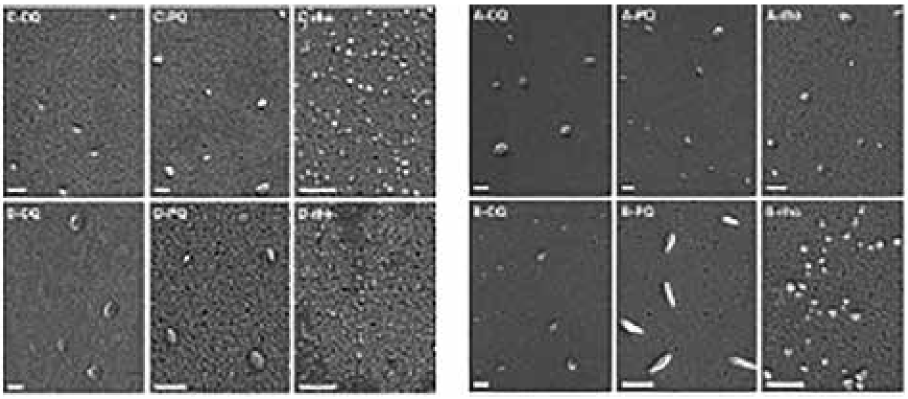

Figure caption: Scanning electron microscopy analysis of the dendritic derivatives encapsulating chloroquine, primaquine, and rhodamine B. Size bar: 500 nm.

Reference:

Julie Movellan , Patricia Urbán , Ernest Moles, Jesús M. de la Fuente , Teresa Sierra , José Luis Serrano , Xavier Fernández-Busquets. Biomaterials 2014, 35, 7940-7950.

ZIF-8 micromembranes for gas separation prepared on laser-perforated brass supports

ZIF-8 is an imidazolate-based metal–organic framework (MOF). ZIF-8 micromembranes of 20–32 mm diameter are prepared by synthesizing the MOF on Nd:YAG laser-perforated 75 mm thick brass sheets (63/37 Cu/Zn). The laser irradiation activates the brass support, promoting ZIF-8 growth. A thick and continuous ZIF-8 membrane is crystallized on the laser irradiation outlet side of the support, while the inlet side and the inner surface of the microperforations are also coated with ZIF-8 intergrowth crystals. Laser perforated brass supports are not only cheap, flexible, strong, and easy to handle and to process as membrane materials; they are also chemically compatible with the ZIF-8 composition because of the shared Zn element. The ZIF-8 membranes obtained are characterized by XRD, SEM, EDX, TGA and N_2 sorption analysis. Furthermore, the membranes are applied to the separation of equimolar H_2–CH_4, He–CH_4, CO_2–CH_4 and O_2–N_2 mixtures confirming the expected molecular sieving effect due to the MOF microporosity. The size, morphology and intergrowth of the ZIF-8 crystals were checked by using a scanning electron microscope (SEM) operating at 5–10 keV (Quanta FEG 250). Besides, EDX (energydispersive X-ray) spectroscopy was used to determine the atomic composition of the phases deposited on the support. Linear patterns were irradiated over brass supports as a starting point to understand the role of laser irradiation in the control of the patterning growth of ZIF-8 crystals. The width of the activated surface (rough groove produced by the irradiation) was about 33 mm with a depth of about 16 mm.

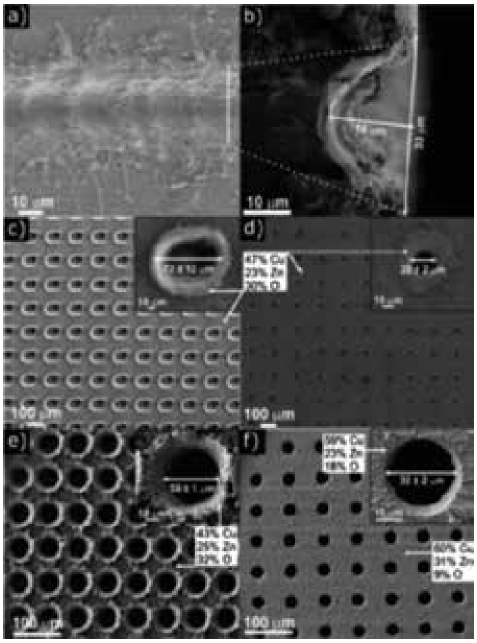

Figure caption: SEM images of (a) laser irradiated brass following a linear path; (b) cross-section of the rough channel produced upon laser irradiation; (c) inlet (rough) and (d) outlet (smooth) sides of a type I brass support; (e) inlet (rough) and (f) outlet (smooth) sides of a type II brass support. Insets of enlarged perforations and EDX atomic compositions are included.

Reference:

Marta Navarro, Beatriz Seoane, Ester Mateo, Ruth Lahoz, Germán F. de la Fuente and Joaquín Coronas. J. Mater. Chem. A, 2014, 2,11177.

Electrospun Au/CeO_2 nanofibers: A highly accessible low-pressure dropcatalyst for preferential CO oxidation

Au/CeO_2 catalysts shaped as nanofibers were obtained by supporting Au nanoparticles (ca. 3 nm) on CeO2 nanofibers of around 200 nm diameter. The CeO_2 support was prepared by calcining electrospun polymer nanocomposite fibers with a high Ce content; then gold nanoparticles were either synthesized in situ or deposited from a suspension. The prepared catalysts were used in the preferential oxidation of CO in a hydrogen-rich stream. The catalysts prepared by deposition of preformed gold nanoparticles were less stable and underwent sintering due to a weaker nanoparticle–support interaction. In contrast, the catalysts with Au nanoparticles synthesized in situ were active (90% conversion and 46% selectivity) and stable. The fiber-shaped catalyst was able to give maximum reactant access at a much lower pressure drop than catalyst in powder form. Solutions with different PVP concentrations and weight ratios of cerium to polymer were prepared and tested under electrospinning conditions. The morphology of the samples obtained was very different, depending on the solution used. Solutions with low polymer concentration (5.8 and 7.3 wt.%) and high $Ce(NO_3)_3$ content produced unstable Taylor cones, and it was not possible to electrospin them. The amount of PVP was found to be an important cause of the change in viscosity of the sol: as expected, the viscosity of the sol increased with increasing PVP content. A minimum viscosity value is necessary to overcome the surface tension effects and produce fibers. The value of viscosity enables electrospinning, but the product consists of beaded fibers, as shown in Fig. 1a

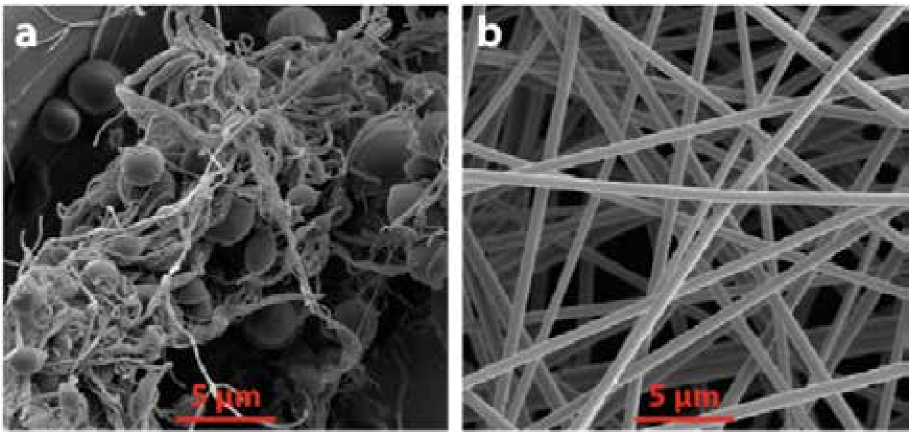

Figure caption: SEM images of as-spun (a) Ce1 fibers, (b) Ce5 fibers, and (c) diameter distribution for Ce5.

Reference:

Iván Moreno, Nuria Navascues, Silvia Irusta and Jesus Santamaria.Journal of Catalysis 2015, 329, 479–489.

Beyond the H_2/CO_2 upper bound: one-step crystallization and separation of nano-sized ZIF-11 by centrifugation and its application in mixed matrix membranes

The synthesis of nano-sized ZIF-11 with an average size of 36 ± 6 nm is reported. This material has been named nano-zeolitic imidazolate framework-11 (nZIF-11). It has the same chemical composition and thermal stability and analogous H_2 and CO_2 adsorption properties to the conventional microcrystalline ZIF-11 (i.e. 1.9±0.9 mm). nZIF-11 has been obtained following the centrifugation route, typically used for solid separation, as a fast new technique (pioneering for MOFs) for obtaining nanomaterials where the temperature, time and rotation speed can easily be controlled. Compared to the traditional synthesis consisting of stirring + separation, the reaction time was lowered from several hours to a few minutes when using this centrifugation synthesis technique. Employing the same reaction time (2, 5 or 10 min), micro-sized ZIF-11 was obtained using the traditional synthesis while nano-scale ZIF-11 was achieved only by using centrifugation synthesis. The small particle size obtained for nZIF-11 allowed the use of the wet MOF sample as a colloidal suspension stable in chloroform. This helped to prepare mixed matrix membranes (MMMs) by direct addition of the membrane polymer (polyimide Matrimid®) to the colloidal suspension, avoiding particle agglomeration resulting from drying. The MMMs were tested for H_2/CO_2 separation, improving the pure polymer membrane performance, with permeation values of 95.9 Barrer of H_2 and a H_2/CO_2 separation selectivity of 4.4 at 35 ºC. When measured at 200 ºC, these values increased to 535 Barrer and 9.1.

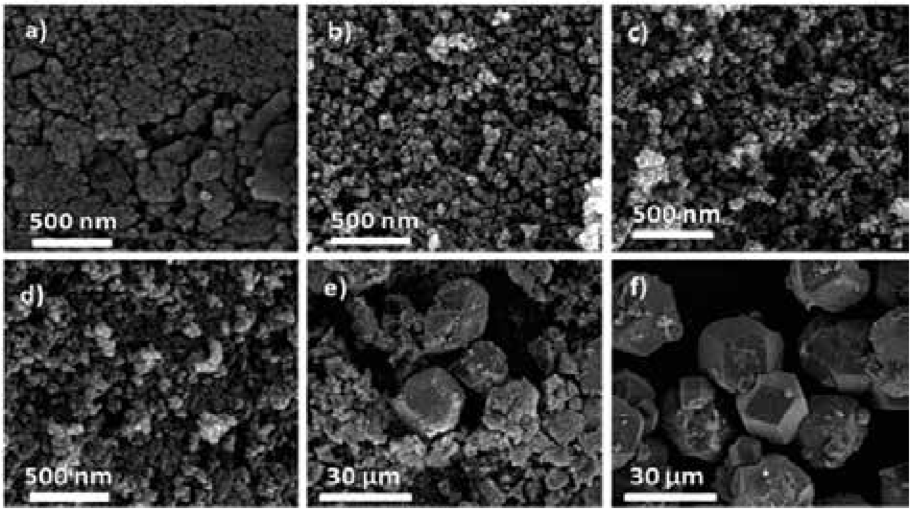

Figure caption: Scanning electron microscopy (SEM) images of MOFs and membranes were imaged using an Inspect F50 model scanning electron microscope (FEI), operated at 20 kV. SEM images of ZIF-11 samples synthesized by centrifugal acceleration at different reaction times: (a) 1 min, (b) 2 min, (c) 5 min,(d) 10 min, (e) 15 min, and (f) 30 min are shown.

Reference:

Javier Sánchez-Laínez, Beatriz Zornoza, Álvaro Mayoral, Ángel Berenguer-Murcia, Diego Cazorla-Amorós, Carlos Téllez and Joaquín Coronas. J. Mater. Chem. A, 2015, 3,6549.

High selectivity ZIF-93 hollow fiber membranes for gas separation

Zeolitic imidazolate framework-93 (ZIF-93) continuous membranes were synthesized on the inner side of P84 co-polyimide hollow fiber supports by microfluidics. MOFs and polymers showed high compatibility and the membrane exhibited H_2–CH_4 and CO_2–CH_4 separation selectivities of 97 (100 ºC) and 17 (35 ºC), respectively.

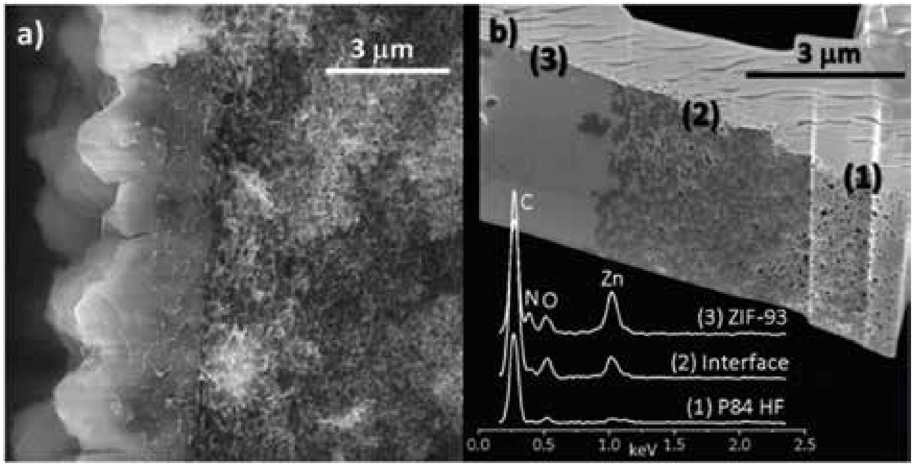

Figure caption: (a) SEM cross-section image of the MOF-coated inner surface of an as-synthesized ZIF-93@P84 membrane; (b) a lamella made with Ga-FIB etching and EDX spectra recorded for the MOF layer, support and interface, showing the MOF attachment to the polymer.

Reference:

Fernando Cacho-Bailo et al. ChemComm (2015) 51, 11283

Preparation of nascent molecular electronic devices from gold nanoparticles and terminal alkyne functionalised monolayer films

A metal–molecule–GNP assembly has been fabricated using an acetylene-terminated phenyleneethynylene molecular monolayer, namely 4-((4 ((4-ethynylphenyl)ethynyl)phenyl) ethynyl)benzoic acid (HOPEA), sandwiched between a gold substrate bottom electrode and gold nanoparticle (GNP) top contact electrode. In the first stage of the fabrication process, a monolayer of directionally oriented (carboxylate-to-gold) HOPEA was formed onto the bottom electrode using the Langmuir–Blodgett (LB) technique. In the second stage, the gold-substrate supported monolayer was incubated in a solution of gold nanoparticles (GNPs), which resulted in covalent attachment of the GNPs on top of the film via an alkynyl carbon–Au s-bond thereby creating the metallic top electrode.

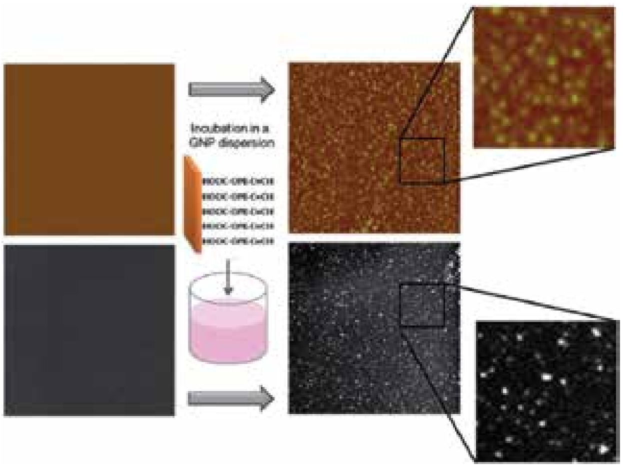

Figure caption: AFM (top) and SEM (bottom) images of a pristine HOPEA monomolecular LB film (left) deposited onto a mica substrate and the same LB film after incubation for 2.5 hours in a dispersion of GNPs (right). Images are 2 x 2 mm^2 in size and the Z range of the AFM images is 30 nm. For a better view of the size and shape of the GNPs both AFM and SEM images have been magnified (500 x 500 nm).

Reference:

Henrry M. Osorio, Pilar Cea, Luz M. Ballesteros, Ignacio Gascón, Santiago Marqués-Gonzáez, Richard J. Nichols, Francesc Pérez-Murano, Paul J. Low and Santiago Martín. J. Mater. Chem. C, 2014, 2,7348.

From an organometallic monolayer to an organic monolayer covered by metal nanoislands: a simple thermal protocol for the fabrication of the top contact electrode in molecular electronic devices.

A novel method for practical uses in the fabrication of the top contact electrode in a metal/organic monolayer/metal device is presented. The procedure involves the thermally induced decomposition of an organometallic compound, abbreviated as the TIDOC method. Monolayers incorporating the metal organic compounds (MOCs) were annealed at moderate

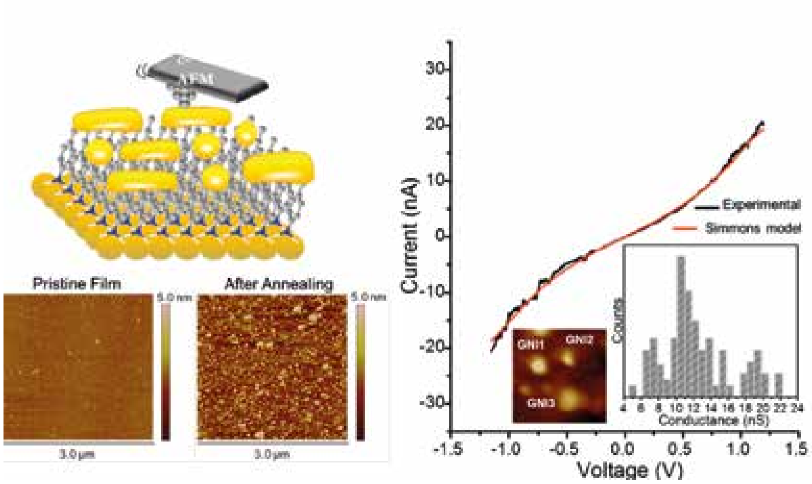

Figure Caption: Left panel: Sketch of the fabrication procedure and AFM images of a pristine film onto a mica substrate and the. Right panel: Representative I–V curve experimentally obtained by positioning the c-AFM tip on top of a GNI when a set-point force of 35 nN was applied. Inset: conductance histogram of the film after annealing.

temperatures resulting in cleavage of the Au-P or Au-C bond and reduction of Au(I) to Au(0) as metallic gold nanoparticles (GNPs). These particles are distributed on the surface of the film resulting in formation of metal/molecule/GNP sandwich structures. Electrical properties of these nascent devices were determined by recording I–V curves with a conductive-AFM. The I–V curves collected from these metal/organic monolayer/GNPs sandwich structures are typical of metal-molecule-metal junctions, with no low resistance traces characteristic of metallic short circuits observed over a wide range of set-point forces.

Reference:

Ballesteros, L. M., Martín, S., Cortés, J., Marqués-González, S., Pérez-Murano, F., Nichols, R. J., Low, P. J., Cea, P. Adv. Mater. Interfaces 2014, 1, 1400128, doi: 10.1002/admi.201400128

Ferromagnetic coupling mechanism in Fe-Phthalocyanine multi-layer assemblies on Au(111)

Molecule-based magnets form a novel class of magnetic materials. Uniquely, they combine their magnetism with electrical and optical properties that are unusual for conventional magnetic compounds. The magnetic coupling in molecule-based magnets might be mediated by a variety of different mechanisms that have to be distinguished in order to tune the material properties at wish. In multi-layer assemblies of Fe-Phthalocyanine (Fe-PC) molecules a strong inter-layer ferromagnetic coupling was found for the iron centers. By means of STM we mapped the exact alignment of the metallic centers and identified the involved magnetic interactions.

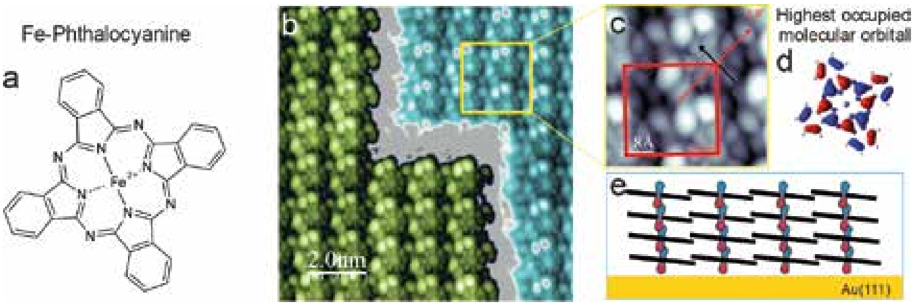

Figure caption: (Omicron LT-qPlus) a) Chemical structure of a Fe-Phthalocyanine molecule, b) STM topography of two subsequent monolayers of Fe-PC on Au(111). Data are used to determine the inter-layer alignment. c) Zoom into individual Fe-PC molecules. The topography is used to determine the relative orientation of the single molecules with respect to the layer plane as well as the single layers unit cell. d) Highest occupied molecular orbital of gas-phase PC, e) relative orientation of the Fe-PC as deduced from the experimental data reveals a direct overlap of the Fe d_{z^2} orbitals.

Reference:

F. Bartolomé, O. Bunau,1 L. M. García,1 C. R. Natoli,2 M. Piantek,1,3 J. I. Pascual,3,4

I. K. Schuller,5 T. Gredig,6 F. Wilhelm,7 A. Rogalev,7 and J. Bartolomé, J. Applied Physics 2015, 117, 17A735, doi: 10.1063/1.4916302

Robust topological surfaces states against surface magnetic impurities on ternary compound Bi_2Se_2Te

3D Topological insulators have great potential in fault-tolerant quantum computating and spintronics. Their key feature is the existence of surface currents with 100% spin polarization which is protected by the crystal non-trivial topology. Here we use low-temperature scanning tunneling spectroscopy to show how the inhomogeneous cleavage surface of a Bi2Se2Te displaces adsorption site of individual Co magnetic away from the high symmetry positions. This precludes the hybridization of atomic magnetic states with the Dirac surfaces states. As a result, the Co surface-doping of Bi2Se2Te is not able to scatter the topological spin currents . Thus, we have found a topological insulator which does not break time-reversal symmetry under magnetic impurities adsorption and a magnetic field influence. This paves the way towards topological magnetoelectronis in which the surface currents can gate the magnetic moment of materials deposited on top of it.

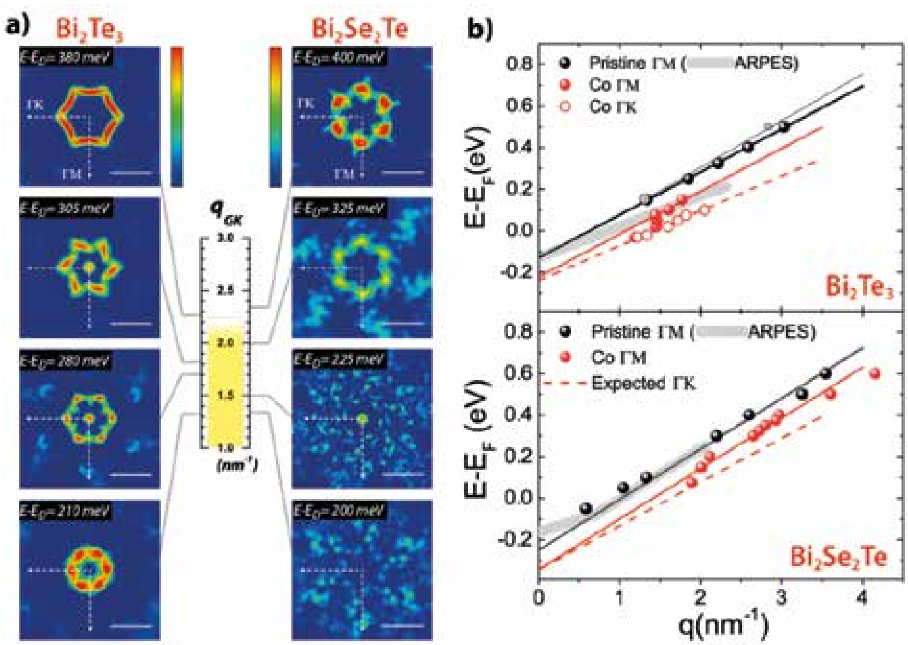

Figure caption: (JT-STM) (a) Energy resolved maps of the reciprocal space interference patters. Comparison a 3D topological insulator that breaks time-reversal symmetry (and so gets a depolarization of the topological spin current) upon Co doping, Bi_2Te_3, and our Bi_2Se_2Te, which does not. (b) Dirac cone relation dispersion obtained from such maps. Depolarization/ preservation of spin current is monitored by the presence/ absenceof backscattering interference spots along the GK direction of the surface Brillouin zone (open cicles), while Dirac dispersion is measured by spin conserving scattering events along GM (filled circles).

Reference:

Martínez-Velarte, M.C.; Kretz, B.; Morellon, L.; Ibarra, M.R.; García-Lekue, A.; Serrate, D. Manuscript in preparation in 2015

Piezoelectric behaviour in atomically thin stacks of polar insulators

Interactions at the atomically precise interface between different polar materials can trigger a variety of novel properties, from induced ferroelectricity [Haeni2004] to superconductivity. Here, we report that atomically thin layers of sodium chloride (NaCl) exhibit inverse piezoelectric behaviour – displacement of the atoms driven by an applied electric field – when deposited on a monolayer of copper nitride (Cu2N) above bulk copper. Unlike analogous van der Waals heterostructures, NaCl is bonded to Cu2N through electrostatic interactions, which distort the NaCl lattice by 7%. Using scanning probe microscopy, we locally manipulate and reverse the atomic dipoles in the NaCl surface, as measured through sharp changes in the tunnel current and force between the surface and a nearby atomically sharp probe tip. These results suggest that NaCl is the first member of a new class of piezoelectrics formed at the interface between ultra-thin insulating polar materials above conducting surfaces, pushing the feasible size of functional multiferroics down to the atomic scale .

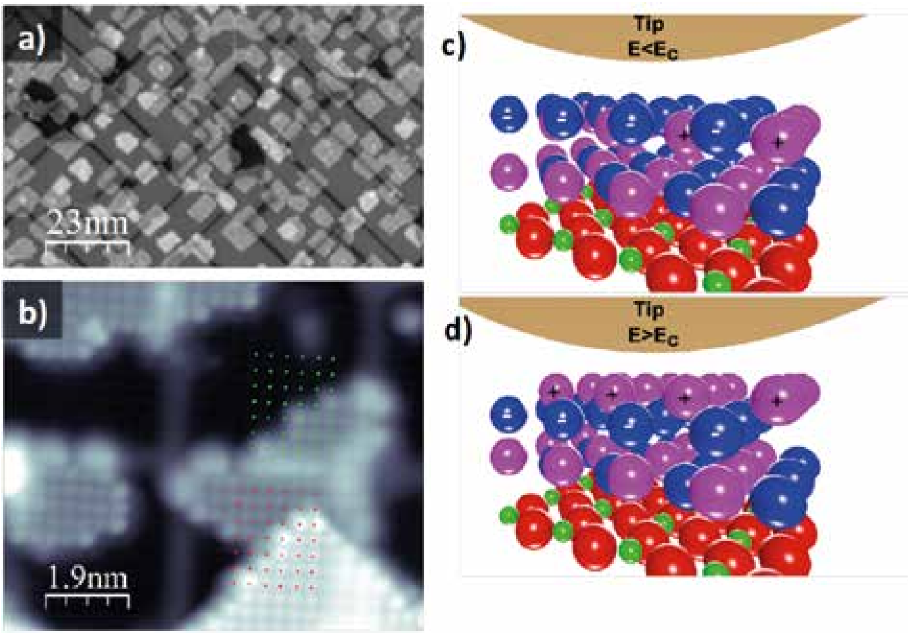

Figure caption: (JT-STM and LT-qPlus)– Ultra-thin NaCl layers on Cu_2N/Cu(001). a) Topographic STM image of a Cu_2N/Cu(001) surface fully covered with monolayers and bilayers of NaCl (72 nm × 116 nm) b) High resolution topographic STM image. Red and greed dots indicate the locations of Cl^- ions in NaCL ML and BL, respectively c) Illustration of the positions of Cu (red), N (green), Na (magenta), and Cl (blue) atoms in NaCl-BL/Cu2N/Cu(001) for the low electric field configuration. In the outermost layer, the Cl- atoms sit above the Na atoms and are thus closer to the tip above. d) Same as (c) for the high electric field configuration, the Cl- atoms are now below the Na atoms, indicating a reversal of surface electric dipole.

Reference:

Martínez-Castro, J.; Piantek, M.;Perssons, M.; Serrate, D.; Hirjibehedin, C.F. Manuscritp in preparation in 2015

Scientific publications

1. Artificial Chemical And Magnetic Structure at the Domain Walls of an Epitaxial Oxide

S. Farokhipoor, C. Magén, S. Venkatesan, J. Íñiguez, C. J. M. Daumont, D. Rubi, E. Snoeck, M. Mostovoy, C. de Graaf, A. Müller, M. Döblinger, C. Scheu & B. Noheda

Nature 515, 379–383, Nov 2014. doi:10.1038/nature13918

IF: 42.351

2. Strain-Induced Coupling of Electrical Polarization and Structural Defects in SrMnO3 films

Becher, C ; Maurel, L ; Aschauer, U ;Lilienblum, M ; Magen, C ; Meier, D ;Langenberg, E ; Trassin, M ; Blasco, J ;Krug, IP ; Algarabel, PA ; Spaldin, NA]; Pardo, JA ; Fiebig, M

NATURE NANOTECHNOLOGY, 10, 8, 661-665, 2015.

IF: 34.048

3. Control of Single-Spin Magnetic Anisotropy by Exchange Coupling

Oberg, JC; Calvo, MR ; Delgado, F; Moro-Lagares, M; Serrate, D; Jacob, D; Fernandez-Rossier, J; Hirjibehedin, CF

Nature Nanotechnology, 9, 1, 64-68, 2014.

IF: 33.265

4. Synthesis of 'Unfeasible' Zeolites

Mazur, M; Wheatley, P; Navarro, M; Roth, W; Polozij, M; Mayoral, A; Eliasova, P; Nachtigall, P; Cejka, J; Morris, R.

NATURE CHEMISTRY, DOI:10.1038/nchem.2374, 2015.

IF: 25.325

5. Enhancement of Long-Range Correlations in a 2D Vortex Lattice by an Incommensurate 1D Disorder Potential

I. Guillamón, R. Córdoba, J. Sesé, J. M. De Teresa, M. R. Ibarra, S. Vieira & H. Suderow

Nature Physics 10, 851–856 (2014), Oct 2014, doi:10.1038/nphys3132

IF: 20.603

6. Achieving Giant Magnetically Induced Reorientation of Martensitic Variants in Magnetic Shape-Memory Ni-Mn-Ga Films by Microstructure Engineering

Ranzieri, P ; Campanini, M ; Fabbrici, S ; Nasi, L ; Casoli, F ; Cabassi, R ; Buffagni, E ; Grillo, V ; Magen, C ; Celegato, F ; Barrera, G ; Tiberto, P ; Albertini, F

ADVANCED MATERIALS, 27, 32, 4760-4766, 2015.

IF: 17.493

7. Synthesis of PbI2 Single-Layered Inorganic Nanotubes Encapsulated Within Carbon Nanotubes
L. Cabana, B. Ballesteros, E. Batista, C. Magén, R. Arenal, J. Oró-Solé, R. Rurali and G. Tobias
Advanced Materials. Volume 26, Issue 13, pages 2016–2021, Apr 2014. doi:10.1002/adma.201305169
IF: 15.409

8. Observation of the Strain Induced Magnetic Phase Segregation in Manganite Thin Films
Marin, L; Rodriguez, LA ; Magen, C; Snoeck, E; Arras, R; Lucas, I; Morellon, L ; Algarabel, PA; De Teresa, JM; Ibarra, MR
NANO LETTERS, 15, 1, 492-497, 2015.
IF: 13.592

9. Position-Controlled Growth of GaN Nanowires and Nanotubes on Diamond by Molecular Beam Epitaxy
Schuster, F; Hetzl, M; Weiszer, S; Garrido, JA; de la Mata, M; Magen, C; Arbiol, J; Stutzmann, M
NANO LETTERS, 15, 3, 1773-1779, 2015.
IF: 13.592

10. Fully Crystalline Faceted Fe-Au Core Shell Nanoparticles
Langlois, C ; Benzo, P ; Arenal, R ; Benoit, M; Nicolai, J ; Combe, N ; Ponchet, A ; Casanove, MJ
NANO LETTERS, 15, 8, 5075-5080, 2015.
IF: 13.592

11. Atomic Scale Strain Relaxation in Axial Semiconductor III–V Nanowire Heterostructures
M. de la Mata, C. Magén, P. Caroff, and J. Arbiol
Nano Letters, Oct 2014, 14 (11), pp 6614–6620. doi:10.1021/nl503273j
IF: 12.940

12. Atomic Configuration of Nitrogen-Doped Single-Walled Carbon Nanotubes
R. Arenal, K. March, C.P. Ewels, X. Rocquefelte, M. Kociak, A. Loiseau, O. Stephan
Nano Letters, 14, 5509–5516 (2014), Aug 2014. doi:10.1021/nl501645g
IF: 12.940

13. Enhanced Magnetotransport in Nanopatterned Manganite Nanowires
L. Marín, L. Morellón, P. A. Algarabel, L. A. Rodríguez, C. Magén, J. M. De Teresa, and M. R. Ibarra
Nano Letters. 14 (2), pp 423–428, Jan 2014. doi:10.1021/nl402911w
IF: 12.940

14. Whispering Gallery Mode Lasing from Hexagonal Shaped Layered Lead Iodide Crystals
Liu, XF; Ha, ST; Zhang, Q; de la Mata, M ; Magen, C; Arbiol, J; Sum, TC; Xiong, QH
ACS NANO, 9, 1, 687-695, 2015.
IF: 12.881

15. Focused Electron and Ion Beam Induced Deposition on Flexible and Transparent Polycarbonate Substrates
Peinado, P; Sangiao, S; De Teresa, JM
ACS NANO, 9, 6, 6139-6146, 2015.
IF: 12.881

16. Electrochemical Single-Molecule Transistors with Optimized Gate Coupling
Henrry M. Osorio, Samantha Catarelli, Pilar Cea, Josef B. G. Gluyas, Frantisek Hartl, Simon J. Higgins, Edmund Leary, Paul J. Low, Santiago Martin, Richard J. Nichols, Joanne Tory, Jens Ulstrup, Andrea Vezzoli, Qiang Zeng, and David Costa Milan
JOURNAL OF THE AMERICAN CHEMICAL SOCIETY, doi:10.1021/jacs.5b08431
IF: 12.113

17. In Situ Formation of Carbon Nanotubes Encapsulated within Boron Nitride Nanotubes via Electron Irradiation
R. Arenal, A. Lopez-Bezanilla
ACS Nano,8 (8), pp 8419–8425, Jul 2014, doi:10.1021/nn502912w
IF: 12.003

18. Arrays of Densely Packed Isolated Nanowires by Focused Beam Induced Deposition Plus Ar+ Milling
J. M. De Teresa and R. Córdoba
ACS Nano. 8 (4), pp 3788–3795. Apr 2014. doi:10.1021/nn500525k
IF: 12.003

19. p-GaN/n-ZnO Heterojunction Nanowires: Optoelectronic Properties and the Role of Interface Polarity
F. Schuster, B. Laumer, R. R. Zamani, C. Magén, J. R. Morante, J. Arbiol, and M. Stutzmann
ACS Nano. 8 (5), pp 4376–4384. Apr 2014. doi:10.1021/nn406134e
IF: 12.003

20. Boron Nitride Materials: an Overview from 0D to 3D (Nano)Structures
Arenal, R ; Lopez-Bezanilla, A
WILEY INTERDISCIPLINARY REVIEWS-COMPUTATIONAL MOLECULAR SCIENCE, 5, 4, 299-309, 2015.
IF: 11.885

21. Dynamic Interplay Between Catalytic and Lectin Domains of GalNAc-Transferases Modulates Protein O-Glycosylation
Lira-Navarrete, E ; de las Rivas, M ; Companon, I ; Pallares, MC ; Kong, Y ; Iglesias-Fernandez, J ; Bernardes, GJL ;Peregrina, JM ; Rovira, C ; Bernado, P ; Bruscolini, P ; Clausen, H ; Lostao, A; Corzana, F ; Hurtado-Guerrero, R
NATURE COMMUNICATIONS, 6, 6937, 2015.
IF: 11.470

22. Dynamic HAADF-STEM Observation of a Single-Atom Chain as the Transient State of Gold Ultrathin Nanowire Breakdown
Lacroix, LM; Arenal, R; Viau, G
Journal of the American Chemical Society, 136, 38, 13075-13077, 2014.
IF: 11.444

23. Supramolecular Architectures from Bent-Core Dendritic Molecules.
Cano M1, Sánchez-Ferrer A, Serrano JL, Gimeno N, Ros MB.
Angew Chem Int Ed Engl. 53(49):13449-53 (2014). doi: 10.1002/anie.201407705
IF: 10.91

24. A 3D Insight on the Catalytic Nanostructuration of Few-Layer Graphene
G. Melinte, I. Florea, S. Moldovan, I. Janowska, W. Baaziz, R. Arenal, A. Wisnet, C. Scheu, S. Begin-Colin, D. Begin, C. Pham-Huu & O. Ersen
Nature Communications 5, Article number: 4109. Jun 2014, doi:10.1038/ncomms5109.
IF: 10.742

25. Low Temperature Stabilization of Nanoscale Epitaxial Spinel Ferrite Thin Films by Atomic Layer Deposition.
M. Coll M., J.M. Montero Moreno, J. Gazquez, C. Nielsch, X. Obradors, and T.Puig
Advanced Functional Materials. Volume 24, Issue 34, pages 5368–5374, Sep 2014.
doi:10.1002/adfm.201400517
IF: 10.439

26. Magnetically Decorated Multiwalled Carbon Nanotubes as Dual MRI and SPECT Contrast Agents

J. Tzu-Wen Wang, L.Cabana, M. Bourgognon, H. Kafa, A. Protti, K. Venner, A. M. Shah, J. K. Sosabowski, S. J. Mather, A. Roig, X. Ke, G. Van Tendeloo, R. T. M. de Rosales, G. Tobias, and K. T. Al-Jamal

Advanced Functional Materials. Volume 24, Issue 13, pages 1880–1894, Ap 2014.

doi:10.1002/adfm.201302892

IF: 10.439

27. High-Temperature Stable Gold Nanoparticle Catalysts for Application under Severe Conditions: The Role of TiO2 Nanodomains in Structure and Activity

Puertolas, B; Mayoral, A; Arenal, R; Solsona, B; Moragues, A;; Amoros, P; Hungria, AB; Taylor, SH; Garcia, T

ACS CATALYSIS, 5, 2, 1078-1086, 2015.

IF: 9.312

28. Na–Vacancy and Charge Ordering in Na≈2/3FePO4

M. Galceran, V. Roddatis, F. J. Zúñiga, J. M. Pérez-Mato, B. Acebedo, R. Arenal, I. Peral, T. Rojo, and M. Casas-Cabanas

Chemistry of Materials. 26 (10), pp 3289–3294. May 2014.

doi:10.1021/cm501110v

IF: 8.535

29. Direct Monolithic Integration of Vertical Single Crystalline Octahedral Molecular Sieve Nanowires on Silicon

Carretero-Genevrier, A; Oro-Sole, J; Gazquez, J; Magen, C; Miranda, L; Puig, T; Obradors, X; Ferain, E; Sanchez, C ; Rodriguez-Carvajal, J; Mestres, N

Chemistry of Materials, 26, 2, 1019-1028, 2014.

IF: 8.535

30. Gas Slug Microfluidics: A Unique Tool for Ultrafast, Highly Controlled Growth of Iron Oxide Nanostructures

Larrea, A ; Sebastian, V ; Ibarra, A ;Arruebo, M ; Santamaria, J

CHEMISTRY OF MATERIALS, 27, 10, 4254-4260, 2015.

IF: 8.354

31. 3D Magnetic Induction Maps of Nanoscale Materials Revealed by Electron Holographic Tomography

Wolf, D; Rodriguez, LA; Beche, A; Javon, E; Serrano, L; Magen, C; Gatel, C; Lubk, A; Lichte, H; Bals, S; Van Tendeloo, G; Fernandez-Pacheco, A; De Teresa, JM; Snoeck, E.

CHEMISTRY OF MATERIALS, 27, 10, 6771-6778, 2015.

IF: 8.354

32. The effect of Surface Charge of Functionalized Fe3O4 Nanoparticles on Protein Adsorption and Cell Uptake
Calatayud, MP; Sanz, B; Raffa, V; Riggio, C; Ibarra, MR; Goya, GF
Biomaterials, 35, 24, 6389-6399, 2014.
IF: 8.312

33. Amphiphilic Dendritic Derivatives as Nanocarriers for the Targeted Delivery of Antimalarial Drugs
Julie Movellan , Patricia Urbán , Ernest Moles, Jesús M. de la Fuente , Teresa Sierra , José Luis Serrano , Xavier Fernández-Busquets.
Biomaterials 2014, 35, 7940-7950.
IF: 8.312

34. Electronic Degeneracy and Intrinsic Magnetic Properties of Epitaxial Nb:SrTiO3 Thin Films Controlled by Defects
Sarantopoulos, A; Ferreiro-Vila, E; Pardo, V; Magen, C; Aguirre, MH; Rivadulla, F.
PHYSICAL REVIEW LETTERS, 115, 166801, 2015.
IF: 7.512

35. Beyond the H-2/CO2 Upper Bound: One-Step Crystallization and Separation of Nano-Sized ZIF-11 by Centrifugation and its Application in Mixed Matrix Membranes
Sanchez-Lainez, J; Zornoza, B; Mayoral, A; Berenguer-Murcia, A; Cazorla-Amoros, D; Tellez, C; Coronas, J
JOURNAL OF MATERIALS CHEMISTRY A, 3, 12, 6549-6556, 2015.
IF: 7.443

36. ZIF-8 Micromembranes for Gas Separation Prepared on Laser-Perforated Brass Supports
Marta Navarro, Beatriz Seoane, Ester Mateo, Ruth Lahoz, Germán F. de la Fuente and Joaquín Coronas
J. Mater. Chem. A, 2014,2, 11177-11184 doi:10.1039/C4TA00547C, Paper
IF: 7.443

37. Spontaneous Formation of Au-Pt Alloyed Nanoparticles Using Pure Nano-Counterparts as Starters: A Ligand and Size Dependent Process
Uson, L; Sebastian, V; Mayoral, A; Hueso, JL; Eguizabal, A; Arruebo, M;Santamaria, J
NANOSCALE, 7, 22, 10152-101561, 2015.
IF: 7.394

38. Facile Production of Stable Silicon Nanoparticles: Laser Chemistry Coupled to in Situ Stabilization Via Room Temperature Hydrosilylation
Malumbres, A ; Martinez, G ; Hueso, JL ;Gracia, J ; Mallada, R ; Ibarra, A ; Santamaria, J]
NANOSCALE, 7, 18, 8566-8573, 2015.
IF: 7.394

39 Lorentz Microscopy Sheds Light on The Role of Dipolar Interactions in Magnetic Hyperthermia
Campanini, M ; Ciprian, R ; Bedogni, E ; Mega, A; Chiesi, V ; Casoli, F ; Fernandez, CD ; Rotunno, E ; Rossi, F ; Secchi, A ; Bigi, F; Salviati, G ; Magen, C ; Grillo, V ; Albertini, F
NANOSCALE, 7, 17, 7717-7725, 2015.
IF: 7.394

40. Electrospun Au/CeO2 nanofibers: A highly accessible low-pressure drop catalyst for preferential CO oxidation
Iván Morenoa, Nuria Navascuesa, Silvia Irusta, Jesus Santamariaa, b,
IF: 7.354

41. Strain-Induced Spatially Indirect Exciton Recombination in Zinc-Blende/Wurtzite CdS Heterostructures
Li, DH ; Liu, Y ; de la Mata, M ; Magen, C ; Arbiol, J ; Feng, YP ; Xiong, QH
NANO RESEARCH, 8, 9, 3035-3044, 2015.
IF: 7.010

42. Te-Seeded Growth of Few-Quintuple Layer Bi2Te3 Nanoplates
Y. Zhao, M. de la Mata, RLJ Qiu, J. Zhang, XL Wen, C. Magen, XPA Gao, J. Arbiol, QH Xiong
Nano Research. Vol: 7. (9) P: 1243-1253. Sep 2014. doi:10.1007/s12274-014-0487-y
IF: 6.963

43. A Novel Co@Au Structure Formed In Bimetallic Core@Shell Nanoparticles
Mayoral, A ; Llamosa, D ; Huttel, Y
CHEMICAL COMMUNICATIONS, 51, 40, 8442-8445, 2015.
IF: 6.834

44. Exfoliated Semiconducting Pure 2H-MoS2 and 2H-WS2 Assisted by Chlorosulfonic Acid
Pagona, G ; Bittencourt, C ; Arenal, R ; Tagmatarchis, N
CHEMICAL COMMUNICATIONS, 51, 65, 12950-12953, 2015.
IF: 6.834

45. High Selectivity ZIF-93 Hollow Fiber Membranes for Gas Separation
Fernando Cacho-Bailo, Guillermo Caro, Miren Etxeberría-Benavides, Oğuz Karvan, Carlos Téllez and Joaquín Coronas
CHEMICAL COMMUNICATIONS, 51, 40, 11283, 2015.
IF: 6.854

46. The Ultimate Step Towards a Tailored Engineering of Core@Shell and Core@Shell@Shell Nanoparticles
D. Llamosa, M. Ruano, L. Martínez, A. Mayoral, E. Roman, M. García-Hernández, Y. Huttel
Nanoscale, Nov 2014,6, 13483-13486. doi:10.1039/C4NR02913E
IF: 6.739

47. Magneto-Plasmonic Nanoparticles as Theranostic Platforms for Magnetic Resonance Imaging, Drug Delivery and NIR Hyperthermia Applications.
Urries, I; Munoz, C; Gomez, L; Marquina, C; Sebastian, V; Arruebo, M; Santamaria, J
NANOSCALE, 6, 15, 9230-9240, 2014.
IF: 6.739

48. Retrieving the Electronic Properties of Silicon Nanocrystals Embedded in a Dielectric Matrix by Low-Loss EELS
Eljarrat, A; Lopez-Conesa, L; Lopez-Vidrier, J; Hernandez, S; Garrido, B; Magen, C; Peiro, F; Estrade, S.
NANOSCALE, 6, 14971-14983, 2014.
IF: 6.739

49. 1SERS Detection of Amyloid Oligomers on Metallorganic-Decorated Plasmonic Beads
Guerrini, L ; Arenal, R ; Mannini, B ;Chiti, F ; Pini, R ; Matteini, P ; Alvarez-Puebla, RA
ACS APPLIED MATERIALS & INTERFACES, 7, 18, 9420-9428, 2015.
IF: 6.723

50. Epitaxial Stabilization of the Perovskite Phase in (Sr1−xBax)MnO3 Thin Films
Langenberg, E; Guzman, R; Maurel, L; Martinez de Banos, L; Morellon, L; Ibarra, MR; Herrero-Martin, J; Magen, C; Algarabel, PA; Pardo, JA
ACS APPLIED MATERIALS & INTERFACES, 7, DOI: 10.1021/acsami.5b06478, 2015.
IF: 6.723

51. Development of Noncytotoxic Chitosan-Gold Nanocomposites as Efficient Antibacterial Materials.
Regiel-Futyra A1, Kus-Liśkiewicz M, Sebastian V, Irusta S, Arruebo M, Stochel G, Kyzioł A.
ACS Appl Mater Interfaces 7(2):1087-99 (2015). doi: 10.1021/am508094e.
IF: 6.723

52. Preparation of Nascent Molecular Electronic Devices from Gold Nanoparticles and Terminal Alkyne Functionalised Monolayer Films.
Osorio, H. M.; Cea, P.; Ballesteros, L. M.; Gascon, I.; Marqués-González, S.; Nichols, R. J.; Pérez-Murano, F.; Low, P. J.; Martín, S.
Journal of Materials Chemistry C, 2, 7348-7355, Jul 2014, doi:10.1039/C4TC01080A
IF: 6.626

53. Tailored Design of CoxMn1-xFe2O4 Nanoferrites: A New Route for Dual Control of Size and Magnetic Properties
Fernandes, C; Pereira, C; Fernandez-Garcia, MP; Pereira, AM; Guedes, A; Fernandez-Pacheco, R; Ibarra, A; Ibarra, MR; Araujo, JP; Freire, C
Journal of Materials Chemistry C, 2, 29, 5818-5828, 2014.
IF: 6.626

54. New Insights Into The Properties and Interactions of Carbon Chains as Revealed by HRTEM and DFT Analysis
G. Casillas, A. Mayoral, M. Liuc, A. Ponce, V. I. Artyukhovc, B. I. Yakobsonc, M. Jose-Yacaman
Carbon. Volume 66, Pages 436–441. Jan 2014. doi:10.1016/j.carbon.2013.09.019
IF: 6.160

55. The Orientation of the Neuronal Growth Process Can Be Directed Via Magnetic Nanoparticles Under an Applied Magnetic Field
C. Riggio, M.P. Calatayud, M. Giannaccini, B. Sanz, T. Torres, R. Fernández-Pacheco, A. Ripoli, M.R. Ibarra, L. Dente, A. Cuschieri
Nanomedicine: Nanotechnology, Biology and Medicine. Volume 10, Issue 7, Oct 2014, Pages 1549–1558. doi:10.1016/j.nano.2013.12.008
IF: 5.978

56. Quantum Dot and Superparamagnetic Nanoparticle Interaction with Pathogenic Fungi: Internalization and Toxicity Profile
N. Rispail, L. De Matteis, R. Santos, A. S. Miguel, L. Custardoy, P. S. Testillano, M. C. Risueño, A. Pérez-de-Luque, C. Maycock, P. Fevereiro, A. Oliva, R. Fernández-Pacheco, M. R. Ibarra, J. M. de la Fuente, C. Marquina, D. Rubiales, and E. Prats.
ACS Applied Materials & Interfaces. 6 (12), pp 9100–9110. May 2014. doi:10.1021/am501029g
IF: 5.900

57. Surface Chemistry on Small Ruthenium Nanoparticles: Evidence for Site Selective Reactions and Influence of Ligands

F. Novio, D. Monahan, Y. Coppel, G. Antorrena, P. Lecante, K. Philippot and B. Chaudret
Chemistry – A European Journal. Volume 20, Issue 5, pages 1287–1297. Jan 2014.
doi:10.1002/chem.201303935
IF: 5.696

58. Towards the Fabrication of the Top-Contact Electrode in Molecular Junctions by Photoreduction of a Metal Precursor.

Martin, S.; Pera, G.; Ballesteros, L. M.; Hope, A. J.; Marqués-González, S.; Low, P. J.; Perez-Murano, F.; Nichols, R. J.; Cea, P.
Chemistry European Journal, Feb 2014, 20, 3421-3426. doi: 10.1002/chem.201303967
IF: 5.696

59. Spatio-Temporal Behaviour of Atomic-Scale Tribo-Ceramic Films in Adaptive Surface Engineered Nano-Materials

Fox-Rabinovich, G; Kovalev, A; Veldhuis, S; Yamamoto, K; Endrino, JL; Gershman, IS; Rashkovskiy, A; Aguirre, MH; Wainstein, DL
SCIENTFIC REPORTS, 5, 8780, 2015.
IF: 5.578

60. Antiferromagnetic Spin Coupling between Rare Earth Adatoms and Iron Islands Probed by Spin-Polarized Tunneling

Coffey, D ; Diez-Ferrer, JL ; Serrate, D ; Ciria, M ; de la Fuente, C ; Arnaudas, JI
SCIENTFIC REPORTS, 5, 13709, 2015.
IF: 5.578

61. Morphological Tunability of the Plasmonic Response: From Hollow Gold Nanoparticles to Gold Nanorings

Prieto, R. Arenal, L. Henrard, L. Gomez, V. Sebastian, M. Arruebo
Journal of Physical Chemistry C, Nov 2014. doi: 10.1021/jp5096129.
IF: 4.835

62 Local Plasmonic Studies on Individual Core-Shell Gold-Silver and Pure Gold Nano-Bipyramids

R. Arenal, L. Henrard, L. Roiban, O. Ersen, J. Burgin, M. Treguer,
Journal of Physical Chemistry C, 118, 25643–25650. Oct 2014. doi:10.1021/jp5066105
IF: 4.835

63. Supramolecular Antimicrobial Capsules Assembled from Polyoxometalates and Chitosan

Laura De Matteis, Scott G. Mitchell and Jesús M. de la Fuente

J. Mater. Chem. B, 2014, 2, 7114-7117. doi:10.1039/C4TB01460J

64. One-Dimensional Molecular Crystal of Phthalocyanine Confined into Single-Walled Carbon Nanotubes

Alvarez, L; Fall, F; Belhboub, A; Le Parc, R ; Almadori, Y; Arenal, R; Aznar, R; Dieudonne-George, P; Hermet, P; Rahmani, A; Jousselme, B; Campidelli, S; Cambedouzou, J; Saito, T; Bantignies, JL

JOURNAL OF PHYSICAL CHEMISTRY C, 119, 9. 5203-5210, 2015.

IF: 4.772

65. Ultrathin Gold Nanowires: Soft-Templating versus Liquid Phase Synthesis, a Quantitative Study

Loubat, A; Lacroix, LM; Robert, A; Imperor-Clerc, M; Poteau, R; Maron, L; Arenal, R; Pansu, B; Viau, G

JOURNAL OF PHYSICAL CHEMISTRY C, 119, 8. 4422-4430, 2015.

IF: 4.772

66. Continuous-Mode Laser Ablation at the Solid Liquid Interface of Pelletized Low-Cost Materials for the Production of Luminescent Silicon Carbide Nanocrystals

Ortega-Liebana, MC; Hueso, JL; Arenal, R; Lahoz, R; de la Fuente, GF ; Santamaria, J

JOURNAL OF PHYSICAL CHEMISTRY C, 119, 4. 2158-2165, 2015.

IF: 4.772

67. Single Gold Atom Containing Oligo(phenylene)ethynylene: Assembly into LB Films and Electrical Characterization

Balesteros, LM ; Martin, S; Marques-Gonzalez, S; Lopez, MC; Higgins, SJ; Nichols, RJ; Low, PJ; Cea, P

JOURNAL OF PHYSICAL CHEMISTRY C, 119, 1, 784-793, 2015.

IF: 4.772

68. High Specific Absorption Rate and Transverse Relaxivity Effects in Manganese Ferrite Nanoparticles Obtained by an Electrochemical Route

Mazario, E; Sanchez-Marcos, J; Menendez, N; Canete, M; Mayoral, A Rivera-Fernandez, S; de la Fuente, JM; Herrasti, P

JOURNAL OF PHYSICAL CHEMISTRY C, 119, 12, 6828-6834, 2015.

IF: 4.772

69. **Structural and Hydrogen Storage Properties of Y2Ni7 Deuterides Studied by Neutron Powder Diffraction**
Charbonnier, V ; Zhang, JX ; Monnier, J ; Goubault, L ; Bernard, P ; Magen, C ; Serin, V ; Latroche, M
JOURNAL OF PHYSICAL CHEMISTRY C, 119, 22, 12218-12225, 2015.
IF: 4.772

70. **Inter-Layer Dependence of G-Modes in Semiconducting Double-Walled Carbon Nanotubes**
D.I. Levshov, T. Michel, R. Arenal, H.-N. Tran, T. Than, M. Paillet, Yu.I. Yuzyuk, J.-L. Sauvajol
JOURNAL OF PHYSICAL CHEMISTRY C, 119, 40, 23196-23202, 2015.
IF: 4.772

71. **Atomic Structural Studies on Thin Single-Crystalline Misfit-Layered Nanotubes of TbS-CrS2**
L. Panchakarla, L. Lajaunie, R. Tenne, R. Arenal
JOURNAL OF PHYSICAL CHEMISTRY C, DOI: 10.1021/acs.jpcc.5b05811, 2015.
IF: 4.772

72. **Nanoscaled M-MOF-74 Materials Prepared at Room Temperature**
M. Díaz-García, Á. Mayoral, I. Díaz, and M. Sánchez-Sánchez
Crystal Growth & Design. 14 (5), pp 2479–2487. Apr 2014.
doi:10.1021/cg500190h
IF: 4.558

73. **Atomic observations of Microporous Materials Highly Unstable Under the Electron Beam: The cases of Ti-doped AlPO4-5 and Zn-MOF-74**
Mayoral, A; Sanchez-Sanchez, A; Alfayete, J; Perez-Pariente, J; Diaz, I.
CHEMCATCHEM, DOI: 10.1002/cctc.201500617, 2015.
IF: 4.556

74. **Enhanced Hydrogen Dissociation by Individual Co Atoms Supported on Ag(111)**
David Serrate, Maria Moro-Lagares, Marten Piantek, Jose I. Pascual, and M. Ricardo Ibarra
J. Phys. Chem. C, 2014, 118 (11), pp 5827–5832
IF: 4.509

75. **Protein-Templated Biomimetic Silica Nanoparticles**
Jackson, E; Ferrari, M; Cuestas-Ayllon, C; Fernandez-Pacheco, R; Perez-Carvajal, J; de la Fuente, JM; Grazu, V; Betancor, L
LANGMUIR, 31, 12, 3687-3695, 2015.
IF: 4.457

76. Tuning Deposition of Magnetic Metallic Nanoparticles from Periodic Pattern to Thin Film Entrainment by Dip Coating Method
J. Dugay, R. P. Tan, A. Loubat, L.-M. Lacroix, J. Carrey, P. F. Fazzini, T. Blon, A. Mayoral, B. Chaudret, and M. Respaud
Langmuir 30 (30), pp 9028–9035, Aug 2014. doi:10.1021/la404044e
IF: 4.384

77. Influence of a Silica Interlayer on the Structural and Magnetic Properties of Sol–Gel TiO2-Coated Magnetic Nanoparticles
L. De Matteis, R. Fernández-Pacheco, L. Custardoy, M. L. García-Martín, J. M. de la Fuente, C. Marquina, and M. R. Ibarra
Langmuir. 30 (18), pp 5238–5247. Apr 2014. doi:10.1021/la500423e
IF: 4.384

78. Growth and Self-Assembly of Ultrathin Au Nanowires into Expanded Hexagonal Superlattice Studied by in Situ SAXS
A. Loubat, M. Impéror-Clerc, B. Pansu, F. Meneau, B. Raquet, G. Viau, and L-M Lacroix
Langmuir, 2014, 30 (14), pp 4005–4012. Mar 2014. doi:10.1021/la500549z
IF: 4.384

79. 3D Reconstruction of Atomic Structures from High Angle Annular Dark Field (HAADF) STEM Images and Its Application on Zeolite Silicalite-1
T. Willhammar, A. Mayoral and X. Zou
Dalton Transactions, 43, 14158-14163, Jul 2014, doi:10.1039/C4DT01904K
IF: 4.097

80. Metal Organic Framework Synthesis in the Presence of Surfactants: Towards Hierarchical MOFs?
Seoane, B; Dikhtiarenko, A; Mayoral, A; Tellez, C; Coronas, J; Kapteijn, F; Gascon, J
CRYSTENGCOMM, 17, 7, 1693-1700, 2015.
IF: 4.034

81. Silica promoted self-assembled mesoporous aluminas. Impact of the Silica Precursor on the Structural, Textural and Acidic Properties
Perez, LL ; Zarubina, V ; Mayoral, A ; Melian-Cabrera, I
CATALYSIS TODAY, 241, 114-124, 2015.
IF: 3.893

82. Vanadium-Doped TiO2 Anatase Nanostructures: the Role of V in solid Solution Formation and Its Effect on the Optical Properties
W. Avansi, Jr., R. Arenal, V. R. de Mendonça, C. Ribeiro and E. Longo
CrystEngComm. 16, 5021-5027. Apr 2014. doi:10.1039/C3CE42356E
IF: 3.858

83. Spin Configuration in Isolated FeCoCu Nanowires Modulated in Diameter
Iglesias-Freire, O; Bran, C; Berganza, E; Minguez-Bacho, I; Magen, C; Vazquez, M; Asenjo, A
NANOTECHNOLOGY, 26, 39, 395702, 2015.
IF: 3.821

84. Nature of Antiferromagnetic Order in Epitaxially Strained Multiferroic SrMnO3 Thin Films
Maurel, L; Marcano, N; Prokscha, T ;Langenberg, E; Blasco, J; Guzman, R; Suter, A; Magen, C; Morellon, L; Ibarra, MR; Pardo, JA; Algarabel, PA
PHYSICAL REVIEW B , 92, 2, 024419, 2015.
IF: 3.736

85. Interfacial Effects on the Tunneling Magnetoresistance in La0.7Sr0.3MnO3/MgO/Fe Tunneling Junctions
Galceran, R ; Balcells, L; Martinez-Boubeta, C; Bozzo, B; Cisneros-Fernandez, J; de la Mata, M; Magen, C; Arbiol, J; Tornos, J; Cuellar, FA; Sefrioui, Z ; Cebollada, A; Golmar, F Hueso, LE; Casanova, F; Santamaria, J; Martinez, B
PHYSICAL REVIEW B , 92, 9, 094428, 2015.
IF: 3.736

86. Antiferromagnetism at T > 500 K in the Layered Hexagonal Ruthenate SrRu2O6
Hiley, CI; Scanlon, DO; Sokol, AA; Woodley, SM; Ganose, AM; Sangiao, S ; De Teresa, JM; Manuel, P; Khalyavin, DD ;Walker, M; Lees, MR; Walton, RI
PHYSICAL REVIEW B , 92, 10, 104413, 2015.
IF: 3.734

87. Simple Hydrothermal Synthesis Method for Tailoring the Physicochemical Properties of ZnO: Morphology, Surface Area and Polarity
H. Silva, C. Mateos-Pedrero, C. Magén, D. A. Pacheco Tanakaa and A. Mendes
RSC Advances, 4, 31166-31176, Jul 2014, doi:10.1039/C4RA05002A
IF: 3.708

88. High-Resolution Imaging of Remanent State and Magnetization Reversal of Superdomain Structures in High-Density Cobalt Antidot Arrays
L A Rodríguez, C Magén, E Snoeck, C Gatel, C Castán-Guerrero, J Sesé, L M García, J Herrero-Albillos,J Bartolomé, F Bartolomé and M R Ibarra
Nanotechnology 25 385703. Sep 2014. doi:10.1088/0957-4484/25/38/385703
IF: 3.672

89. Magnetic Antidot to Dot Crossover in Co and Py Nanopatterned Thin Films
C. Castán-Guerrero, J. Herrero-Albillos, J. Bartolomé, F. Bartolomé, L. A. Rodríguez, C. Magén, F. Kronast, P. Gawronski, O. Chubykalo-Fesenko, K. J. Merazzo, P. Vavassori, P. Strichovanec, J. Sesé, and L. M. García
Physical Review B 89, 144405. Apr 2014.
doi:http://dx.doi.org/10.1103/PhysRevB.89.144405
IF: 3.664

90. Nanoscale Constrictions in Superconducting Coplanar Waveguide Resonators
M. D. Jenkins, U. Naether, M. Ciria, J. Sesé, J. Atkinson, C. Sánchez-Azqueta, E. del Barco, J. Majer, D. Zueco, and F. Luis
Applied Physics Letters 105, 162601 (2014), Oct 2014. arXiv:1409.1040
IF: 3.515

91. Real-Time Monitoring of Breathing of MIL-53(Al) by Environmental SEM
Seoane, B; Sorribas, S; Mayoral, A; Tellez, C; Coronas, J
MICROPOROUS AND MESOPOROUS MATERIALS, 203, 17-23, 2015.
IF: 3.453

92. Amino-Modified Periodic Mesoporous Biphenylene-Silica
Lourenco, MAO; Mayoral, A; Diaz, I; Silva, AR; Ferreira, P
MICROPOROUS AND MESOPOROUS MATERIALS, 217, 167-172, 2015.
IF: 3.453

93. Growth Factor Choice is Critical for successful Functionalization of Nanoparticles
Pinkernelle J1, Raffa V2, Calatayud MP3, Goya GF4, Riggio C5, Keilhoff G6.
Front Neurosci. 2015 Sep 2;9:305. doi: 10.3389/fnins.2015.00305
IF: 3.398

94. Evaluation of Gold-Decorated Halloysite Nanotubes as Plasmonic Photocatalysts.
Gomez, L; Hueso, J. L.; Ortega-Liebana, M. C.; Santamaria, J., Cronin, S.
Catalysis Communications. Volume: 56 Pages: 115-118. Published: Nov 2014.
doi:10.1016/j.catcom.2014.07.017
IF: 3.320

95. VOCs Abatement Using Thick Eggshell Pt/SBA-15 Pellets With Hierarchical Porosity.
L. Usón, M. G. Colmenares, J. L. Hueso, V. Sebastián, F. Balas, M. Arruebo , J. Santamaría.
Catalysis Today. Volume: 227. Pages: 179-186. May 2014.
doi:10.1016/j.cattod.2013.08.014
IF: 3.309

96. Sequential Binding of FurA from Anabaena sp. PCC 7120 to Iron Boxes: Exploring Regulation at the Nanoscale
M.C. Pallarés, C. Marcuello, L. Botello-Morte, A. González, M. F. Fillat, A. Lostao
Biochimica et Biophysica Acta (BBA) – Proteins and Proteomics, Volume 1844, Issue 3, Pages 623–631. Mar 2014. doi:10.1016/j.bbapap.2014.01.005
IF: 3.191

97. Gold-coated Halloysite Nanotubes as Tunable Plasmonic Platforms.
Zieba, M ; Hueso, JL ; Arruebo, M ; Martinez, G ; Santamaria, J.
New Journal of Chemistry. Volume: 38. Issue: 5. Pages: 2037-2042. Published: May 2014.
doi:10.1039/C3NJ01127E
IF: 3.159

98. Photoresponsive Supramolecular Gels Based on Amphiphiles with Azobenzene and Maltose or Polyethyleneglycol Polar Head
María José Clemente, Rosa María Tejedor, Pilar Romero, Juliette Fitremann and Luis Oriol
New J. Chem., 2015,39, 4009-4019. doi:10.1039/C4NJ02012J
IF: 3.159

99. Key Residues Regulating the Reductase Activity of the Human Mitochondrial Apoptosis Inducing Factor
Villanueva, R; Ferreira, P; Marcuello, C; Uson, A; Miramar, MD; Peleato, ML; Lostao, A ; Susin, SA; Medina, M
BIOCHEMISTRY, 54, 33, 5175-5184, 2015.
IF: 3.015

100. Structural Characterization and EXAFS Wavelet Analysis of Yb doped ZnO by Wet Chemistry Route
Otal, EH; Sileo, E; Aguirre, MH; Fabregas, IO; Kim, M
JOURNAL OF ALLOYS AND COMPOUNDS, 622, 115-120, 2015.
IF: 2.999

101. Morphology of the Asymmetric Iron-Silicon Interfaces
Badia-Romano, L; Rubin, J; Bartolome, F; Magen, C; Bartolome, J; Varnakov, SN; Ovchinnikov, SG; Rubio-Zuazo, J ; Castro, GR
JOURNAL OF ALLOYS AND COMPOUNDS, 627, 136-145, 2015.
IF: 2.999

102. Synthesis and Plasmonic Properties of Core–Shell Bimetallic Silver–Gold Nanoprisms Obtained through an Organometallic Route
J. Crespo, A. Ibarra, J. M. López-de-Luzuriaga, M. Monge, and M. E. Olmos
European Journal of Inorganic Chemistry.Volume 2014, Issue 14, pages 2383–2388. May 2014. doi:10.1002/ejic.201400023
IF: 2.965

103. Effect of Thermal Treatments on the Morphology, Chemical State and Lattice Structure of Gold Nanoparticles Deposited onto Carbon Structured Monoliths
Ballestero, D; Juan, R ; Ibarra, A; Gomez-Gimenez, C; Ruiz, C; Rubio, B; Izquierdo, MT
COLLOIDS AND SURFACES A-PHYSICOCHEMICAL AND ENGINEERING ASPECTS, 468, 140-150, 2015.
IF: 2.752

104. Mixed Matrix Membranes Based on 6FDA Polyimide with Silica and Zeolite Microsphere Dispersed Phases
Zornoza, B; Tellez, C; Coronas, J; Esekhile, O; Koros, WJ.
AIChE Journal, 61, 12, 4481-4490, 2015.
IF: 2.748

105. Quaternary Organization in a Bifunctional Prokaryotic FAD synthetase: Involvement of an Arginine at its Adenylyltransferase Module on the Riboflavin Kinase Activity
Serrano, A; Sebastian, M; Arilla-Luna, S ; Baquedano, S; Pallares, MC; Lostao, A; Herguedas, B; Velazquez-Campoy, A; Martinez-Julvez, M; Medina, M]
BIOCHIMICA ET BIOPHYSICA ACTA-PROTEINS AND PROTEOMICS, 1854, 8, 897-906, 2015.
IF: 2.747

106. Electrical Characterization of Single Molecule and Langmuir-Blodgett Monomolecular Films of a Pyridine-Terminated Oligo(Phenylene-Ethynylene) Derivative
Osorio, HM ; Martin, S ; Lopez, MC ; Marques-Gonzalez, S ; Higgins, SJ ;Nichols, RJ ; Low, PJ ; Cea, P
BEILSTEIN JOURNAL OF NANOTECHNOLOGY, 6, 1145-1157, 2015.
IF: 2.670

107. Influence of the Shape and Surface Oxidation in the Magnetization Reversal of Thin Iron Nanowires Grown by Focused Electron Beam Induced Deposition
Rodriguez, LA ; Deen, L; Cordoba, R; Magen, C; Snoeck, E; Koopmans, B; De Teresa, JM
BEILSTEIN JOURNAL OF NANOTECHNOLOGY, 6, 1319-1331, 2015.
IF: 2.670

108. Quantitative Use of Electron Energy-Loss Spectroscopy Mo-M-2,M-3 Edges for the Study of Molybdenum Oxides
Lajaunie, L; Boucher, F; Dessapt, R; Moreau, P
ULTRAMICROSCOPY, 149, 1-8, 2015.
IF: 2.436

109. α-Alkyl cysteine-Coated Gold Nanoparticles: Effect of Cα-Tetrasubstitution on Colloidal Stability
I. Osant, E. Polo, G. Revilla-López, J. M. de la Fuente, C. Alemán, C. Cativiela, D. Díaz Díaz
Journal of Nanoparticle Research. Jan 2014. doi:10.1007/s11051-013-2224-y
IF: 2.278

110. Exploratory Catalyst Screening Studies on the Base Free Conversion of Glycerol to Lactic Acid and Glyceric Acid in Water Using Bimetallic Au-Pt Nanoparticles on Acidic Zeolites
RKP Purushothaman, J. van Haveren, A. Mayoral, I. Melian-Cabrera, HJ Heeres
Topics in Catalysis. Vol: 57. 17-20. P: 1445-1453. Nov 2014. doi:10.1007/s11244-014-0316-2
IF: 2.220

111. Role of Magnetic Anisotropy on the Magnetic Properties of Ni Nanoclusters Embedded in a ZnO Matrix
W. C. Nunes, R. P. Borges, M. M. Cruz, R. C. da Silva, U. Wahl, A. Cuchillo, P. Vargas, C. Magen and M. Godinho
Journal of Applied Physics, 116, 033916, Jul 2014, doi:10.1063/1.4890498
IF: 2.185

112. Heteroepitaxial ZnO Films on Diamond: Optoelectronic Properties and the Role of Interface Polarity
F. Schuster, M. Hetzl, C. Magén, J. Arbiol, J. A. Garrido and M. Stutzmann
Journal of Applied Physics115, 213508. Jun 2014, doi:10.1063/1.4880161.
IF: 2.185

113. Iron Silicide Formation at Different Layers of (Fe/Si)3 Multilayered Structures Determined by Conversion Electron Mössbauer Spectroscopy
L. Badía-Romano, J. Rubín, C. Magén, D. E. Bürgler and J. Bartolomé
Journal of Applied Physics, 116, 023907, Jul 2014, doi:10.1063/1.4887522
IF: 2.185

114. Magnetic Behavior of NiCu Nanowire Arrays: Compositional, Geometry and Temperature Dependence.
E. M. Palmero, C. Bran, R. P. del Real, C. Magén and M. Vázquez
Journal of Applied Physics, 116, 033908, Jul 2014, doi:10.1063/1.4890358
IF: 2.185

115. Molecular Tilting and Columnar Stacking of Fe Phthalocyanine Thin Films on Au(111)
Bartolome, F ; Bunau, O ; Garcia, LM ; Natoli, CR ; Piantek, M ; Pascual, JI ; Schuller, IK; Gredig, T ; Wilhelm, F ; Rogalev, A ; Bartolome, J
JOURNAL OF APPLIED PHYSICS, 117, 17, 17A735, 2015.
IF: 2.183

116. Formation of Strained Interfaces in AlSb/InAs Multilayers Grown by Molecular Beam Epitaxy for Quantum Cascade Lasers
Nicolai, J; Warot-Fonrose, B; Gatel, C; Teissier, R; Baranov, AN; Magen, C; Ponchet, A
JOURNAL OF APPLIED PHYSICS, 118, 3, 035305, 2015.
IF: 2.183

117. Validity of the Néel-Arrhenius Model for Highly Anisotropic CoxFe3−xO4nanoparticles
Torres, TE; Lima Jr, E; Mayoral, A; Ibarra, A; Marquina, C; Ibarra, MR
JOURNAL OF APPLIED PHYSICS, 118, 3, 183902, 2015.
IF: 2.183

118. Zeolites Are No Longer a Challenge: Atomic Resolution Data by Aberration-Corrected STEM
Mayoral, A; Anderson, PA; Diaz, I
MICRON, 68, 146-151, 2015.
IF; 1.998

119. Characterization of Langmuir and Langmuir-Blodgett Films of an Octasubstituted Zinc Phtalocyanine.
Torrent-Burgués, J.; Cea, P.; Giner, I.; Guaus, E.
Thin Solid Films Apr 2014, 485-494. doi: 10.1016/j.tsf.2014.01.045
IF: 1.867

120. Generation of Gold Nanoparticles According to Procedures Described in the Eighteen Century
Mayoral, A; Agundez, J; Pascual-Valderrama, IM; Perez-Pariente, J
GOLD BULLETIN, 47, 3, 161-165, 2014.
IF: 1.840

121. Present and Future Applications of Magnetic Nanostructures Grown by FEBID
J. M.De Teresa, A. Fernandez-Pacheco
Applied Physics A. Volumen: 117. Número: 4. Páginas: 1645-1658. Dec 2014. doi:10.1007/s00339-014-8617-7
IF: 1.694

122. Fabrication of Cobalt Trifluoride (CoF3) Phase from Metallic Cobalt by XeF2-Assisted Focused Electron Beam Induced Processing
J.M. De Teresa, P. Holuj, R. Córdoba, R. Fernández-Pacheco, J.M. Michalik
Microelectronic Engineering Volume 125, Pages 78–82, Aug 2014. doi:10.1016/j.mee.2014.01.002
IF: 1.338

123. Thin-Film Microsusceptometer with Integrated Nanoloop
D. Drung, J. H. Storm, F. Ruede, A. Kirste, M. Regin, Th. Schurig, A. Repollés, J. Sesé, F. Luis
IEEE Trans Appl. Superc. 24, 1600206 (2014). doi:10.1109/TASC.2014.2318322
IF: 1.324

124. Silica-Based Nanoporous Materials
Han, L; Ohsuna, T; Liu, Z; Alfredsson, V; Kjellman, T; Asahina, S; Suga, M; Ma, YH; Oleynikov, P; Miyasaka, K; Mayoral, A; Diaz, I ; Sakamoto, Y; Stevens, SM; Anderson, MW; Xiao, CH; Fujita, N; Garcia-Bennett, A; Yoon, KB; Che, SN; Terasaki, O
Zeitschrift fur Anorganische Und allgemeine chemie, 640, 3-4, 521-536, 2014.
IF: 1.251

125. Synthesis, Crystal structure, Electric and Magnetic Properties of LaVO2.78N0.10
S Yoon, AE Maegli, L Karvonen, A Shkabko, S Populoh, K Gałązka, Leyre Sagarna, Myriam H Aguirre, Peter Jakes, Rüdiger A Eichel, Stefan G Ebbinghaus, Simone Pokrant, Anke Weidenkaff
Zeitschrift fur Anorganische Und allgemeine chemie, 640, 5, 797-804, 2014.
IF: 1.251

126. Nanostructuring Superconducting Vortex Matter with Focused Ion Beams
I. Guillamón, H. Suderow, P. Kulkarni, S. Vieira, R. Córdoba, J. Sesé, J. M. De Teresa, M.R. Ibarra, G. Shaw, S.S. Bannerjee,
Physica C: Superconductivity, Volume 503, Aug 2014, Pages 70–74 doi:10.1016/j.physc.2014.04.031
IF: 1.110

127. Synthesis and Optical Properties of Homogeneous Nanoshurikens
Morla-Folch, L. Guerrini, N. Pazos-Perez, R. Arenal, R. Alvarez-Puebla
ACS Photonics 1, 1237–1244, Oct 2014. doi:10.1021/ph500348h
IF: No impact factor assigned in 2014

128. From an Organometallic Monolayer to an Organic Monolayer Covered by Metal Nanoislands: a Simple Thermal Protocol for the Fabrication of the Top Contact Electrode in Molecular Electronic Devices.
Ballesteros, L. M.; Martin, S.; Cortés, J.; Marqués-Gonzalez, S.; Pérez-Murano, F.; Nichols, R. J.; Low, P. J.; Cea, P.
Advanced Materials Interfaces.Jun 2014, doi:10.1002/admi.201400128.
IF: No impact factor assigned in 2014

Organization of scientific events

LMA Scientific Meetings

A series of topical colloquia on the three scientific áreas (TEM, Dual & SPM), devoted to informing local researchers about the capabilities of our infrastructures and to promote interdisciplinar work.

> I Scientific Seminar TEM area: November 11, 2014

> II Scientific Seminar SPM area: December 16, 2014

> III Scientific Seminar DUAL BEAM area: February 10, 2015

> IV Scientific Seminar TEM area: March 3, 2015

> V Scientific Seminar SPM area: June 24, 2015

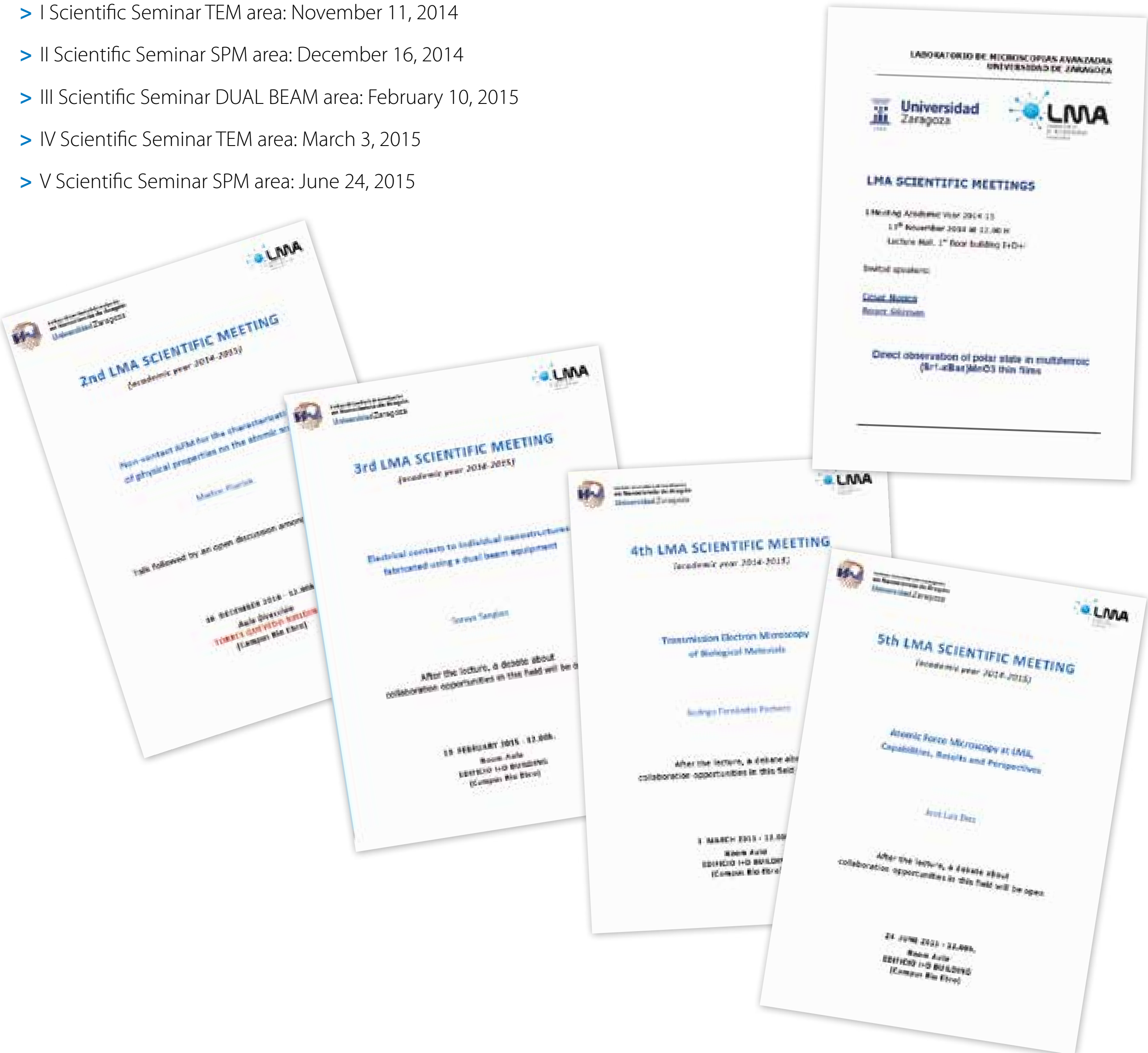

6th Spanish Workshop on Nanolithography–Nanolito 2014

Since its creation the Network of nanolithography, NANOLITO, has achieved an optimization in the use and coordination of the scientific-technological infrastructures that exist today in Spain in the field of nanolithography and has made it possible to hold meetings, schools and workshops, as well as to foster a program of short stays between centers aimed at students and researchers..

The 6º Spanish Workshop on nanolithography was held in October 2014 in the framework of the network Nanolito, with the aim to exchange and transfer knowledge between Spanish agents (research groups, centers and companies) in this field. The scientific program, which took place in the premises of the Institute of Nanoscience of Aragon from 28 to 30 October, consisted of 50 contributions, divided into 5 invited talks, 24 oral presentations and 21 posters, including also an industrial meeting with the attendance of companies like Cetemmsa, EIF, Raith-Vistec, Zeiss and Graphene Nanotech. The invited lectures were given by the prestigious researchers Ivo Rangelow (Ilmenau University, Germany), Rainer Hillenbrand (Nanogune, Spain), Isabel Rodríguez (Imdea, Spain) and Amalio Fernández-Pacheco (U. Cambridge, United Kingdom). The most prominent subjects addressed during the Workshop were related with the development of nanofabrication techniques in order to achieve new applications in the fields of electronics, photonics, magnetism and spintronics, superconductivity, smart surfaces, sensors and biosensors.

Pictures of the 6th Spanish Workshop on Nanolithography

CIBA-LMA seminar on Electronic and Scanning Probe Microscopy for Biomedical Applications

The Laboratory of Advanced Microscopies the Nanoscience Institute of Aragon (LMA-INA) and the Aragon Institute of Health Sciences (IACS) organized the seminar "Electronic Microscopy and Local probe for biotechnological applications", which was taught by Rodrigo Fernández Pacheco, Technician at LMA-INA.. This seminar took place on January 21 at 5 p.m. in the Biomedical Research Center of Aragon (CIBA). The lecture presented the techniques, with practical examples applied to research in Biotechnology of the Scanning Electron Microscopy (SEM), Transmission Electron Microscopy (TEM) and Dual Beam electrons/ion (SEM/FIB), as well as the Atomic Force and Local Probe (AFM-SPM) Microscopy. The objective of this seminar was to introduce to CIBA's scientific community the services offered by the Laboratory of Advanced Microscopies.

Seminars

February 12, 2014

An introduction to Scanning Probe Microscopies

Richard Nichols (University of Liverpool, UK)

June 6, 2014

One-Step Generation of alloy, Core@Shell and Core@Shell@Shell Nanoparticles under Ultra High Vacuum Conditions

Yves Huttel (ICMM-CSIC, Madrid)

October 22, 2014

Magneto-thermoelectric transport in ferromagnetic La2/3Sr1/3MnO3 thin films

Bui Cong Tinh (Centro Singular de Investigación en Química Biológica y Materiales Moleculares –CIQUS, Santiago de Compostela)

December 18, 2014

Magnetic and Structural Properties of nanometric La1-xCaxMnO3 superlattices.

Pedro Prieto (Centro de Excelencia en Nuevos Materiales CENM, Cali, Colombia)

Seminars given by indutry in collaboration with the LMA

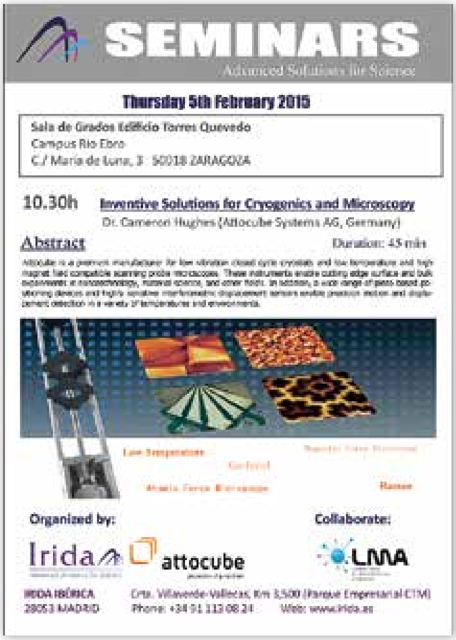

Visibility actions

Presentation of the Laboratory of Advanced Microscopies in business and industry forums

> IMAGINENANO 2015Industrial Forum. March 11, 2015

> MESIC 2015 International Conference. July 1, 2015

In both forums, Dr. Guillermo Antorrena, technical manager of the LMA took part with the presentation "Advanced Microscopy Services for Industrial Applications" which showed the capabilities of the Laboratory of Advanced Microscopie focused on applications to the industrial sector.

Visits to the facilities

With the objective of increasing the interest of society in general in Science, giving visibility and stressing the value of the daily work of researchers, the INA stands for the realization of guided tours and open days in its installations, in which the Laboratory of Advanced Microscopies acquires special importance to seize the interest of its visitors. The most significant visits received throughout 2014 and 2015 are listed below::

> IV Scientific Circuits: This edition took place along March and April and it received more than 300 students from that of different secondary institutes from all over Aragon.

> Alumni of the University Master in Nanostructured Materials for Applications in Nanotechnology. September 18, 2014.

> Students of 4th, 5th and 6th grade of primary school "CEIP Labordeta" visited the facilities of the LMA along the month of November as winners of the first edition of the Science Fair.

> Visit of the participants at the Characterization of Nanocomposites Workshop. February 20, 2014

> AIN TECH Technological Center - 24 February.

> Podoactiva. June, 5

> Leads RCT. October 20, 2014

> HENKEL October 23, 2014

> Visit of the participants at the 6th Spanish Workshop on Nanolithgraphy October 30, 2014

> Arcelor Mittal. November 4, 2014

> ARACLON BIOTECH (Group Grifols). December 2, 2014.

> Compañía Logística de Hidrocarburos CLH December 10, 2014

> V Scientific Circuits: Within the framework of this program organized by the University of Zaragoza and co-financed by FECYT, along the months of April and May, LMA has been visited by students of 4º course of Secondary Education from all over Aragon, especially from the rural countryside.

> BSH. January 14, 2015. R&D managers from the plants of BSH in Zaragoza and Germany visited INA to learn first hand the facilities, including in particular the LMA, where the company carries out some of its technological projects

> Chamber of Commerce and Industry of Zaragoza. March 9, 2015. In the framework of the meeting held between representatives of the Chamber of Commerce and Industry of Zaragoza and INA management, a visit was made to LMA.

> REPSOL. April 20, 2015. Representatives of the R+D department toured the facilities of the INA and the LMA to learn its capabilities and address possible ways of collaboration..

> Valeo Térmico. May 6, 2015. The company, which already is a user of LMAL, wanted to get to know the facilities and the instruments on which perform the characterization services they use.

> LEAR Corporation. May 18, 2015. After a previous meeting that was maintained with the company at its facilities in Valls (Tarragona), the LMA received the visit of this company to learn about our facilities and, as a result, LMA has already provided several services..

Training actions

Course on Micro- and nano-Characterization of Materials and Surfaces for industrial users

Within the framework of activities of NANOARACAT, LMA organized a practical course on advanced microscopy techniques especially addressed to industrial users. It took place on October 5-7, 2015 and was devoted to techniques on Micro and Nano characterization of surfaces and materials. Hands-on training was carried out by LMA scientific and technical staff and participants coming from all over the country had the chance to get to know the great possibilities provided by an installation which is accredited as Singular Scientific and Technical Installation (ICTS for its English acronym) by the Ministry of Economy and Competitiveness and therefor giving service to the industrial sector in Spain is one of its inherent objectives.

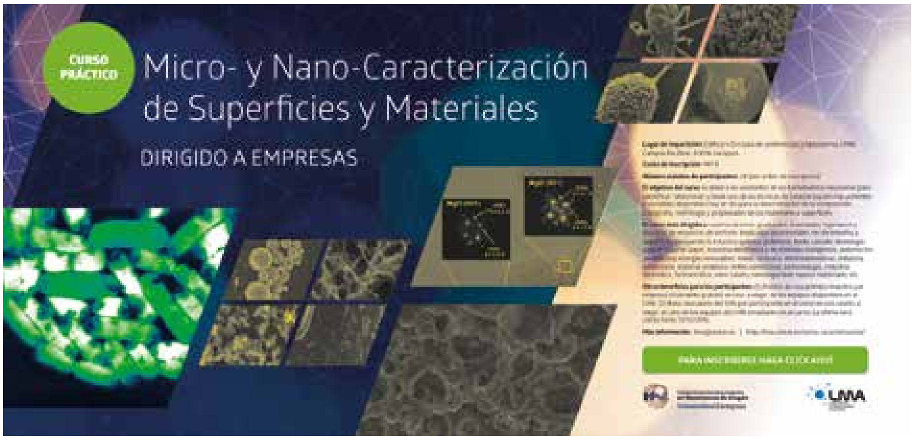

Above: Image of the Promotional Leaflet of the course.
Below: (left) Group of students in a practical lesson at the Clean Room. (right) Group photo of students and teachers of the course

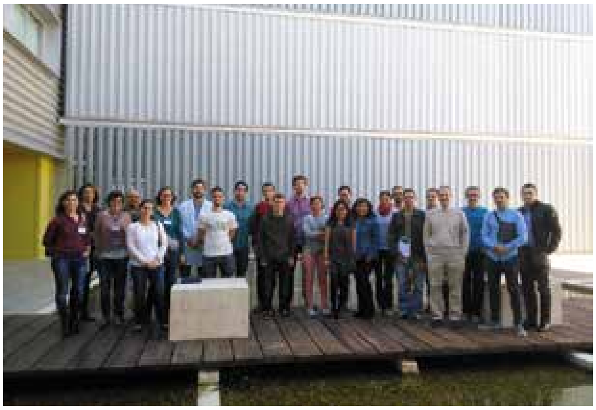

Basic course on Transmission Electron Microscopy.

The objective of the course is to give the student the sufficient training to operate the instrument as an autonomous user and to interpret by himself the results obtained. For this reason the course was primarily aimed at those people who have a continuing need of this very versatile tool. he course was structured in a theoretical part and a very practical part in laboratory and iwas delivered by the technical staff of the TEM area-tem.

Masters Courses

LMA makes available its facilities and technical staff to the Master in nanostructured materials for applications in nanotechnology (Nanomat), Erasmus Mundus Masters course in Engineering of membranes and masters degree in Physics and Physical Technologies, so that students of the University of Zaragoza can have access to the most advanced infrastructures in nanomanufabrication and nanocaracterización. We understand that this is yet another way to promote our facilities to future scientists, to contribute to train highly qualified professionals and to increase the internationalisation of the University of Zaragoza (all Erasmus Mundus students and a most of the students of the Nanomat come from abroad).

Other actions

A new web page of the Laboratory of Advanced Microscopies was launched. The bilingual site collects all the capabilities of the installation and provides detailed information on how to use the services available both to the scientific and industrial communities.

http://lma.unizar.es

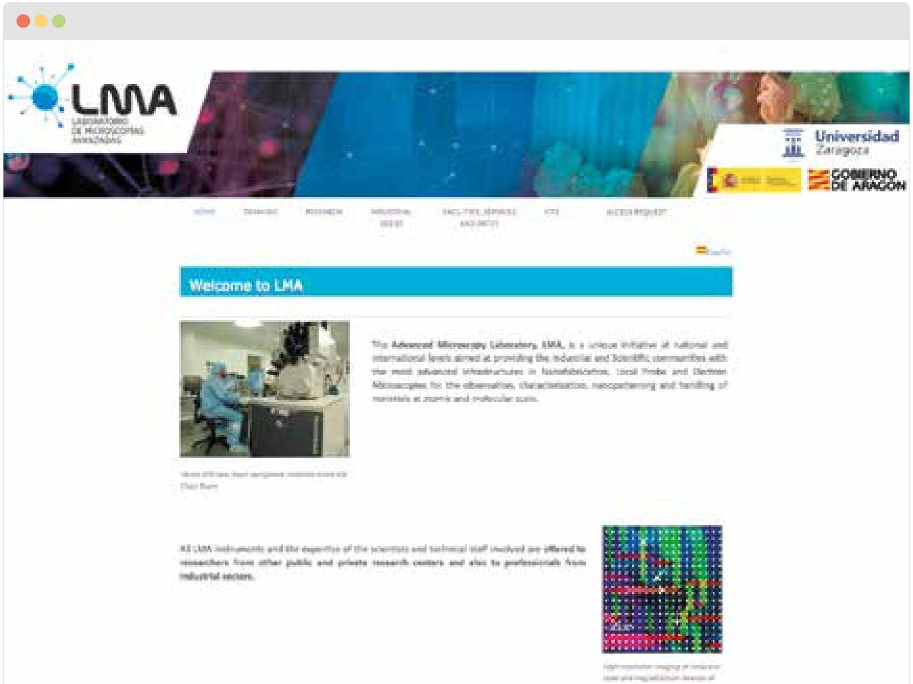

A corporate video on LMA in Spanish and English was also recorded with the objective of having an audiovisual tool to help disseminate the capabilities available at LMA.

https://www.youtube.com/watch?v=VCPKBUUGf-U

LMA and the industry

LMA and the industry

Along 2014 and 2015, the Advanced Microscopy Laboratory has offered the experience of their researchers and technical staff to provide service to several private companies in order to help them to solve production problems and advance in their R&D programs. They have been able to benefit from the transfer of our technical knowledge and experience in highly advanced characterization and fabrication techniques. These companies belong to branches of industry as diverse as electronics and microelectronics, biotechnology, white goods industry, telecommunications, chemistry, logistics or automotive industry. A list of several private companies both from Spain and abroad which have benefited from these services is provided below.

- Abengoa Research, S.L.
- Aitex
- Bsh Electrodomesticos, S.A.
- Eficiencia Energética
- Enagas, S.A.
- Essilor
- Faci Metalest, S.L.
- Fitex
- Grupo Arbotante
- Grupo Torras
- Konsberg Group
- Laboratorios Argenol, S.L.
- Mondragon Corporation
- Nanoimmunotech, S.L.
- Nurel, S.A.
- Quionne
- Sesderma
- Tecnalia Research & Innovation
- Teltronic, S.A.U.
- Valeo Termico
- Worldpathol
- Abalonyx, S.A.
- Araclon Biotech
- Enagas, S.A.
- Lear Corporation
- Nanoimmunotech, S.l.
- Next Services Iberia, S.L.
- Valeo Termico

aitex textile research institute

enagas

ESSILOR SEEING THE WORLD BETTER

LABORATORIOS ARGENOL

NUREL

tecnalia Corporación Tecnológica

Abalonyx Innovative materials

Araclon Biotech GRIFOLS

LEAR CORPORATION

ABENGOA RESEARCH

B/S/H/

Eficiencia Energética Aplicada

FACI metalest FACI S.p.A. Spain Branch

fitex FUNDACIÓ PER A LA INNOVACIÓ TEXTIL

Arbotante Equipo de Investigación

KONGSBERG

SENTIDO HUMANO DEL TRABAJO MONDRAGON Finanzas Industria Distribución Conocimiento

nanoimmunotech global solutions in nanobiotechnology

QUIONNE

sesderma listening to your skin

teltronic Part of the Sepura Group

Valeo

Henkel

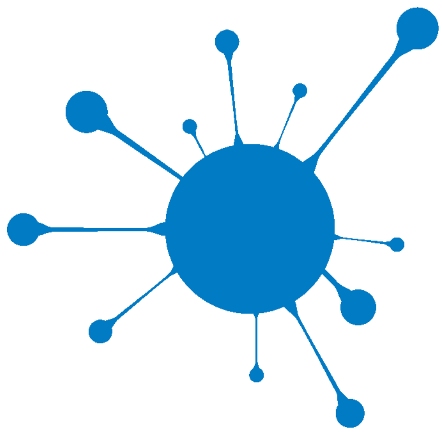

GOBIERNO DE ESPAÑA
MINISTERIO DE ECONOMÍA, INDUSTRIA Y COMPETITIVIDAD

Universidad Zaragoza
1542

GOBIERNO DE ARAGON